An Electromechanical Valve Drive Incorporating a Nonlinear Mechanical Transformer

by

Woo Sok Chang

S.M., Mechanical Engineering, Massachusetts Institute of Technology (1999)
M.S., Electrical Engineering, Seoul National University (1990)
B.S., Electrical Engineering, Seoul National University (1988)

Submitted to the Department of Electrical Engineering and Computer Science
in Partial Fulfillment of the Requirements for the Degree of

Doctor of Philosophy

in Electrical Engineering and Computer Science
at the

Massachusetts Institute of Technology

September 2003

© 2003 Massachusetts Institute of Technology
All rights reserved

Signature of Author .....
Department of Electrical Engineering and Computer Science
July 15, 2003

Certified by .....
John G. Kassakian
Professor of Electrical Engineering and Computer Science
Thesis Supervisor

Accepted by .....
Arthur C. Smith
Chairman, Department Committee on Graduate Students

MASSACHUSETTS INSTITUTE OF TECHNOLOGY
SEP 13 2005
LIBRARIES

ARCHIVES

An Electromechanical Valve Drive Incorporating a Nonlinear Mechanical Transformer

by

Woo Sok Chang

Submitted to the Department of Electrical Engineering and Computer Science
on July 15, 2003 in Partial Fulfillment of the
Requirements of the Degree of
Doctor of Philosophy
in Electrical Engineering and Computer Science

ABSTRACT

In traditional internal combustion engines, a camshaft acts on the valve stems to open and close the valves. Valve timing is fixed relative to piston position. On the other hand, if a valve is flexibly controlled by a variable valve actuation (VVA) system, we can achieve significant improvements in fuel efficiency, engine performance, and emissions. One of the most advanced variable valve actuation systems is the VVA operated by an electromechanical actuator without a camshaft, the so-called bi-positional electromechanical valve drive (EMVD). Existing EMVDs characteristically use a spring to provide the required mechanical power for operating a valve. The use of a spring provides many benefits to the design of the system, but it also results in difficult design challenges. The large holding force against the spring at the ends of the stroke suggests the use of a normal-force electromagnetic actuator, which, from a servomechanical point of view, is considerably inferior to a shear-force actuator. Furthermore, the large holding force generates a large jerk at the beginning and the end of a stroke and makes it difficult to achieve soft valve landing. An innovative electromechanical valve drive (EMVD) design is proposed, which incorporates a nonlinear mechanical transformer and a shear-force actuator. This allows not only fast but also smooth valve motion, almost zero seating velocity, zero holding power, and improved control with acceptable electric power. This proposed concept is modeled, analyzed, simulated, designed, and implemented. Experimental results show the beneficial features of the promising proposed concept.

Thesis Supervisor: John G. Kassakian
Professor of Electrical Engineering

Thesis Committee: Thomas A. Keim
Principal Research Scientist

Wai K. Cheng
Professor of Mechanical Engineering

David J. Perreault
Assistant Professor of Electrical Engineering

Acknowledgements

I would like to thank people who directly and indirectly enabled me to complete this thesis work. This thesis research would not have been possible without their effort.

- Professor John G. Kassakian, Dr. Thomas A. Keim, and Professor David Perreault for guide, support, patience, and encouragement during the course of this thesis research as not only thesis but also personal advisors.
- Professor Wai Cheng and his colleagues in Sloan Automotive Lab at MIT for valuable comments and useful information on my thesis research.
- Tushar, Wayne, Mike, and Yihui for helping me to implement the apparatus, especially for the preparation of 3-D drawings and the construction, measurement setup, and testing of the electrical/mechanical components and systems.
- Dr. John Miller of Ford and Dr. David Turner of Eaton for donating cylinder heads and Dr. Bruno Lequesne of Delphi for useful information.
- Joshua for proof-reading.
- The Shiela and Emanuel Landsman Fund for supporting this project.

Many other people helped me in a number of different ways. I would like to thank these people too.

- All labmates, officemates, and staff in Laboratory for Electromagnetic and Electronic Systems. Especially, Vahe, Vivian, Tim, and Dave Wentzloff for useful discussion and friendship.
- Drs. June Dong Kim and Sang-Gook Kim at Daewoo Electronics for support.
- Professors Song-yop Hahn and Il Hong Suh for guide and encouragement.
- KGSA members. Especially, Drs. Jae-Hyuk Oh and Sangjoon Shin.

Above all, I would like to thank my wife, Eunchan, and my children, Yehna and Hweedo for their patience and understanding, my and Eunchan's parents for their prayer and encouragement. This thesis is dedicated to my family.

Contents

1 Introduction

1.1 Brief Background and Motivation

In internal combustion engines, variable valve actuation (VVA) systems offer a flexible valve profile and may significantly improve fuel efficiency, engine performance, and emissions compared with conventional, fixed profile valvetrains [1], [2], [3]. One of the most advanced VVA systems is the electromechanical valve drive (EMVD), an electrically actuated, camless VVA which can flexibly control the duration, phase, and lift of a valve profile. The EMVD is expected to become a more viable candidate for future VVA systems with the advent of 42 V automotive electrical systems. Arguably, the most difficult challenge for existing EMVDs is achieving soft valve landing within acceptable power consumption limits, especially while counteracting gas forces.

1.2 Thesis Objectives and Contributions

The objectives of this thesis are:

- To propose an innovative EMVD design which solves the technical problems of existing EMVDs.
- To design and construct an experimental apparatus which demonstrates the basic operation of the proposed concept.
- To confirm the benefits of the proposed design with experimental results.

In this thesis, an EMVD incorporating a nonlinear mechanical transformer (NTF) is proposed. The mechanical transformer introduces an effective nonlinear spring or inertia into the otherwise linear valve mechanics, generating a smooth valve acceleration curve

and soft valve landing. The NTF, moreover, improves control performance by allowing the use of a single bi-directional shear-force electromagnetic actuator instead of two uni-directional normal-force electromagnetic actuators. The design proposed in this thesis exhibits low driving current and near zero holding current, and consumes less power than other EMVDs. It tolerates kinematic overshoot in the actuator, allowing fast actuator rise times, which improves overall system response speed. The valve seating velocity is almost zero – without brute-force actuator effort – as long as the mechanical compliance across the NTF is negligible.

The proposed EMVD system is mathematically modeled, analyzed, and simulated. To demonstrate the feasibility of the NTF concept, an experimental apparatus is designed and constructed. The performance of the NTF-based EMVD is confirmed with test results.

The major contributions of the thesis are:

- Proposal of an innovative EMVD incorporating an NTF.
- Mathematical modeling, analysis, and simulation of the EMVD.
- Design and construction of an experimental apparatus.
- Design of controllers for the initial, holding, and transition modes of valve motion.
- Measurements and characterization of the experimental apparatus.
- Conceptual design of a lash-adjustment device and a lift-control mechanism.
- Optimization of the NTF to minimize actuator size.

1.3 Thesis Organization

The thesis has three major parts:

- Proposal of an innovative EMVD.
- A report of the design and construction of the experimental EMVD apparatus.
- Experimental results from the prototype system.

In the first part, Chapter 2 describes the technical issues of valvetrains and the benefits of VVA systems. Chapter 3 describes existing EMVD designs and details of their technical problems. To address the main technical challenges of experimental systems, Chapter 4 proposes the incorporation of an NTF in the EMVD and shows the results of simulating the novel design.

In the second major division, a description of the design and construction of an experimental EMVD apparatus is presented in four chapters:

- System requirements and design considerations (Chapter 5).
- Electrical and mechanical components and subsystems (Chapters 6 and 7).
- Operation and control (Chapter 8).

Chapter 9 describes experimental results which confirm the benefits of the NTF concept. Chapter 10 introduces the conceptual design of a lash-adjustment device, a description of a lift-control mechanism, and the optimization of the NTF for minimized actuator torque. Finally, Chapter 11 presents conclusions and suggests topics for further research.

2 Background

This chapter describes the background of conventional valvetrains and variable valve actuation systems. This fundamental background is useful for the design of an electromechanical valve drive (EMVD).

2.1 Conventional Valvetrains

An internal combustion engine converts chemical fuel energy to mechanical energy. This section explains the operation of the engine, and in particular, the function of the valvetrain. Also discussed are technical issues such as valve kinematics, gas forces, and valvetrain power consumption.

Fig. 2.1 shows the structure of an internal combustion engine [4]. A piston is connected to a crankshaft through a connecting rod, and the crankshaft is connected to a camshaft through a belt. As the piston moves up and down, the crankshaft and the camshaft rotate. As the camshaft rotates, intake and exhaust valves open and close and enable the exchange of gases in the cylinder. The intake valve controls the opening and closing of the air-fuel mixture flow channel, and the exhaust valve controls the exhaust gases flow channel. In conventional valvetrain systems, the intake and exhaust valves' opening and closing is geometrically fixed relative to the camshaft angle, the crankshaft angle, and the piston position.

Internal combustion engines usually operate on a four-stroke cycle: an intake stroke, a compression stroke, a power stroke, and an exhaust stroke. Fig. 2.2 shows a 4 stroke cycle and corresponding valve controls [4]. During the intake stroke, an intake valve opens, and the piston moves down. So, the stroke provides a fresh air-fuel mixture flow through the intake valve using a pressure difference. During the compression stroke, both

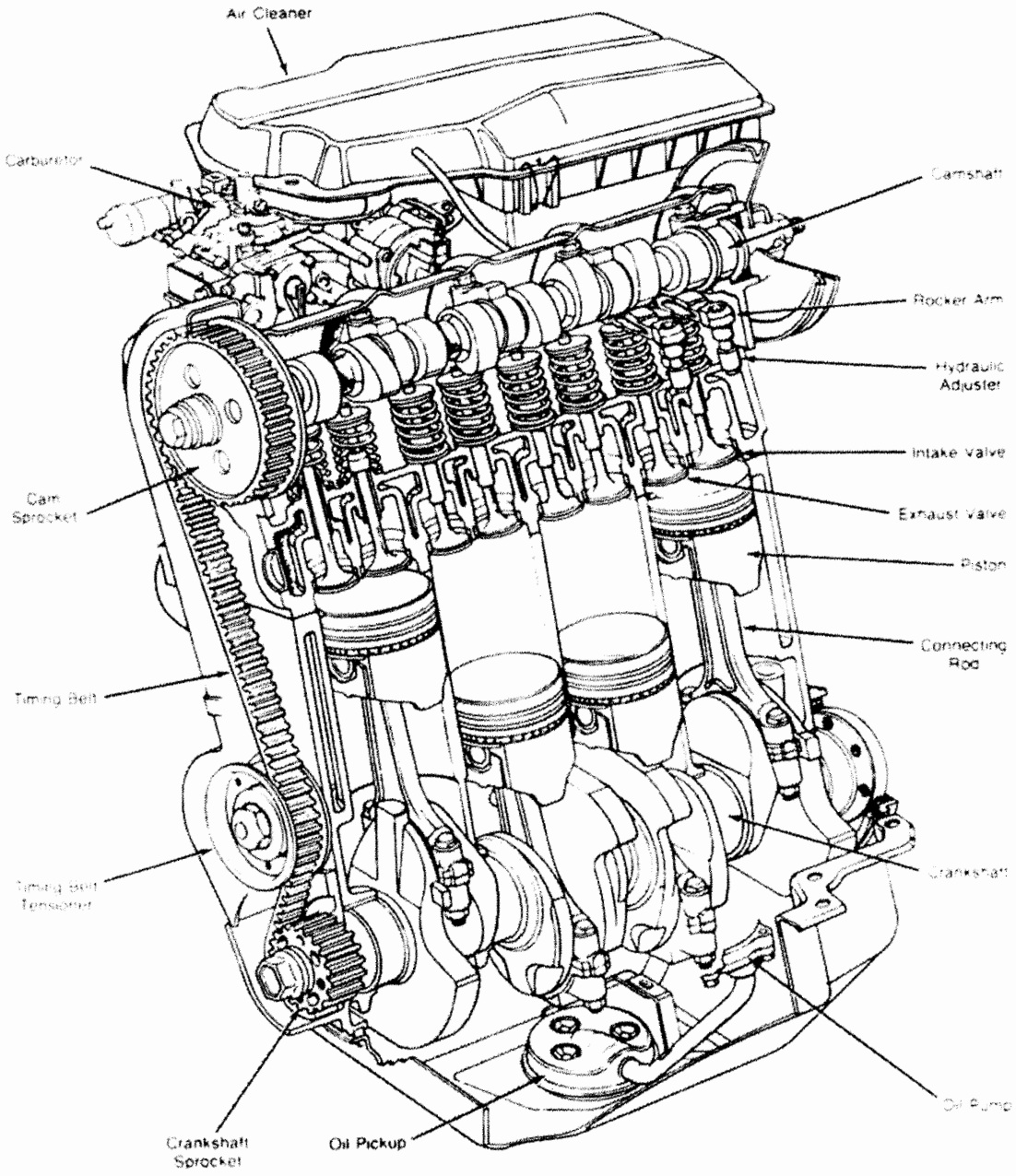

Fig. 2.1. A structure of an internal combustion engine [4].

valves are closed, and the air-fuel mixture is compressed as the piston moves up. Near the end of the stroke, an electrical discharge across the spark plug starts the combustion process, and the cylinder pressure rises rapidly. During the power stroke, the high pressure and high temperature gases push down the piston and deliver power to the crankshaft. Near the end of the power stroke, the exhaust valve opens so that burned gases may exit the cylinder using a pressure difference. The exhaust valve stays open during the exhaust stroke, in which the piston rises and expels burned gas from the cylinder. During two rotations of the crankshaft, intake and exhaust cams perform one cycle of opening and closing. Therefore, two rotations of the crankshaft correspond to one rotation of each camshaft.

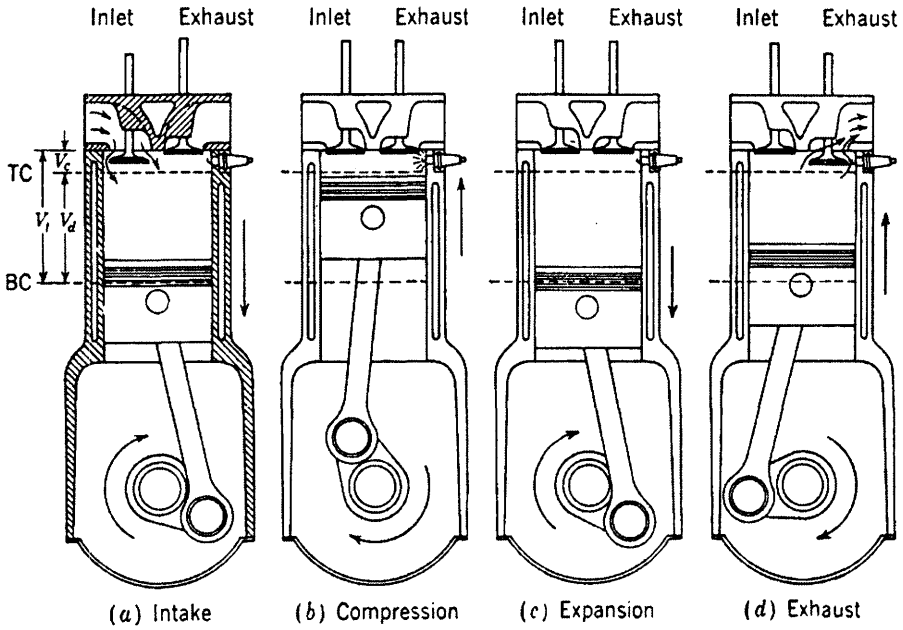

Fig. 2.2. Four stroke operating cycle [4].

Fig. 2.3 shows representative valve opening and closing times of intake and exhaust valves with respect to crankshaft angle. The opening and closing times are fixed with respect to camshaft angle which generally has a fixed relationship to crankshaft angle. The times are determined by the compromise among maximum power, fuel efficiency, and emissions [5].

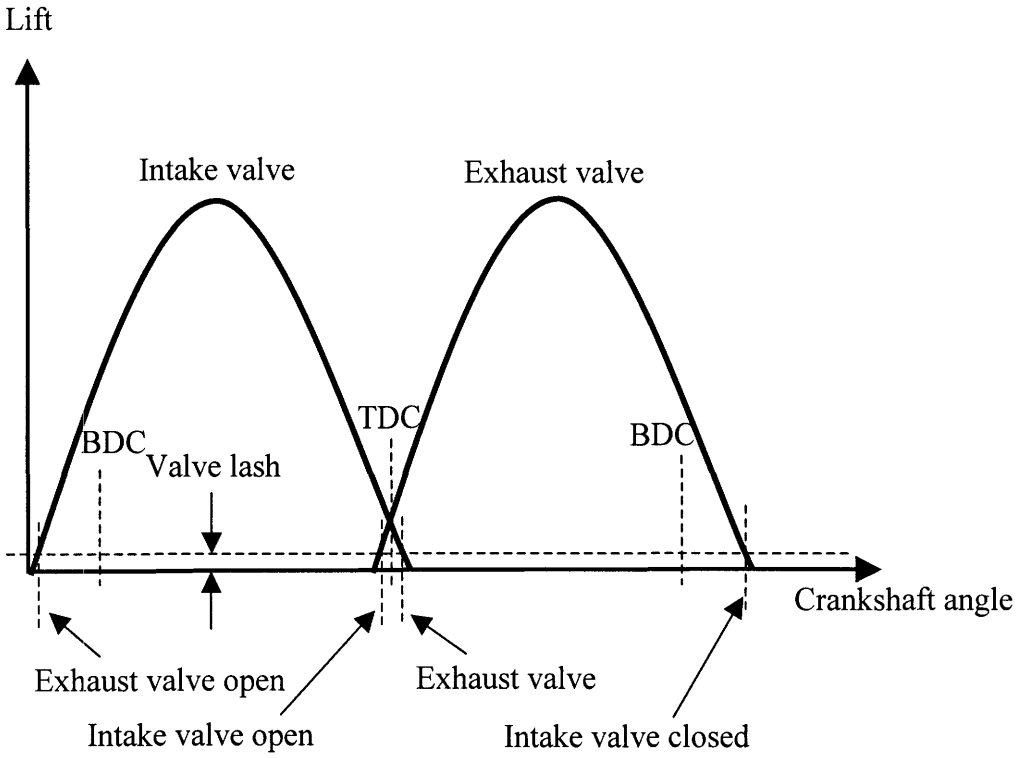

Fig. 2.3. Intake and exhaust valves timing [5].

The shape of a cam lobe determines valve kinematics. In particular, abrupt changes in acceleration (jerk) in valve kinematics introduce shock loading in the valvetrain, thus creating deflections and vibrations in linkage components [6]. To avoid excessive jerk, the opening and closing parts of the acceleration curve need to be rounded. The transition between the base circle and flank of the cam should be carefully designed. A ramp is used on the opening and closing sides of the cam. Fig. 2.4 shows a cam and ramp design. The ramp compensates for length changes in the valvetrain that result from wear or thermal effects when solid tappets are used, or from leak down effects when hydraulic tappets are used. Fig. 2.5 shows typical valve position, velocity and acceleration profiles with respect to camshaft angle [7]. Two small acceleration spikes in Fig. 2.5 are due to the transition between the cam's base circle and constant velocity ramp. Ramp velocity is about 0.0005 in/cam angle degree for quiet valvetrain operation in passenger cars [6]. This ensures the valves' low opening and closing velocities, which are about 23 cm/s at 6 krpm engine speed. In industrial or commercial engines, where noise is not a serious

problem, ramp velocity may be as high at 0.0015 in/deg [6]. Another reference gives seating velocity requirement of less than 3 cm/s at an engine speed of 600 rpm and 30 cm/s at 6000 rpm [8]. An electromechanical valve drive should have as smooth valve kinematics as possible and meet the seating velocity specification.

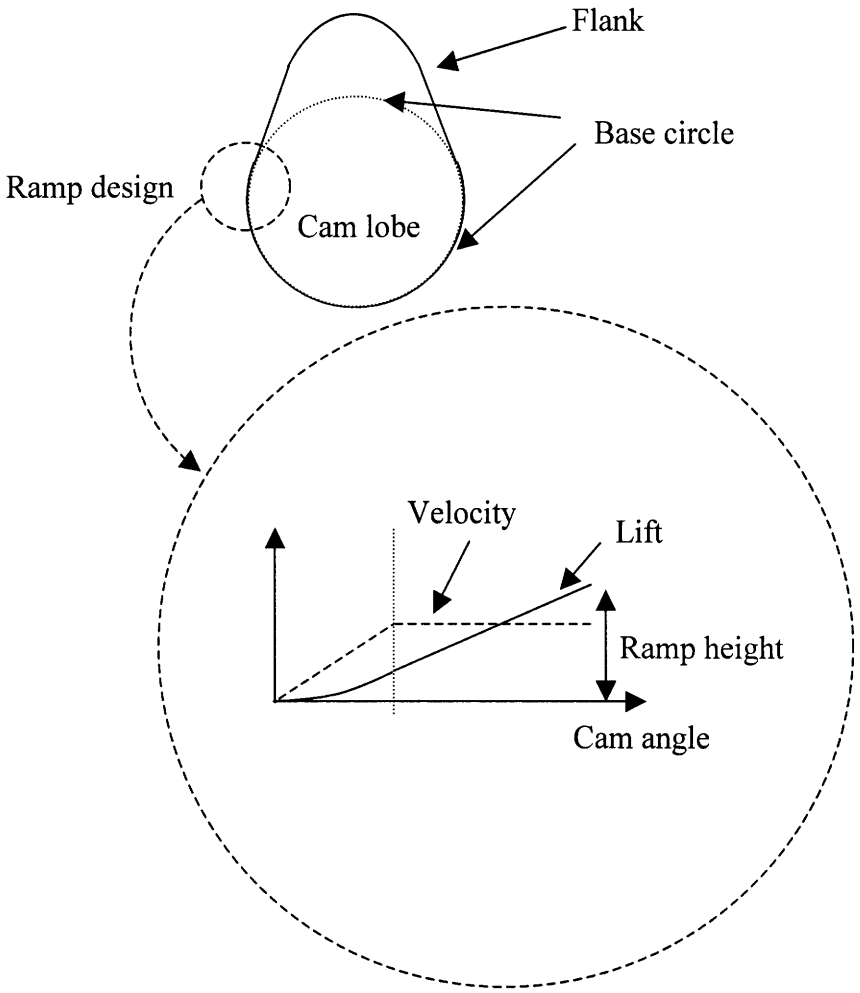

Fig. 2.4. A cam and ramp design.

Valves' opening and closing positions are defined as valve-lift positions of approximately 0.15 mm [4]. An approximate valve opening period based on the definition of valve's opening and closing positions is about a third of one revolution of the camshaft, or approximately 120° cam angle. At 6 krpm engine speed, the crankshaft rotates at 100 (rev/s), and the camshaft rotates at 50 (rev/s). Therefore, a valve opening duration time at 6 krpm engine speed is (120/360) x (1/50) = 6.67 ms. An electromechanical valve drive

should meet this valve opening duration time to permit operation of 6000 rpm engine speed.

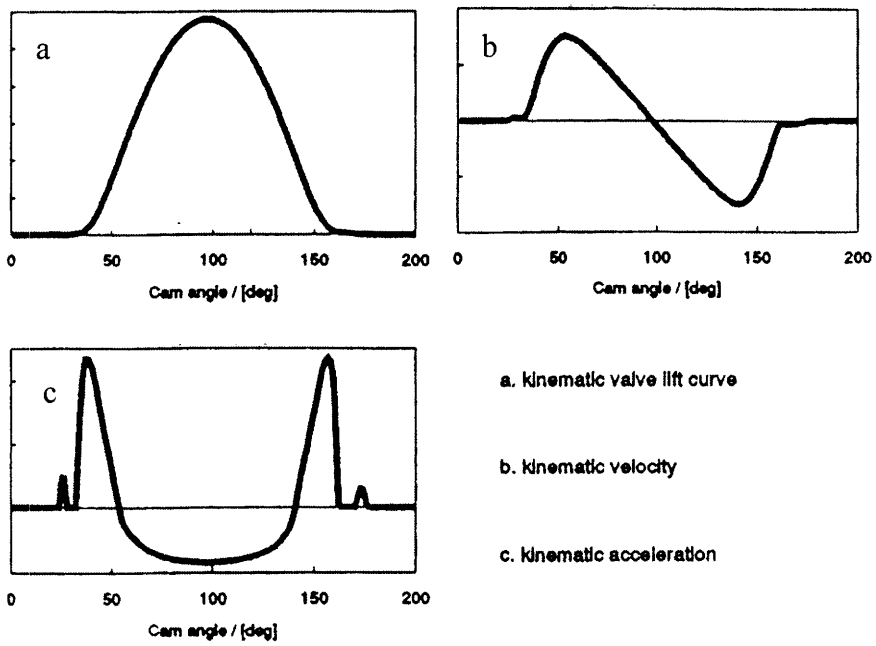

Fig. 2.5. Valve position, velocity, and acceleration profiles [7].

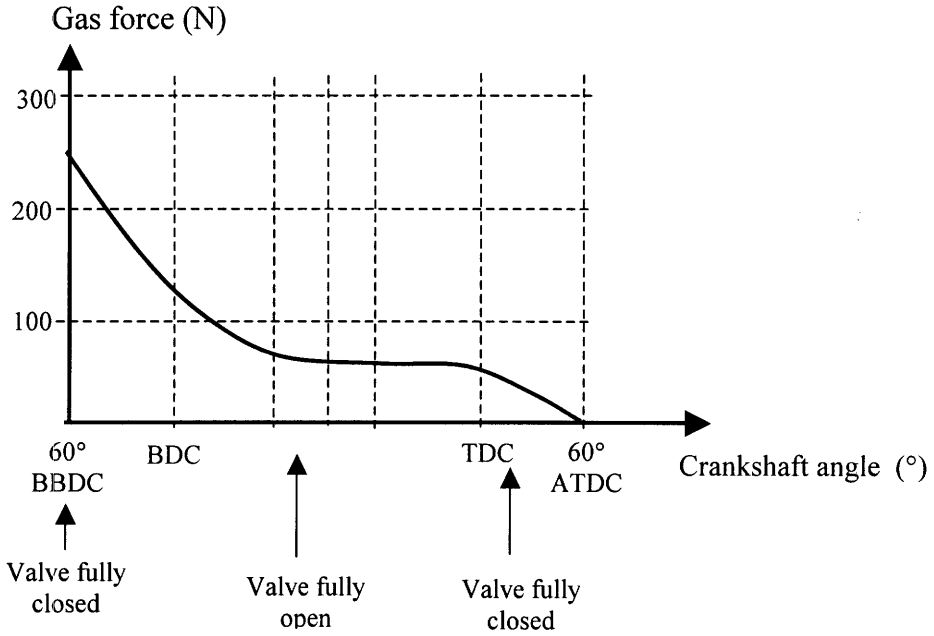

Fig. 2.6. Gas force acting on an exhaust valve at full engine speed and load [1].

After an exhaust valve opens, the cylinder pressure drops monotonically. Fig. 2.6 shows a gas force profile acting on an exhaust valve at maximum engine speed and full load for a 2.0 L engine [1]. The camshaft provides power to compensate for the work done against gas force during valve opening and receives power from the gas during the closing of the valve. The work per cycle to compensate for only the gas work is approximately 0.7 J. The net power per exhaust valve to compensate for the gas work at 6 krpm and wide open throttle is about 35 W. No corresponding requirement applies to intake valves, so an electromechanical valve drive for an exhaust valve needs more power than for an intake valve.

In a conventional spark ignition internal combustion engine, typical use of available energy is as follows [4]: At mid-open-throttle, from total available fuel energy of 100%, gross indicated work (the work delivered to the piston over the compression and expansion strokes only) is 36%, consisting of brake (or useful) work of 25% and friction work of 11%. The friction work of 11% consists of pumping work (the work transfer between the piston and the cylinder gasses during the intake and exhaust strokes) of 3.5% and mechanical friction loss of 7.5%. Friction loss in a valvetrain, including friction losses in camshafts, cam followers, and valve actuation systems, is about 0.75% of the available energy, about 10% of the mechanical loss, about 2% of the indicated work, and about 3% of the brake work. Since a typical brake mean effective pressure (the brake work per cycle divided by the cylinder volume displaced per cycle, *bmep*) is about 1000 kPa, valvetrain friction mep, 3% of the *bmep*, is about 30 kPa, which is almost uniform over engine speeds. Power, P (kW) is calculated as follows:

$$P = bmep \times N \times V_d / 2000, \tag{2.1}$$

where *bmep* represents the brake mean effective pressure (kPa), N engine speed (rev/s), V_d engine displacement (L), 2000 is the conversion factor to get P in kW. For a 2 L engine, typical brake power is about 100 kW at 6 krpm engine speed, and the power consumption due to valvetrain friction is 3 kW at 6 krpm, 0.75 kW at 1.5 krpm [4]. The valvetrain friction can be reduced by 50% by using roller cams [4]. It is desirable for the

power consumption of an electromechanical valve drive to be comparable to that of a conventional valvetrain with roller cams, i.e., 1.5 kW.

2.2 Benefits of Variable Valve Actuation Systems

In conventional valvetrains, valve opening/closing timing, speed, and lift are fixed geometrically relative to camshaft angle. Timing and lift are a compromise among fuel efficiency, performance, and emission. On the other hand, we can improve fuel efficiency by 15-20% or more over a driving cycle, torque by 5-13% or more, depending on engine speeds, and emissions significantly with a fully flexible variable valve actuation system that can adjust phase, duration and lift independently and flexibly [1], [2], [3]. The greater the flexibility which can be incorporated in the valvetrain, the greater the benefits that can be achieved. This section defines a variable valve actuation system and discusses its potential benefits.

A variable valve actuation (VVA) system is a device to control a valve's opening profile. The profile is characterized by duration, phase, lift, and opening/closing speed, as shown in Fig. 2.7. Duration is the length of the time or the range of angle during which a valve is open, as shown in Fig. 2.7 (a). Phase is a shift with respect to crankshaft angle of the valve's opening profile, as shown in Fig. 2.7 (b). In industry, control of the valve's phase is generally referred to as variable valve timing (VVT). In this document, we use the term to refer to variable phase, variable duration, or both. Lift defines the height of the valve profile as in Fig. 2.7 (c). Both valve timing and lift control are desired according to engine operating conditions. Detailed operating conditions will be explained with corresponding benefits later in this section. A valve's opening/closing speed is defined as the opening/closing speed of a valve profile, namely full lift divided by transition time when the valve opens and closes, respectively. Fig. 2.7 (d) shows profile shapes having different opening/closing speeds. In general, a faster opening and closing speed is useful in order to control gas exchanges more precisely. In particular, a faster opening/closing speed is desired at high engine speeds to achieve better volumetric efficiency and higher torque [2].

For intake valves at high engine speeds, sufficient lift is desired in order to achieve cylinder filling and high power. On the other end, at low engine speeds, small lift is desired in order to increase air velocity as it passes through the valve, which leads to a faster burn rate, and improved idle quality [2]. Flexible lift control of the intake valve can be used as a throttling means or even as a means of deactivating valves/cylinders to improve fuel efficiency.

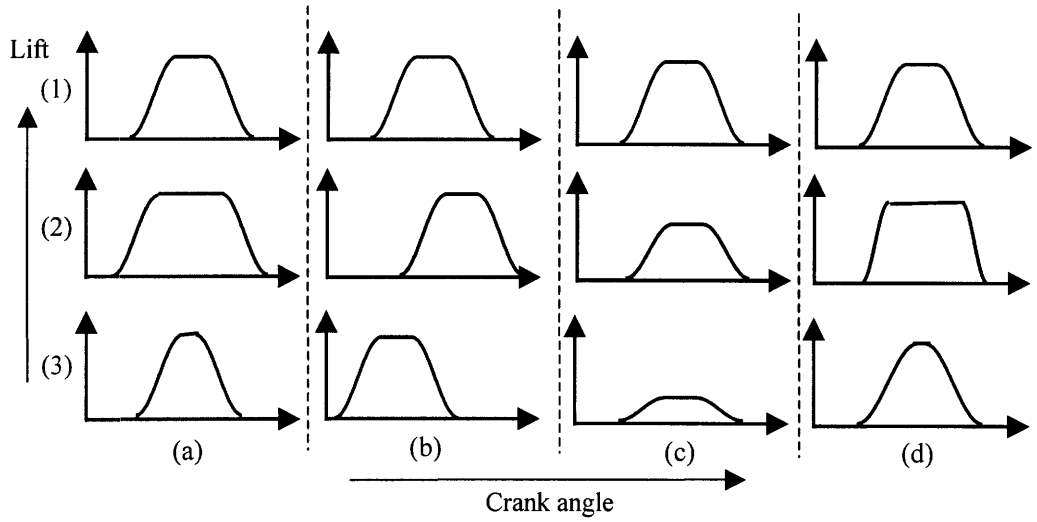

Fig. 2.7. Characteristics of a valve's opening profile.

(a1) baseline (a2) increased duration (a3) decreased duration
(b1) baseline (b2) retarded phase (b3) advanced phase
(c1) baseline (c2) reduced lift (c3) further reduced lift
(d1) baseline (d2) faster valve actuation (d3) slower valve actuation

Fig. 2.8 shows one proposal for optimal valve timing for an engine to achieve better performance, fuel efficiency, and emission [9]. Optimal valve timing depends on engine speeds and loads and other operating conditions. In Fig 2.8, an exhaust valve is opened at 70° BBDC (before bottom dead center) at high engine speeds to provide sufficient time for discharging of the burned gas, at 45° BBDC at low engine speeds, and is closed at 15° ATDC (after top dead center) at high engine speeds to reduce residual gas, and at 15° BTDC (before top dead center) at low engine speeds to reduce HC, Nox. Therefore, the recommended timing for an exhaust valve, at low engine speeds, has an opening duration of 210° crankshaft angle, but at high engine speed, an opening duration of 265° is

required. Note that the higher duration of high speed independent of load provides some relief in transition time requirement relative to static timing. In particular, 265° crankshaft angle at 6000 rpm engine speed requires 7.36 ms duration time, so a 3.68ms opening transition followed immediately by a 3.68 ms closing transient, should permit operation at this speed. On the other hand, at low speeds and load, an intake valve is desired to open at 25° BTDC and to close at 53° ABDC (after bottom dead center) in order to achieve high torque, and at 70° ABDC at a high engine speed in order to get a higher maximum power. Consequently, for the intake valve, opening durations of 258° crankshaft angles at low engine speed and high load and 275° crankshaft angles for all other cases are desired.

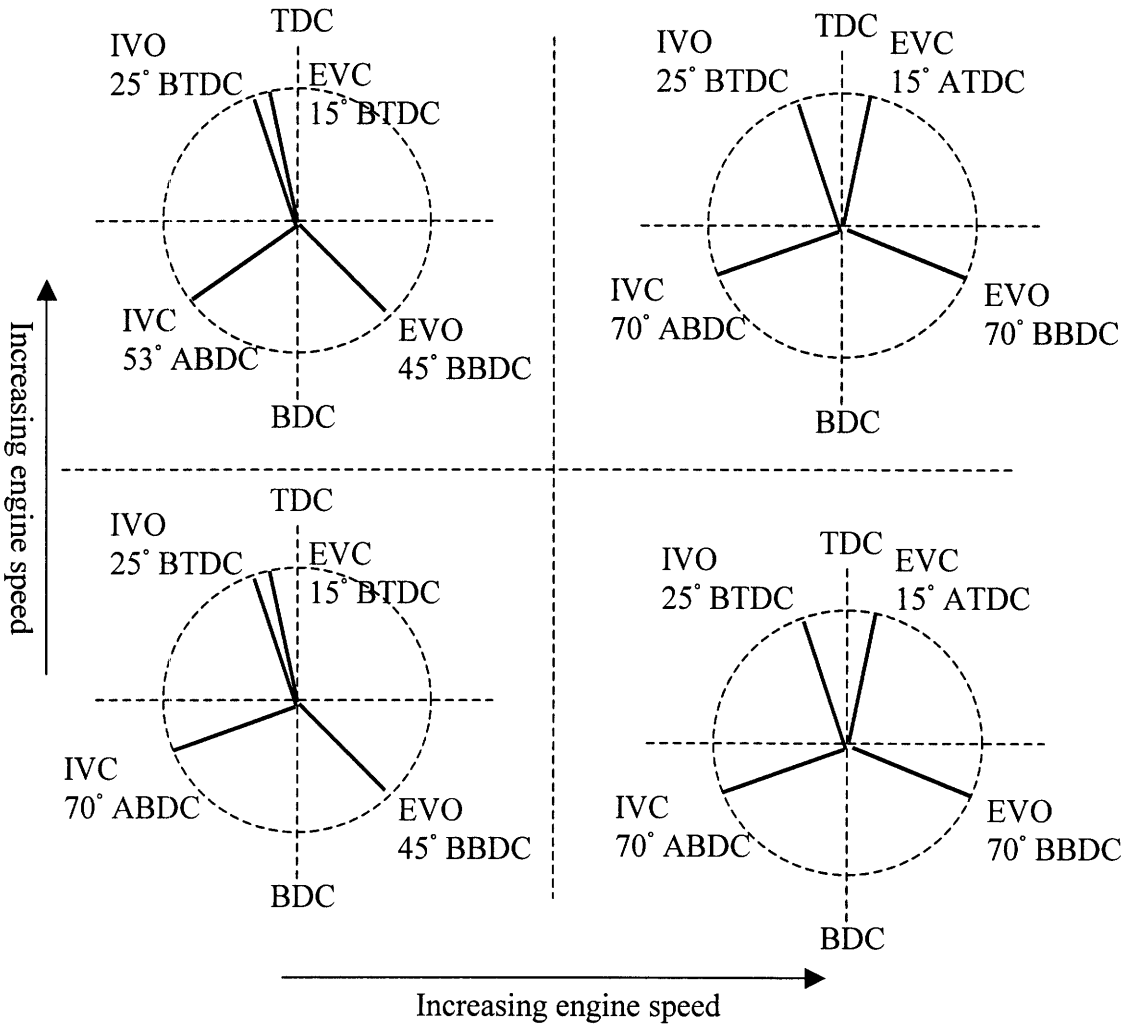

Fig. 2.8. A valve timing strategy [9].

If the valve open-duration and overlap can be optimized as a function of engine speed, pumping losses are minimized, and volumetric efficiency is improved [3]. It has been reported that a net fuel efficiency gain (gas mileage) of up to 15% over a typical driving cycle was achieved over a conventional valvetrain system [3]. Fuel efficiency can also be improved by variable engine displacement. The most efficient and most common form of variable engine displacement is to cut off all flow in and out of the inactive cylinders. With half the cylinders disabled, fuel efficiency is improved by 25% at low speed cruise and 40% at idle speed [2], [3]. Unequal lifts of paired valves can provide a variety of in-cylinder charge swirls and improve fuel efficiency by up to 3% in addition to better combustion stability, improved idle quality and lower emissions [2]. Also, reduced intake valve lift at low engine speeds increases inlet air velocity and reduces fuel consumption by 8-9% [2]. It is predicted that average fuel efficiency gain over a conventional valvetrain system of up to 20% or higher is possible, using combined variable valve timing, variable engine displacement, and intake valve throttling [3].

VVT can broaden the maximum torque vs. speed curve. Torque can be increased by 5-13% at low engine speeds and up to 23% at high engine speeds [10]. The torque increase results from the reduction of pumping losses and the increase of volumetric efficiency. Engine torque is largely determined by the amount of fuel delivered to and efficiently burned in each cylinder. The fuel charge can be changed rapidly from idle load to full load by an electronic fuel injection system in a conventional valvetrain. However, the air charge required to burn the fuel cannot be varied as rapidly as the fuel charge. Intake valve timing control does not need the throttle plate, and there is no delay in filling the intake manifold. Therefore, the intake valve timing control can change the air charge rapidly to match the fast response capability of the electronic fuel injection system. In principle, an engine employing the intake valve throttling can run at idle in one cycle and switch to full load in the very next cycle, while maintaining a proper air-to-fuel ratio. This improves the transient response of an engine [2].

VVA systems can reduce emissions by controlling the fraction of residual gases retained in a cylinder. An increase of the residual fraction reduces combustion temperature, and thereby directly reduces NOx emissions. A NOx reduction of 91% at a residual fraction

of 29% has been reported [3]. An increase of the residual fraction also reduces hydrocarbons (HC) emissions if the residual is a final portion of the gases that would otherwise leave the cylinder, which has the highest unburned HC concentration. However, the reduction of combustion temperature and mixture dilution tend to offset this effect, and HC emissions start increasing if the residual fraction is too large. HC emissions almost always increase as the residual fraction increases if the retained gases are not the last portion of the gases that would otherwise leave the cylinder. An effective way to decrease HC emissions even with the increased residual fraction is to advance exhaust valve closing, and to assure that the retained portion is the last portion leaving the cylinder [3]. The fuel efficiency improvement of a VVA system reduces emissions directly by reducing the consumed fuel and by burning the fuel more completely. Variable engine displacement affects emissions as well. Changing the number of cylinders from 8 to 4 reduces HC by 40% and CO by 47% at idle, and HC by 12.5% and CO by 45% at road load [3]. Adjusting the exhaust valve's closing timing and the intake valve's corresponding opening timing, that is, controlling valve overlap, can minimize residual gas quantity and contribute to better idle stability [2].

VVA systems can improve engine braking by increasing pumping losses when braking is desired [3]. To perform a dynamic braking function, exhaust valves and fuel injectors may be deactivated while intake valves are open during each piston down-stroke [2]. Instead of being dumped into the atmosphere, the compressed air can be pumped into a reservoir and then used for engine supercharging when the vehicle is accelerated. This provides a regenerative braking function, and further improves fuel efficiency.

There are other potential benefits of fully flexible variable valve actuation systems. An EMVD could eliminate the heavy and complicated mechanical components such as camshafts, timing chains, etc., which take up a lot of space on the top of a conventional cylinder head [11]. As a result, the height and weight for the EMVD could be lower than those for the case of cam-driven conventional valvetrains [11]. Also, all valves can be opened at the beginning of engine start-up, relieving compression and greatly reducing the crank torque needed [2], so that a smaller battery and starter motor could be used [11]. In fact, the peak power of the starter motor might be close to that of the alternator,

so that a combined starter/alternator might become feasible [11]. When combined with direct fuel injection, an EMVD may be able to start an engine statically. If the static starting should prove feasible, the battery could be designed for energy storage only, not for cranking power, and its size and weight could be reduced [11].

3 Motivation

Owing to the benefits of VVA systems mentioned in the previous chapter, various VVA designs have been introduced into some production vehicles. In this chapter, some of these VVA systems are described. In addition, the operating principle of an EMVD having two normal-force actuators, which is one of the most advanced types of EMVD, is described. Technical issues and/or problems of this EMVD are discussed and provide the motivation for the proposal of a new EMVD in this thesis.

3.1 Previous VVA Designs

There are many different types of VVAs. Benefits of each VVA depend on its design and functions. References [12] and [13] classify VVAs and briefly evaluate those functions and benefits. Among the VVAs, the variable cam phasing (VCP) and cam profile switching (CPS) types are the most popular owing to their simplicity and significant benefits. These types will be briefly explained. After that, some existing EMVDs are described including the normal-force actuator based EMVD.

A VCP type VVA system can shift a valve position profile with respect to time, as shown in Fig. 2.7 (b). The intake and exhaust camshafts rotate with relative and/or absolute shifts, which are controlled by the actuation system. VCP VVAs control only cam phasing, not duration or lift. Several car manufacturers have employed this approach in production already [14], [15], [16].

Another popular system is the CPS type VVA, which switches among sets of pre-determined cam profiles. The cam profiles can have discrete steps or be continuously variable. Fig. 3.1 shows a two-step CPS and a continuously variable CPS, respectively. Honda's early VTEC engines use a two-step CPS VVA [17], and Fiat engines use a

continuously variable CPS VVA [18]. A CPS VVA provides not only duration and phase control functions but also a lift control function. However, these functions are not independent, and flexibility is limited. Since lift control is not necessary for the exhaust camshaft, except for the purpose of a variable engine displacement function, a CPS approach is usually applied to the intake camshaft only. A two-step CPS is simple and practical. A continuously variable CPS VVA gives more flexible valve profiles, which even enables intake valve throttling.

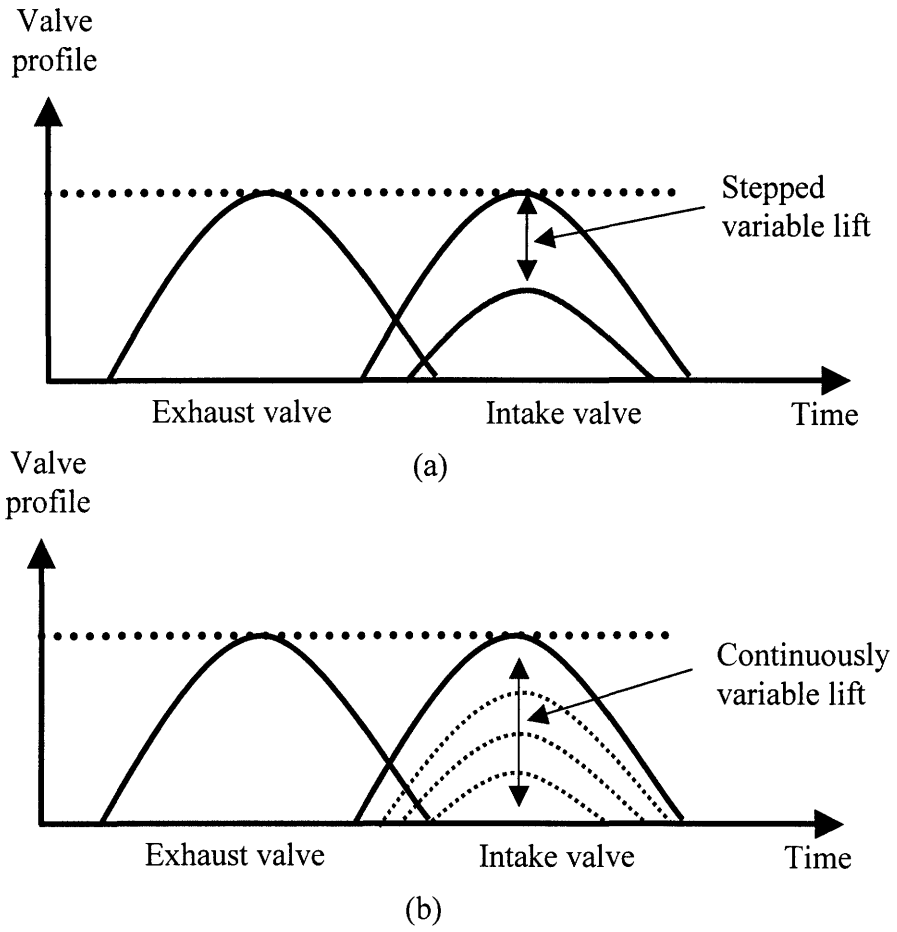

Fig. 3.1. A valve profile of a cam profile switching (CPS) type VVA system: (a) two step type and (b) continuously variable type.

A combined VCP and CPS VVA is the most advanced design in production. BMW's mechanical Valvetronic^{TM} VVA system uses a continuously variable CPS for the intake valve in addition to VCP VVAs for the intake and exhaust camshafts [19]. This design

offers independent phase control for the intake and exhaust camshafts and combined lift and duration control for the intake camshaft. Lift and duration controls are interdependent. Variable engine displacement is not available with this mechanism, and independent control of each valve is not possible.

One of the most advanced VVAs is the EMVD. Electropneumatic, electrohydraulic, and electromagnetic actuators have been considered as candidates for an EMVD actuation system. An electropneumatic actuator inherently has a relatively large compliance and a smaller dynamic bandwidth compared to other actuators [20]. An electrohydaulic actuator is complex due to the employment of an hydraulic system [2]. An EMVD employing two normal-force actuators (electromagnets) and one or more springs has been considered a viable candidate for future VVA systems owing to its simple structure and design [21], [22]. All of the EMVDs mentioned above use springs as a regenerative means to save power. Details of the two normal-force actuator based EMVD designs will be discussed in the next section.

Another interesting design is GM's rotary motor type EMVD [8], which uses inertia instead of springs as the regenerative device. The design needs power to provide VVA functions in addition to power to compensate for external forces and losses, and the flexibility of this design is limited in practice. For example, at high engine speeds, it is very hard to change valve profiles from base profiles for duration and/or lift control due to power limitations [8].

3.2 Normal-Force Actuator Based EMVD Design

The most viable EMVD candidate demonstrated to date is the normal-force actuator based electromechanical valve drive (NFEMVD) having two normal-force (electromagnet) actuators and one or more springs [21]-[30]. This design can offer both fully flexible duration and phase control, and limited lift control. However, it is difficult to provide fully flexible lift control in practice, but easy to position a valve at the two extreme positions (fully open and closed). In other words, valve/cylinder deactivation is

practical. This design is expected to become a more viable candidate for future VVA systems owing to the advent of 42 V automotive electrical systems [11], [19], [25], [28]. This section explains the operation of this design.

Several companies have developed prototype NFEMVDs. These include FEV [21], [22], [24], BMW [19], [25], GM [23], Renault [26], [27], Siemens [28], [29], and Aura [30]. Fig. 3.2 shows a schematic view of an NFEMV. In exploring fully flexible VVAs, people have frequently used the NFEMVD as a basis for contrast and comparison.

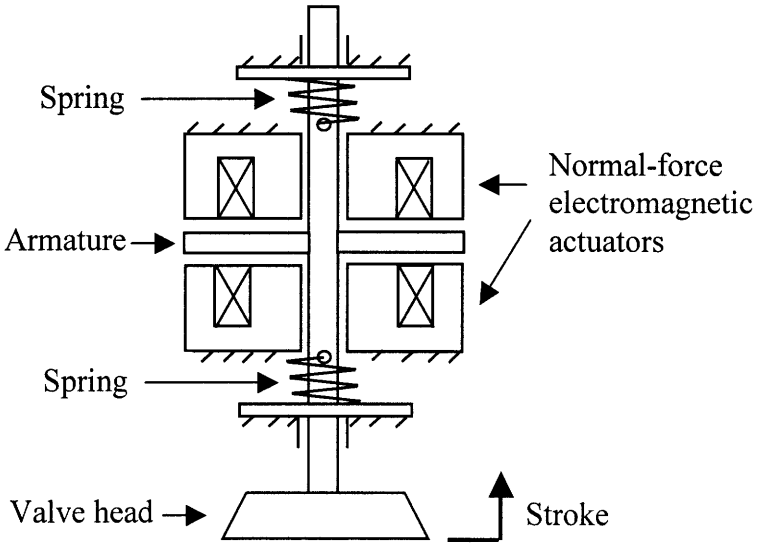

Fig. 3.2. Schematic view of a normal-force electromechanical valve drive (NFEMVD, one of the previously proposed EMVDs).

Basically, all of the reported NFEMVDs have the same fundamental operating principle, illustrated in Fig. 3.2. This basic design consists of a valve, one or more springs, and two electromechanical actuators. In this EMVD, normal-force electromagnetic actuators are used. These actuators have the following properties: the force is uni-directional in the direction of decreasing magnetic gap. In the absence of saturation, the force is proportional to the square of the actuator current, and is a decreasing function of gap (approximately 1/gap). The zero-force position for the spring (or system of springs) is the midpoint of the valve stroke. Fig. 3.3 shows the spring and electromagnet forces with respect to stroke at constant currents.

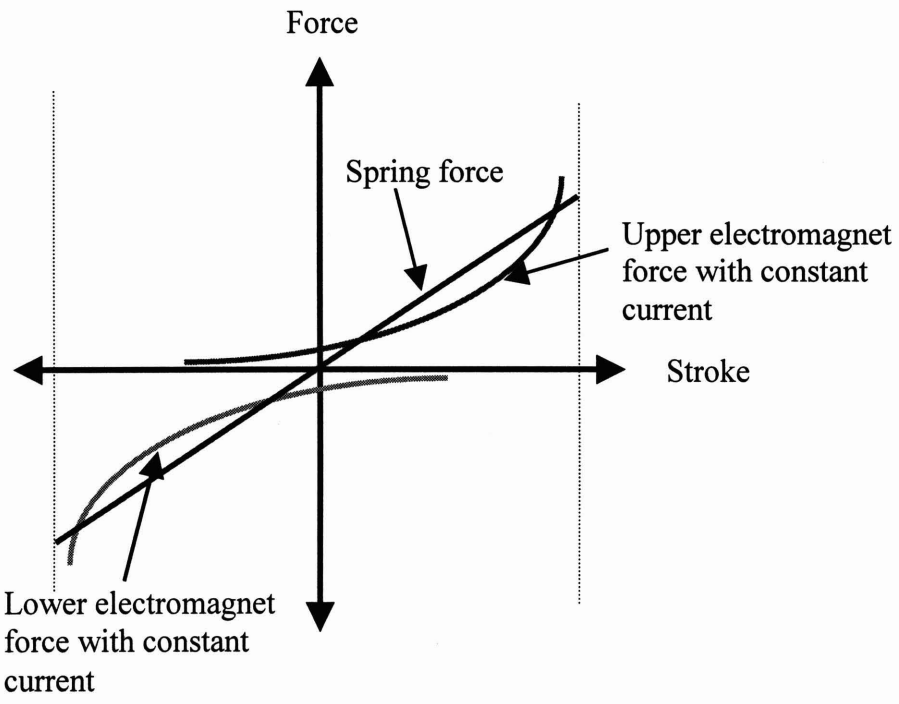

Fig. 3.3. Two electromagnet forces and spring force with respect to stroke.

The NFEMVD operates in three modes: initial, holding, and transition. The initial mode moves the valve from the middle of the stroke to the end of the stroke at start up. A way to traverse this mode with little force is to excite the system at its natural frequency until the amplitude of the valve displacement reaches the fully open or closed position. As soon as the valve is within a pre-determined distance from the end of the stroke, feedback control is employed to move the valve to the end and complete the initial mode. With minimal holding current, the valve is then held at its extreme positions. This is the holding mode.

The transition mode moves the valve from one end of the stroke to the other. This mode can be easily understood. Suppose we hold the valve at a non-equilibrium position at one end of the stroke by using, for example, the upper normal-force actuator in Fig. 3.2. Now let the valve be instantly released. The valve is accelerated by the springs. Neglecting friction, gravity and gas force, it flies freely beyond the equilibrium position until it reaches the opposite end of the stroke. The valve comes naturally to a stop at the lower

end of the stroke. The lower actuator is then turned on, holding the valve in this position and completing the transition. The process is depicted in Fig. 3.4.

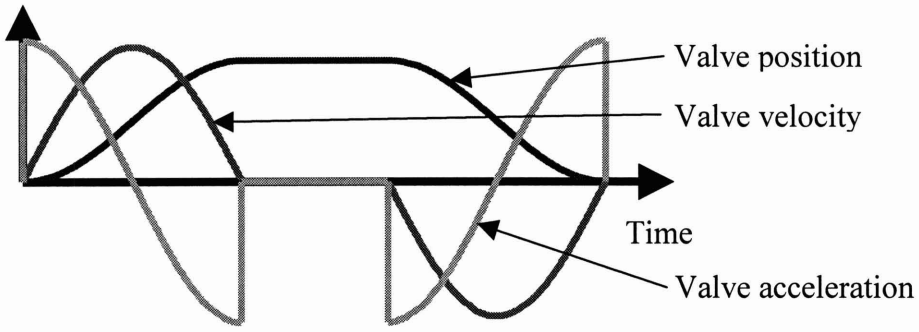

Fig. 3.4. Free flight dynamics of an idealized bi-positional electromechanical valve drive (EMVD).

Note that in the idealized action described above, the actuators do no work because they apply force only when the valve has zero velocity. From a thermodynamic point of view, the power consumed in the EMVD is limited to the mechanical and electrical loss in the system and the power to compensate for external disturbances such as gas force acting on the valves.

The valve system spends virtually all of its time in either the fully open or fully closed position. The transition between the two positions is swift and occurs in large measure independent of the electromechanical actuators. In this sense, we would like to call this design a bi-positional EMVD.

In this mechanism, the spring plays an important role. The idealized operation described above requires huge inertial power (inertial force times velocity), on the order of 2 or 3 kW per valve. The springs supply this inertial power to accelerate the valve during the first half of the stroke and absorb the inertial power during deceleration. The power absorbed during the second half of the stroke is not dissipated, but stored in the springs for use in the next cycle. If the springs were not used, the actuator would need to supply this inertial power. Even at a relatively optimistic 80% efficiency, the losses would be troubling. Instead, the springs automatically regenerate the inertial energy at high

efficiency. It is this automatic regeneration which makes the NFEMVD such a strong candidate for an EMVD.

The spring stiffness and moving mass determine the natural frequency of the EMVD. Half of the inverse of the natural frequency should be the transition time, which is the time for the moving mass to travel from one end of the stroke to the other, more specifically, from 2% of full stroke to 98% of full stroke, or vice versa. The transition time should be no longer than approximately 3-4 ms, half of the valve opening time in a conventional valvetrain at maximum engine speed (6 krpm). Once the EMVD meets this requirement, it can easily offer fully flexible phase and duration controls by combining holding and transition modes in time. In addition, it provides faster valve opening/closing speed at low or mid engine speed and enables more precise control of gas exchanges. Moreover, a valve/cylinder deactivation function is available to enable variable displacement. A limited lift control function can also be implemented. Since lift control is limited, intake valve throttling could be performed with duration control. However, this might deteriorate combustion stability at low engine speeds because the speed of the air-fuel mixture becomes slow compared to that of a conventional valvetrain. Valve deactivation could improve combustion stability at low engine speeds since this can increase the speed of the air-fuel mixture.

3.3 Technical Problems of the Normal-Force Actuator Based EMVD Designs

There are many technical challenges in previous EMVD designs. Two of particular importance are achieving soft landing and reducing power consumption. This section explains these challenges in detail.

One desirable characteristic of EMVD systems is that the valves achieve soft landing; that is, landing at the hold point with small velocity and acceleration. In previous EMVD designs, as that in Fig. 3.2, there are two technical challenges to achieving soft landing of a valve. First, the acceleration curve in the idealized EMVD design shown in Fig. 3.4 has

infinite jerk (time rate of change of acceleration) not only at the end of the stroke, but at the beginning of the stroke as well. This contrasts with the acceleration curve of a conventional valvetrain, as shown in Fig. 3.5, which is smooth and has finite jerk [6]. Infinite jerk requires a step in holding force. If the actuators provide a step in holding force, the reaction force where the actuator mounts to the engine experiences a step load. This impulsive excitation is a source of acoustic noise. For the operation of a system at high speed, it is desirable to avoid discontinuous acceleration, i.e., high values of jerk [31].

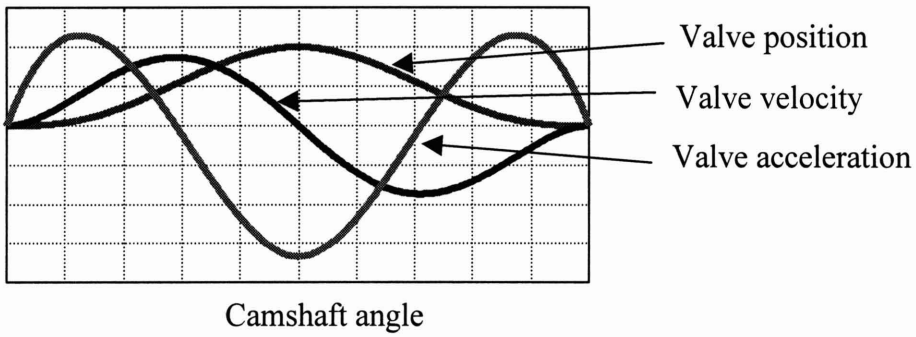

Fig. 3.5. Valve profile of a conventional valvetrain.

For example, the step of force at the beginning of a valve transition can be softened by turning the actuator off slowly. If this is done, some of the spring work that in the ideal case goes to accelerating the valve is instead converted to electrical energy. The spring work removed at the start of the event adds to the actuator work which must be done on the valve before the end of the stroke. An active control like this can reduce the large jerk and generate smooth valve kinematics in order to achieve soft landing. However, the electrical energy transfer to/from the power source results in significant power loss in practice. In addition, any work done to overcome mechanical losses or gas forces must be restored to the valve and spring system before the end of the stroke. If the losses are not made up, the valve will not arrive at its destination, but will stop short and begin to move away from the destination.

The stiffness of the springs in the NFEMVD should be large enough to achieve a fast transition time, resulting in a large spring force at the end of the stroke. Consequently, a large holding force is required. Normal-force actuators as in Fig. 3.2 are well suited to the holding function since in the closed position the actuators produce large force with small current.

A normal-force actuator is uni-directional. Consequently, for bi-directional motion, we need two normal-force actuators, two control channels, two actuator drives, etc., which increases system cost and complexity. Also, control action over a stroke is limited. Only the landing-end actuator can do work during the transition. Because this actuator is relatively ineffective at the beginning of the stroke, most of the work that it must do will be done in the later portion of the transition. This limited control action makes it hard to achieve a soft landing. Moreover, the force constant of the normal-force actuator is not uniform over a stroke. This non-uniformity is not good from a servomechanical point of view. This is the second reason why it is hard to achieve soft landing of a valve with the NFEMVD.

If the actuator does exactly the required work, the valve arrives at its resting place with zero velocity. However, if the actuator does any more than the exactly required work, the excess work will cause the valve to have non-zero velocity when it arrives at its resting place, resulting in an impact, which can result in acoustic noise and decreased life of colliding parts. This, then, is the fundamental control challenge of the EMVD: the landing-end actuator needs to provide exactly enough work and no more, in a time short compared to the transition time, while the valve is in the vicinity of its resting position. Since the amount of energy required cannot be known precisely in advance, this represents a substantial feedback control problem. Note that if the landing-end actuator does too much work, and the error is detected, it is formally possible to correct that error by use of the initiating-end actuator. But this choice, although formally possible, is unattractive, because the actuator requires a very large current to make a meaningful force. Because the actuator is highly inductive, very large reactive power is required to produce a large current. Overshoot in position, velocity, and acceleration is unacceptable in practice.

The NFEMVD design has great features: use of a regenerative device like a spring; holding with low holding current. But this design has technical challenges to achieve soft landing and reduce power consumption, which motivates the proposal for a new EMVD [32]-[35], which will be described in the following chapter.

4 An Electromechanical Valve Drive Incorporating a Nonlinear Mechanical Transformer

In this chapter, an EMVD design is proposed which addresses the technical challenges of the NFEMVD presented in Chapter 3. The benefits of the novel design are presented in a conceptual overview, and its performance predicted by mathematical modeling and simulation.

4.1 Conceptual Design of the Proposed EMVD

A practical valve-drive design must incorporate power-saving and energy-regeneration features to reduce actuator force requirements. An EMVD design should use springs as the regenerative device, as in the NFEMVD, to achieve a fast bi-positional stroke with minimal power input. A candidate design should furthermore move valves smoothly, with low jerk, to reduce undesirable impacts and losses. A mechanical design in which smooth actuation follows natural dynamic trajectories, and does not require large actuator forces to enforce control, is a particularly desirable means of reducing peak actuator power.

To understand the benefits of reduced actuator force, first consider the ideal NFEMVD dynamics in detail. The free-flight kinematics of the valve are described by

$$\text{Inertial force} + \text{Spring force} = 0. \tag{4.1}$$

The inertia represents valve mass plus actuator inertia. If the inertial and spring forces are linear, the force balance becomes

$$m\frac{d^2x}{dt^2} + kx = 0, \tag{4.2}$$

where m and k are inertia and stiffness, respectively. The spring stiffness must be large enough to meet a minimum transition time requirement, and the holding force must be large enough to compensate for the large spring force at each end of the stroke. Abrupt release of a valve from an end of the stroke results in an abrupt change of acceleration – a large jerk – due to the large end-stroke spring force in an ideal EMVD. The NFEMVD counteracts this jerk directly with actuator force, at the expense of large peak actuator power.

A valve-drive design with small spring force and/or large inertial force at both ends of the stroke, as shown in Figs. 4.1 (a) and (b), smoothes valve kinematics and reduces jerk without large driving forces. If the reference input (i.e., the commanded valve position vs. time) follows the natural valve trajectory, then the actuator supplies only power to correct for losses and gas force during the valve stroke, even when the valve dynamics are nonlinear.

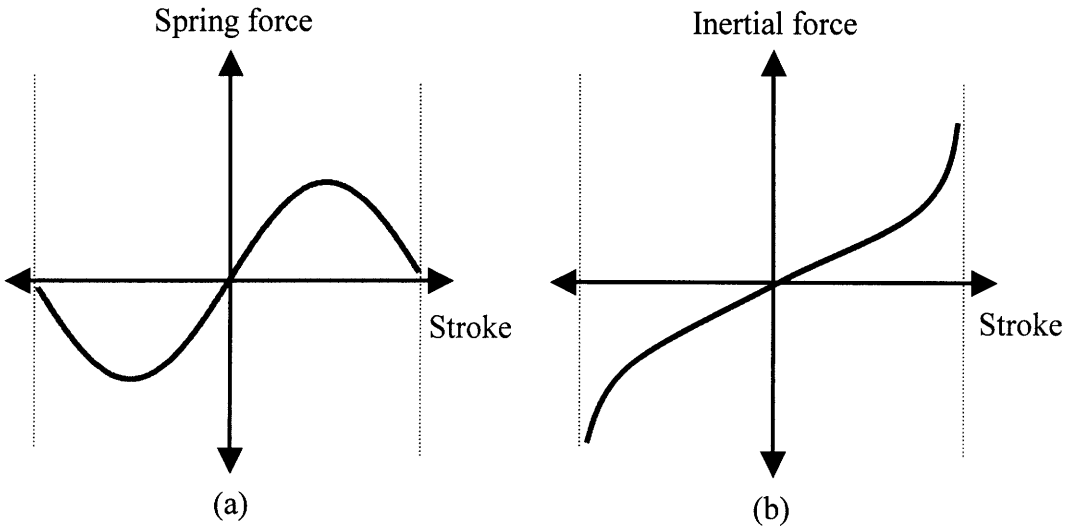

Fig. 4.1. Desired characteristics of (a) spring force and (b) inertial force.

The nonlinear characteristics of Fig. 4.1 can be realized either directly, using a nonlinear spring and/or inertia, or indirectly, using a nonlinear transformer (NTF) to shape the force-position relationships of the linear mechanical elements.

In the EMVD application, direct implementation of nonlinear springs or inertias seems impractical from a case-by-case consideration of reported designs. The nonlinear disc spring (e.g., Belleville washers [36]) of Fig. 4.2 demonstrates typical limitations. Fig. 4.2 (a) shows top and side views of the spring, and Fig. 4.2 (b) shows its force vs. stroke relationship. Stacks of disc springs in series or parallel can realize the force-stroke characteristic of Fig. 4.1 (a), but since a disc spring stack has a uni-directional force-stroke relationship, two sets of stacks are required for the complete bi-directional characteristic. The resulting structure would have undesirable impacts and losses during operation, and is not suitable for an EMVD application.

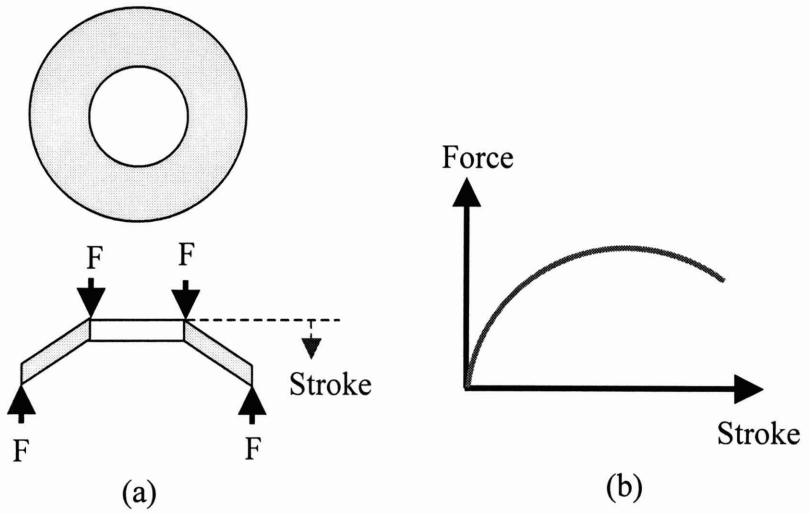

Fig. 4.2. A nonlinear spring. (a) Top and side views. (b) Force vs. stroke characteristic.

An effective nonlinear spring or inertia may be implemented quite easily with an NTF. Suppose two energy domains (domain 1 and domain 2 in Fig. 4.3) consist of a linear spring and/or linear inertia, and are related by a nonlinear transformation. If the equation of motion is expressed with state variables of domain 1 only, all of the components in domain 2 can be reflected to domain 1. Consider a mass in domain 1 (m_1) to be reflected to domain 2 (m_2). If the transformer is ideal and has a constant modulus, r, the transformer satisfies the following equations.

$$f_1 = \mathrm{r} \cdot f_2, \tag{4.3}$$

$$v_1 = \frac{v_2}{\mathrm{r}}, \tag{4.4}$$

where $f_1 = \mathrm{m}_1 \frac{\mathrm{d}v_1}{\mathrm{d}t}$, $f_2 = \mathrm{m}_2 \frac{\mathrm{d}v_2}{\mathrm{d}t}$. The mass reflected from domain 1 to domain 2 is

$$\mathrm{m}_2 = \frac{\mathrm{m}_1}{\mathrm{r}^2}. \tag{4.5}$$

Similarly, the spring stiffness reflected from domain 1 (k_1) to domain 2 (k_2) is

$$\mathrm{k}_2 = \frac{\mathrm{k}_1}{\mathrm{r}^2}. \tag{4.6}$$

Since the transformer is linear, the reflected spring and/or inertia are also linear. If the modulus is nonlinear, the reflected elements have nonlinear characteristics, and can assume various reflected values as a function of stroke, e.g., as shown in Figs. 4.1 (a) and (b).

Before deriving the equations of motion for EMVD designs employing an NTF, consider first, in a general fashion, design cases which have small spring force and/or large inertia at both ends of the valve stroke. Fig. 4.4 shows four possible EMVD design cases having two dominant inertias (valve mass and actuator inertia), springs, and an appropriate NTF.

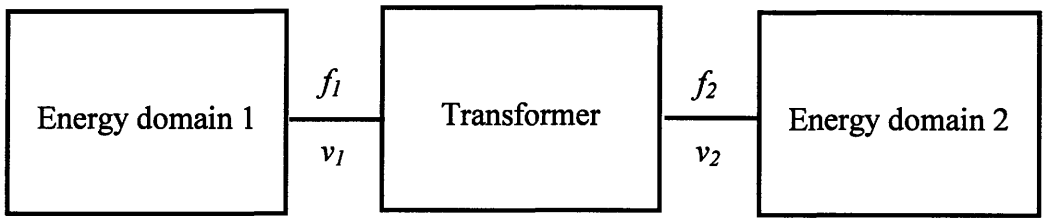

Fig. 4.3. Connection of two energy domains using a transformer.

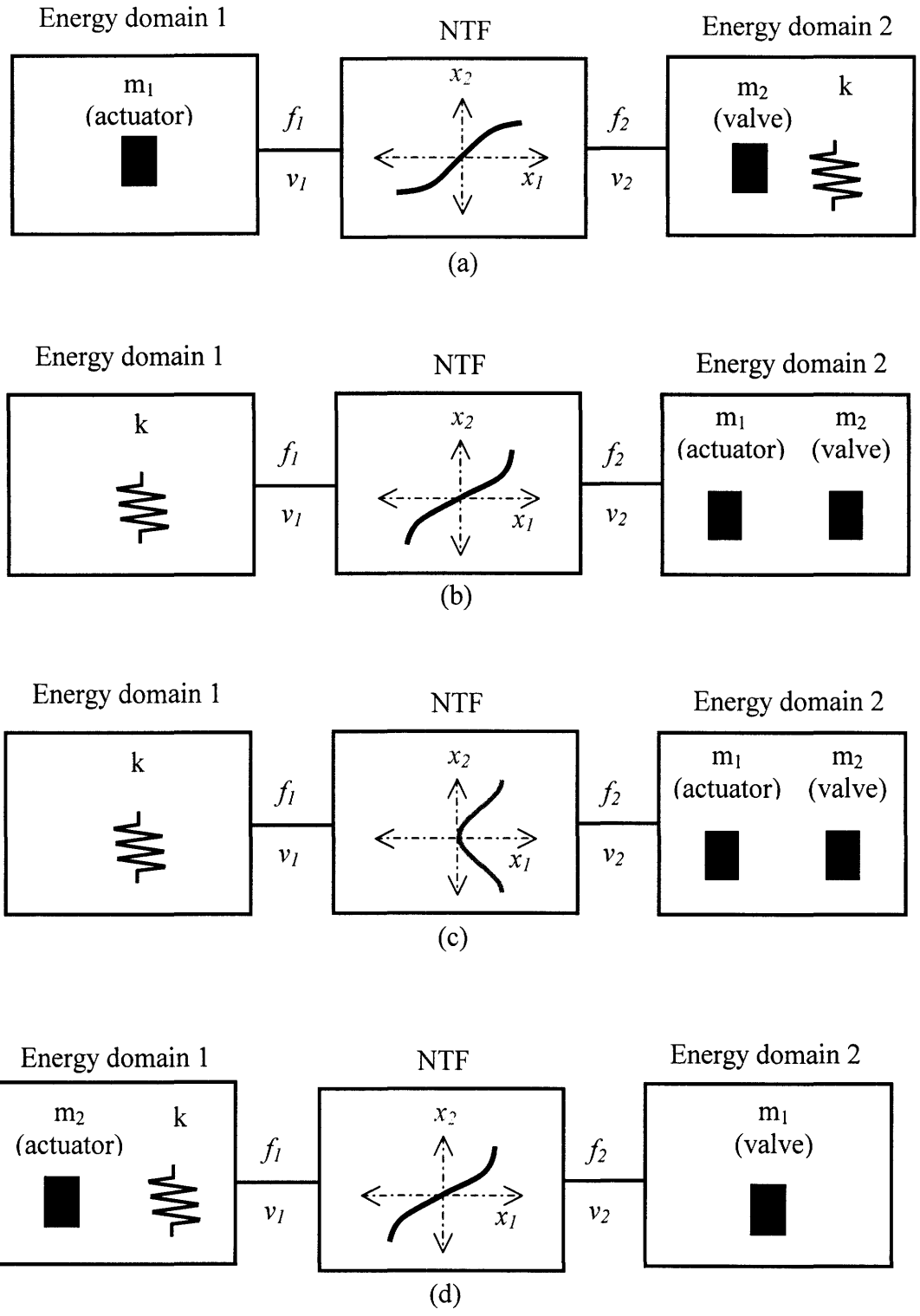

Fig. 4.4. Four possible connection designs using a nonlinear mechanical transformer (NTF) to achieve smooth valve kinematics.

Assume that all inertias and springs are constant in their own domains. Fig. 4.4 (a) shows the first case, in which the actuator inertia is in domain 1, and the valve mass and springs are in domain 2. To represent the equation of motion using the state variables in domain 2, reflect the actuator inertia in domain 1 to domain 2. The NTF having a small transformer modulus (gear ratio) at both ends of the stroke makes the effective inertia – consisting of the original inertia plus the reflected inertia –large at both ends of the stroke, resulting in smooth free-flight kinematics. Note that the transformer modulus should be large in the middle of the stroke to reduce transition time. The transformer is nonlinear, and its modulus varies according to valve position as shown in Fig. 4.4 (a).

Fig. 4.4 (b) and (c) show the second design case, where springs are in domain 1, and valve mass and actuator inertia are in domain 2. In this case, the transformer has a large modulus at both ends of the stroke so that the spring force reflected to domain 2 is small.

Fig. 4.4 (d) shows the last design case. Actuator inertia and springs are in domain 1, and the valve is in domain 2. The transformer again has a large modulus at both ends of the stroke so that the reflected spring force from domain 1 to domain 2 remains small. Since a valve moves up and down in EMVD applications, domain 1 is translational. Domain 2 can be either translational or rotational, however, depending on the actuator type.

All of the design cases mentioned above have smooth valve kinematics without large driving force. Only those design cases with low holding current or force, however, are suitable for an EMVD application. The design cases of Fig. 4.4 (a), (b), and (c) require only a small holding force, and allow the use of a shear-force actuator instead of two normal-force actuators. A shear-force actuator provides bi-directional motion even with a single control channel, and is easier to control because its force or torque constant can be uniform, independent of valve displacement. Design (d) of Fig. 4.4, on the other hand, requires a large holding force since the springs and the actuator are in the same domain. A normal-force actuator can, indeed, provide large holding force with small current as in the NFEMVD design, but it requires two channels for bi-directional actuation. Design (d) has a large modulus at both ends of the stroke, amplifying the reflected kinematics of domain 1 in domain 2. A very high resolution displacement sensor is therefore required

in domain 1, which, with the drawbacks of a normal-force actuator, make design (d) impractical.

Designs (b) and (c) of Fig. 4.4, where both the valve and actuator are in the same domain, is a direct-acting EMVD in which, as in the NFEMVD, actuator kinematics affect valve kinematics directly. The direct-acting system suffers from two drawbacks. First, overshoot in the actuator dynamics causes the valve to hit the valve seat hard as in the NFEMVD, the prevention of which poses a severe servomechanical challenge. Second, gas force is at a maximum when the exhaust valve starts opening at full engine speed and load. This resistance determines the maximum torque or force required of the actuator and oversizes the actuator relative to other designs.

Design (a) of Fig. 4.4 is not direct-acting because the actuator is not in the same domain as the valve. Furthermore, the transformer modulus is small at both ends of the stroke, and the reflected position errors from the actuator domain to the valve domain are small in the valve domain. This mechanical arrangement permits the use of an inexpensive, low-resolution position sensor in the actuator domain. If the slope of the nonlinear transformer is almost flat at both ends of the stroke, as shown in Fig. 4.5 (a), the seating velocity (unless there is compliance between valve kinematics and actuator kinematics) and the holding force are almost zero. Moreover, the extended flat region of the nonlinear transformer of Fig. 4.5 (b) allows overshoot in actuator kinematics, improving the speed of system response. Maximum gas force occurs when an exhaust valve starts opening, but the maximum reflected gas force/torque – approximately in the middle of the stroke – determines the maximum actuator force/torque requirement. Peak actuator effort is substantially less for design (a) of Fig. 4.4, which is clearly the most suitable for EMVD applications.

There are two types of shear-force actuators: linear and rotary. Fig. 4.6 shows the EMVD design of Fig. 4.4 (a) based on a linear shear-force actuator. In this design, a slotted cam and roller act as an NTF. The linear motor shaft is rigidly connected to the cam, and the roller – connected to the valve – rolls over either the top or bottom surface of the cam slot. The cam is free to move horizontally, and the valve and roller shaft are free to move

vertically, as constrained by the slot. Fig. 4.7 shows the EMVD design of Fig. 4.4 (a) based on a rotary shear-force actuator, which is the proposed design here.

The benefits of this proposed EMVD over the NFEMVD can be summarized as follows:

- Smooth valve kinematics
- Low seating velocity
- Lower power consumption
- The use of a rotary shear-force actuator instead of two normal-force actuators
- Allowance of overshoot

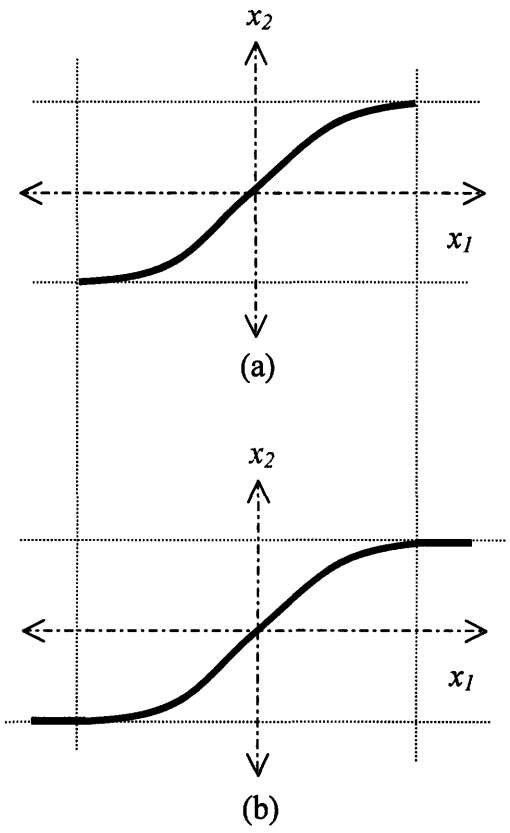

Fig. 4.5. Desired characteristics of a nonlinear mechanical transformer (NTF) (a) with almost flat slope at both ends of the stroke and (b) with an extended flat region in addition to (a).

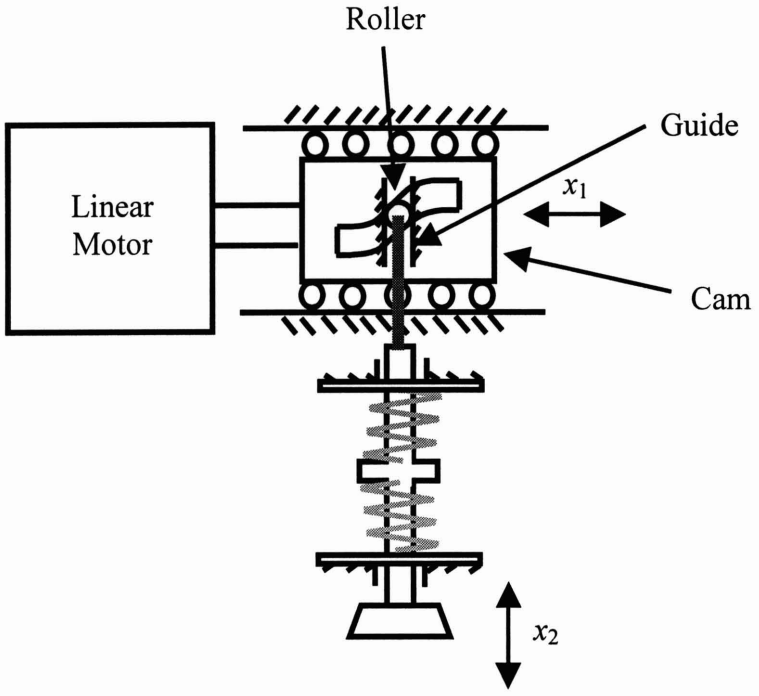

Fig. 4.6. A linear shear-force actuator based EMVD.

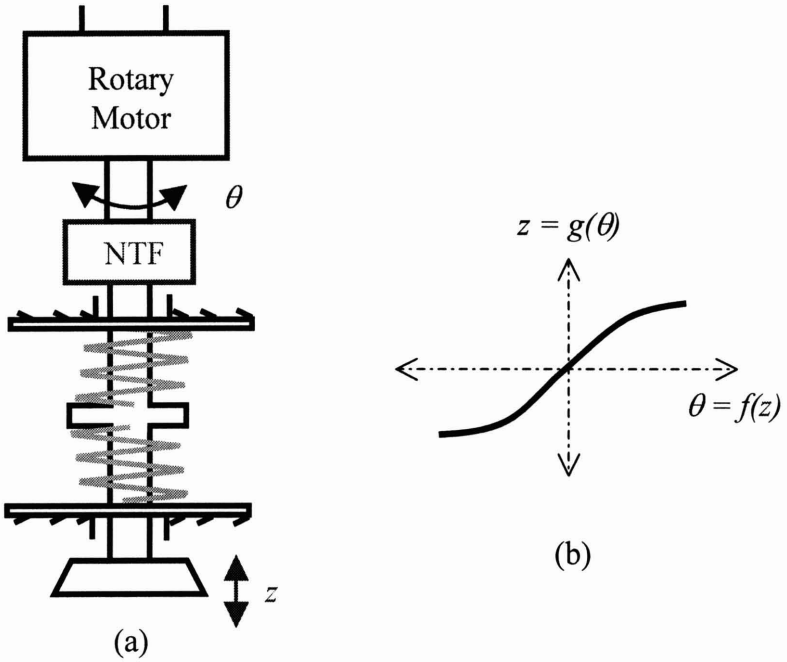

Fig. 4.7. (a) Conceptual design of a proposed electromechanical valve drive incorporating a rotary actuator and a nonlinear mechanical transformer (NTF); (b) A desired characteristic of the NTF.

Proposed EMVDs with different NTF structures are shown in Fig. 4.8, Fig. 4.9, and Fig. 4.10. Fig. 4.8 shows an EMVD incorporating a rotary cam with the desired nonlinear-transformer characteristic. The motor shaft is free to rotate about its axis but is fixed in all other directions. The rotary cam is connected to the motor axis and is free to rotate, and the rollers are free to rotate about their axes and roll over the surfaces of the rotary cam. The turret is connected to the roller shafts and the valve and is free to move up and down against a linear spring force. With this mechanical configuration, the nonlinear transformer characteristic can be designed with substantial flexibility.

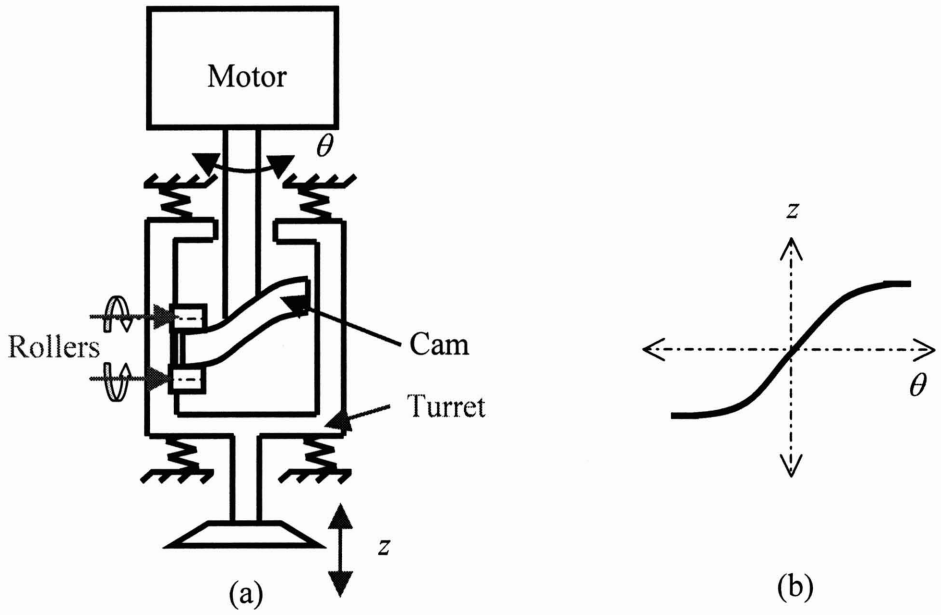

Fig. 4.8. (a) A proposed EMVD with a rotary cam as an NTF; (b) A desired nonlinear characteristic of the NTF.

Alternatively, a disc-cam and roller can be used as an NTF, as shown in Fig. 4.9. This simple design was proposed for the first time by Professor Kassakian. The motor shaft is rigidly connected to the disc-cam, which has a shaped slot. A roller is connected to the valve and rolls over either the top or bottom surface of the cam slot. The disc cam is free to rotate with the motor shaft, to which it is connected rigidly, and the valve and roller shaft are free to move vertically as constrained by the slot. This design is simple and compact, but additional power is required to compensate for the losses due to the slip between the roller surface and the disc-cam surface. There is always slip in mid-stroke

because the rotational direction of the roller reverses at this point in each cycle. However, this power loss is small relative to the power supplied to counteract gas force and other friction forces. Due to its structural simplicity, we use this NTF design for the first experimental apparatus. The conjugate disc-cam of Fig. 4.10 can reduce the slip loss because there is no reversal of the roller rotational direction in the middle of the stroke.

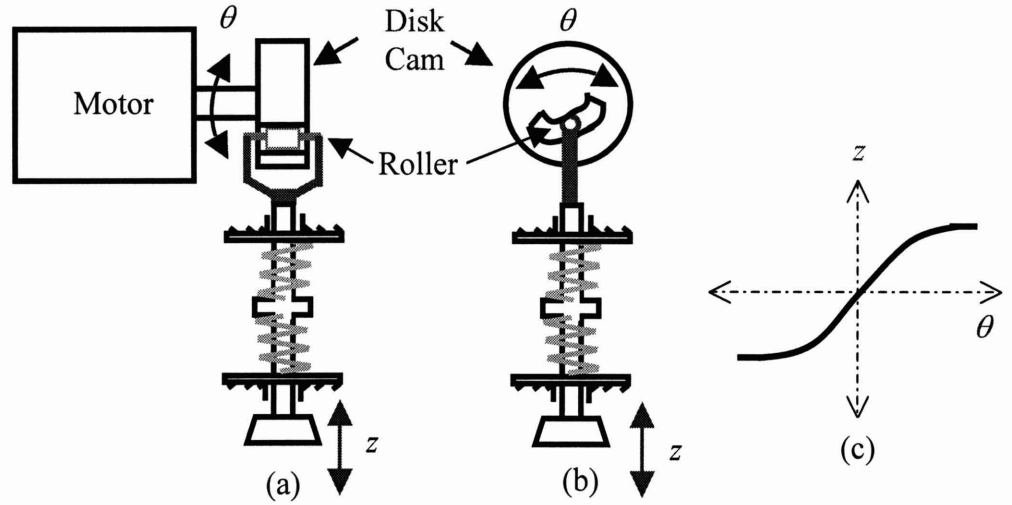

Fig. 4.9. (a) Front view of a proposed EMVD with a disk cam as an NTF; (b) Side view of the proposed EMVD; (c) A desired nonlinear characteristic of the NTF.

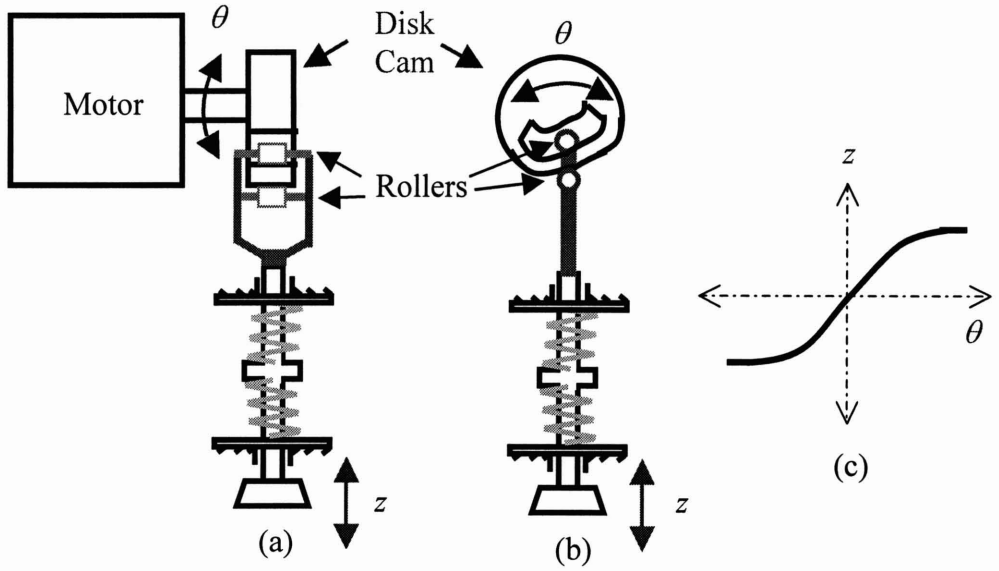

Fig. 4.10. (a) Front view of a proposed EMVD with a conjugate disk cam as an NTF; (b) Side view; (c) A desired nonlinear characteristic of the NTF.

4.2 Mathematical Modeling and Analysis of the Proposed EMVD

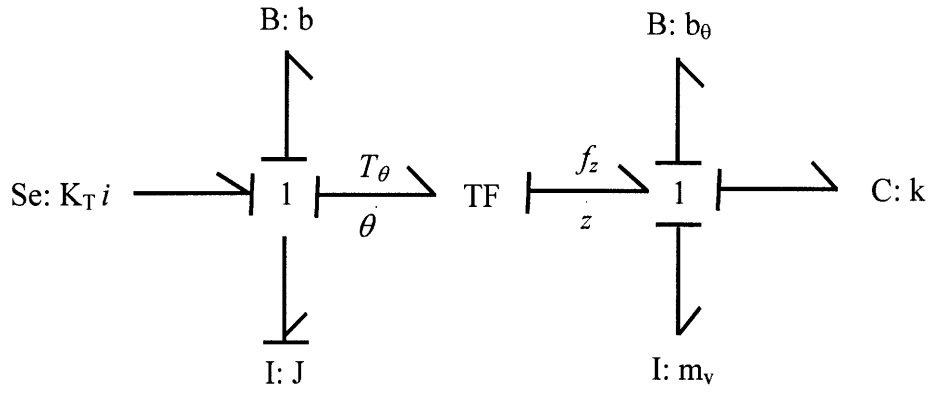

Fig. 4.11. A simplified bond graph model of the proposed EMVD.

Fig. 4.11 shows a bond graph model [37] of the proposed EMVD in Fig. 4.7. The simplified equations of motion for this system are:

$$J\frac{d^2\theta}{dt^2}+b\frac{d\theta}{dt}+T_\theta = K_T i, \tag{4.7}$$

$$F = m_v\frac{d^2 z}{dt^2}+ b_v\frac{dz}{dt}+ kz, \tag{4.8}$$

where i is motor current, J and m_v represent inertia present in the actuator side and in the valve side respectively, b and b_v represent viscous friction in each side, K_T and k are the torque constant of the rotary motor and the spring constant, respectively, T_θ and F represent the torque and force related by the nonlinear transformer modulus, and θ and z are rotational and vertical displacements. Equations (4.7) and (4.8) show the torque and force balance equations in the actuator side (θ domain) and the valve side (z domain), respectively. The variables θ and z have the following relation:

$$\theta = f(z),$$

$$\frac{d\theta}{dt} = \frac{df}{dz}\frac{dz}{dt},$$

$$\frac{d^2\theta}{dt^2} = \frac{d^2 f}{dz^2}\left(\frac{dz}{dt}\right)^2 + \frac{df}{dz}\frac{d^2 z}{dt^2}. \tag{4.9}$$

T_θ and F are related by:

$$F = T_\theta \frac{df}{dz}. \tag{4.10}$$

Equations (4.9) and (4.10) constitute a mathematical model of the NTF, which relates the rotational domain to the translational domain. After combining (4.7) and (4.8) with (4.9) and (4.10) and substituting (4.9) into the combined equation, we obtain the equation of motion in either the θ or z domain. The equations of motion in the z domain can be represented in state-equation form as follows:

$$\begin{aligned} \frac{dx_1}{dt} &= x_2, \\ \frac{dx_2}{dt} &= A(x_1, x_2) + B(x_1, x_2)i, \end{aligned} \tag{4.11}$$

where x_1 and x_2 represent valve position and velocity, respectively, and

$$A(x_1, x_2) = \frac{-1}{m_v + J\left(\frac{df}{dz}\right)^2}\left\{\left(b_v + b\left(\frac{df}{dz}\right)^2\right)x_2 + J\frac{d^2 f}{dz^2}\frac{df}{dz}x_2^{\,2} + kx_1\right\}, \tag{4.12}$$

$$B(x_1, x_2) = \frac{1}{m_v + J\left(\frac{df}{dz}\right)^2}\frac{df}{dz}K_T. \tag{4.13}$$

Since the mechanical transformer is nonlinear, linear relationships in one domain are nonlinear in the other.

Similarly, the equation of motion in the θ domain is as follows:

$$\begin{aligned} \frac{dy_1}{dt} &= y_2, \\ \frac{dy_2}{dt} &= A(y_1, y_2) + B(y_1, y_2)i, \end{aligned} \tag{4.14}$$

where

$$A(y_1, y_2) = \frac{-1}{J + m_v\left(\frac{dg}{d\theta}\right)^2}\left\{\left(b + b_v\left(\frac{dg}{d\theta}\right)^2\right)y_2 + m_v\frac{d^2g}{d\theta^2}\frac{dg}{d\theta}y_2^{\,2} + kg(\theta)\frac{dg}{d\theta}\right\}, \tag{4.15}$$

$$B(y_1, y_2) = \frac{1}{J + m_v\left(\frac{dg}{d\theta}\right)^2}K_T, \tag{4.16}$$

and y_1 and y_2 represent rotor position and velocity, respectively, and $z = g(\theta)$.

With the NTF, we can qualitatively design the desired relation between the rotational displacement of the motor and the translational displacement of the valve, change effective inertia and/or stiffness, and reduce holding and driving torques. Fig. 4.7 (b) shows a desired characteristic of the NTF, but a detailed specification of the NTF is reserved for Chapter 7.

The use of the NTF in Fig. 4.7 (b) can increase the free-flight travel time from one end of the stroke to the other because the acceleration at both ends of the stroke is very low. The problem is solved by creating impulses of actuator force at both ends of the stroke. Simulation results for the ideal free flight dynamics of the proposed EMVD both with

and without force pulses created by applying current pulses to the actuator confirm the benefits of this technique, as shown in Fig. 4.12.

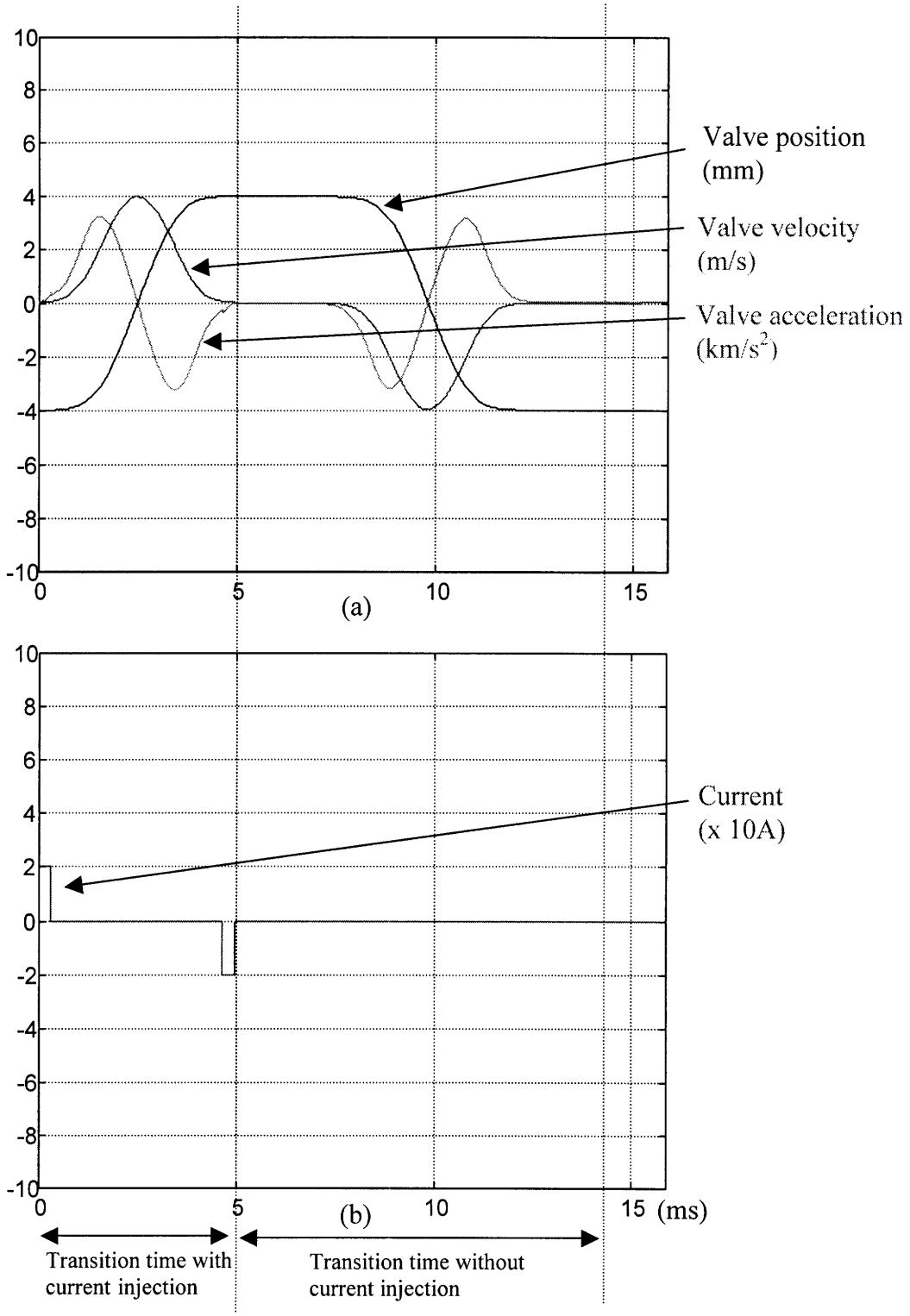

Fig. 4.12. (a) Free flight characteristic of the proposed EMVD (with and without current injection); (b) associated current.

From 0 to 5 ms, current pulses are injected at the ends of each stroke. The first pulse at one end of the stroke is for accelerating the valve, and the second one is for keeping the total internal energy of the system to be the same at the other end of the stroke for the ideal case. After 5 ms, for comparison, no current pulses are applied. As expected, the travel time is significantly reduced with the current injection technique. See Appendix A.1 for the Matlab simulation program and parameters. Note that during transitions, valve kinematics are extremely smooth "naturally," without large actuator exertion. The second current pulse in each cycle does not have to be applied in practice since the first current impulse can be used to compensate for gas and friction forces. A practical control technique for the EMVD system with the NTF will be discussed in detail in Chapter 8.

The proposed EMVD performs three basic valve-profile shaping functions (initial, transition, and holding modes). It enables fully flexible duration and phase control, and limited lift control, as in the NFEMVD. Further details of EMVD operation will be described in Chapter 8. Lift control could be included if a second nonlinear mechanical transformer is added to control the amplitude of the original nonlinear transformer-modulus curve. Details of this fully flexible EMVD design will be described in Chapter 10.

5 System Design

This chapter describes the system-level performance specifications and design considerations of the proposed EMVD. Simulation is used to confirm the performance of proposed designs. Further details of the components and subsystems will be described in Chapters 6 and 7.

5.1 System Requirements and Design Considerations

Fig. 5.1 shows a model of the proposed EMVD control system, consisting of a reference input, external disturbances, a sensor, and the EMVD electromechanical plant. The EMVD electromechanical plant comprises an actuator drive, an actuator, and the EMVD mechanical plant consisting of an NTF, a valve, and springs. From a servomechanical point of view, the EMVD must follow a commanded reference input in the presence of external disturbances – such as gas force – within acceptable power consumption limits.

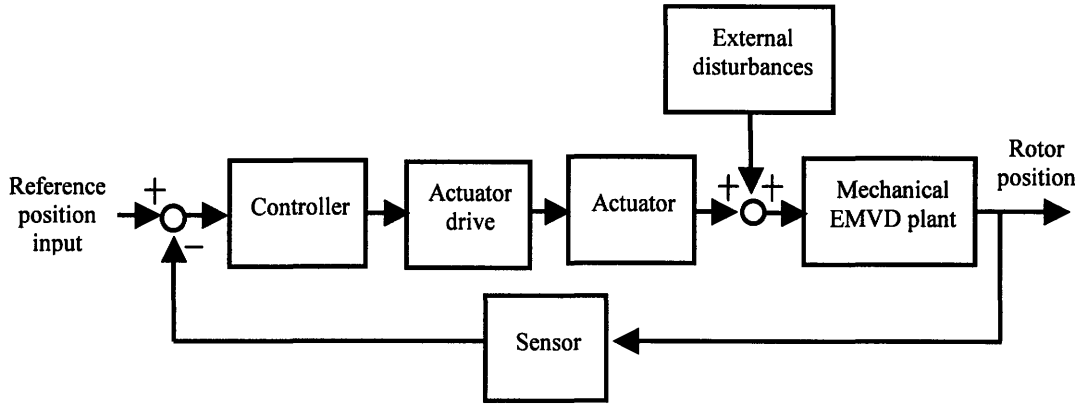

Fig. 5.1. A block diagram of an EMVD control system.

There are two inputs to the proposed EMVD control system: a reference input (a desired profile of valve-position with respect to time) and external disturbances (e.g., gas force), both of which depend on the engine operating conditions. Important mechanical and electrical output quantities of the EMVD control system include the valve position, from which the valve transition time and the seating velocity are estimated, and motor voltage and current, from which instantaneous and average actuator powers are computed.

The first step in the design of the EMVD system is to determine the natural mechanical frequency (approximately 150 Hz, in the prototype system) which is compatible with the maximum allowable valve transition time of 3-4 ms. This minimum natural frequency allows the EMVD to operate at the maximum engine speed of 6000 rpm, as explained in Chapter 2. For a given z domain inertia, comprising the reflected rotary inertia and the total mass in the z domain, the minimum stiffness is constrained by the minimum natural frequency. From valve mass and motor inertia, the nominal modulus of the NTF (i.e., the full lift of the valve divided by the full rotational angle of the rotor) is chosen so that the maximum θ domain power is delivered to the z domain load in midstroke. This constraint requires that the θ domain inertia should be impedance-matched with the mass in the z domain in the middle of the stroke. Taking account of the reflected inertia based on the chosen modulus, the minimum spring stiffness can then be calculated.

The ideal free-flight valve kinematics of the proposed EMVD – a function of the inertia, springs, and NTF – determines the valve transition time. The ideal smooth free-flight trajectory of the valve is used as the reference input, which relieves the motor of any duty except correction for losses, gas force, and control errors. The amplitude of the reference input is the maximum lift of the valve, approximately 8 mm in the prototype apparatus. Proper combination of holding and transition modes in the reference input provides phase, duration, and limited lift control in the valve profile. It is difficult to find the reference input analytically due to the nonlinearity of the NTF, but simulation easily yields a numerical valve-profile sequence which can be experimentally refined.

The gas-force profile (gas force vs. time) depends on the valve profile and engine operating conditions. For simplicity, a typical gas force profile in Fig. 5.2 (a) is assumed

for the prototype design. The reflected torque of the gas force is largest at approximately the middle of the stroke, as shown in Fig. 5.2, since the modulus of the NTF is largest in midstroke. The maximum reflected gas torque determines the peak motor torque, and is an important measure of design practicality, an issue which will be discussed in detail in Chapter 10.

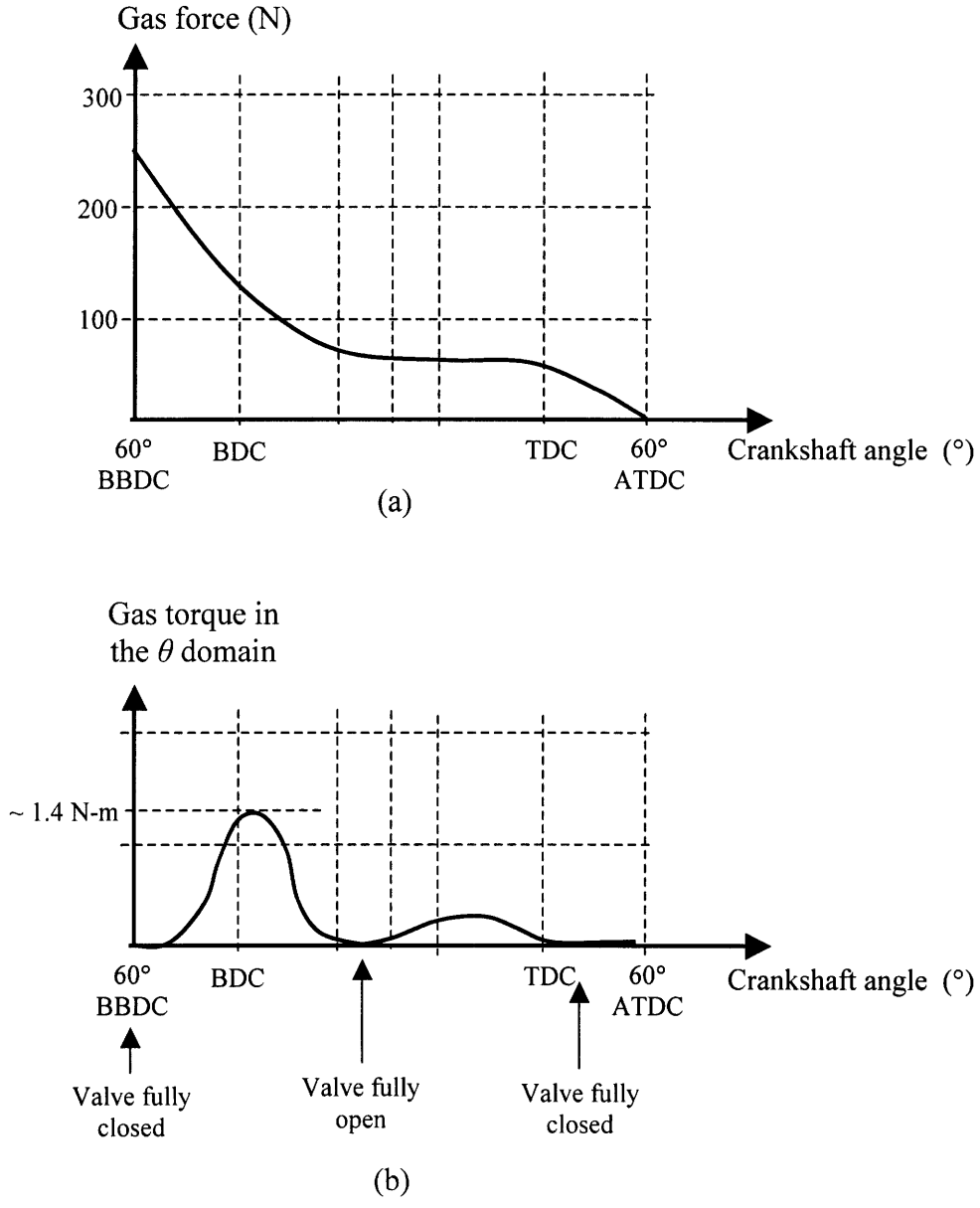

Fig. 5.2. (a) Gas force from Fig. 2.6 and (b) corresponding gas torque reflected to the θ domain.

Before designing controllers to achieve the target valve-profile performance, we first consider the stability of the EMVD plant in the absence of static friction. Given any nonzero viscous friction, the plant has a stable equilibrium point in the middle of the stroke (origin), as is easily proven by the indirect Lyapunov method [38]. If the slope of the NTF characteristic is perfectly flat for $|\theta| \geq \theta_o$, as shown in Fig. 5.3, all extreme points for which $|\theta| \geq \theta_o$ are equilibrium points. All of these points are marginally stable except for the two points at $\theta = +/- \theta_o$, since perturbation toward the origin from rest at $\theta = +/- \theta_o$ results in instability. If friction forces are considered, even the equilibrium points at $\theta = +/- \theta_o$ are stable. The bistability of the proposed EMVD (i.e., the equilibrium regions at stroke extremes) is one of its greatest benefits over the NFEMVD.

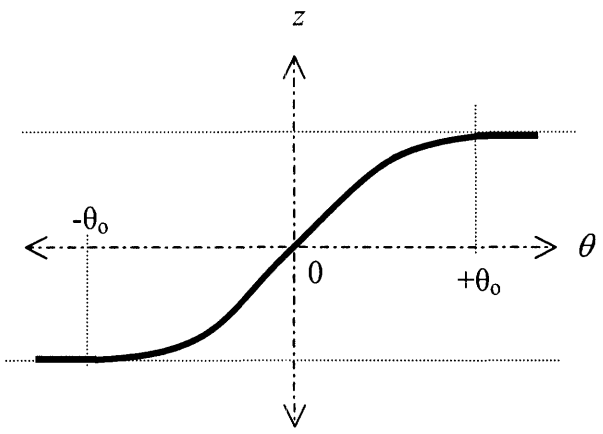

Fig. 5.3. Equilibrium points of an NTF with an extended flat region: $\theta = 0$; $|\theta| \geq \theta_o$.

The EMVD control is designed subject to a minimum valve transition time, a maximum disturbance rejection, and a minimum reference-tracking error. Since the proposed EMVD is nonlinear, it is hard to predict gas-force rejection and command-tracking performance without simulations.

A linear controller for the proposed EMVD can be designed based on the nominal model of the proposed EMVD, in which the transformer has a constant modulus (the full lift of the valve divided by the full rotation angle of the rotor). This model has significant inaccuracies at the extremes and midpoint of the valve stroke, but the controller designed with a linear model is useful — with some ad hoc adjustments — in the nonlinear system

since the linear model can be considered approximately an averaged model for the extremes and midpoint just as the nominal model of the NTF can be considered approximately an average model.

More complicated controllers can be designed directly from the nonlinear EMVD model: a gain-adjusting linear controller, a nonlinear controller based on the feedback-linearization technique [38], etc. Detailed designs of such controllers will be discussed in Chapter 8.

The power consumed by the EMVD is an important measure of the practicality of a specific design. The actuator must provide power to compensate for gas force and losses inside the system. Since net gas force over a cycle is approximately 0.7 J, the power to compensate the net gas force is approximately 35 W per exhaust valve at full engine speed and load, as mentioned in Chapter 2. Further input power compensates for friction forces, which can be approximately estimated, for simplicity, by assuming that the transformer modulus is constant with respect to valve displacement. The equation of motion for the system becomes:

$$m_e \frac{d^2x}{dt^2} + b_e \frac{dx}{dt} + k_e x = f, \tag{5.1}$$

where m_e, b_e, and k_e are the effective inertia, viscous friction coefficient, and spring constant, respectively, f is the effective actuator force, and x is the displacement. Assume that x_i and x_a are the free-oscillation displacements (zero-input responses) during the transition with and without friction force, respectively. In other words, x_i and x_a satisfy, the following equations:

$$m_e \frac{d^2x_i}{dt^2} + k_e x_i = 0, \tag{5.2}$$

$$m_e \frac{d^2x_a}{dt^2} + b_e \frac{dx_a}{dt} + k_e x_a = 0. \tag{5.3}$$

Assume that an actuator force f_p makes the system follow the reference x_i perfectly, so that f_p satisfies:

$$m_e \frac{d^2 x_i}{dt^2} + b_e \frac{dx_i}{dt} + k_e x_i = f_p . \tag{5.4}$$

Then the displacement error, x_e, defined as

$$x_e \equiv x_i - x_a , \tag{5.5}$$

satisfies

$$m_e \frac{d^2 x_e}{dt^2} + b_e \frac{dx_e}{dt} + k_e x_e = f_p , \tag{5.6}$$

and the power P during the transition is:

$$P = f_p \cdot \frac{dx_i}{dt} = (m_e \frac{d^2 x_e}{dt^2} + b_e \frac{dx_e}{dt} + k_e x_e) \cdot \frac{dx_i}{dt} . \tag{5.7}$$

Therefore, given m_e, b_e, and k_e, we can estimate the instantaneous and average powers needed to compensate for friction force during the transition time. For a given motor winding resistance (R), electrical loss (i^2R) is easily calculated from the actuator current required to provide f_p. Note that the maximum actuator force necessary to compensate for friction force can also be obtained from (5.6).

A position sensor can be located on the valve or actuator side of the EMVD plant. Although a direct measure of valve position offers (theoretically) the greatest immunity to noise and modeling errors, it is difficult to locate the position sensor on the valve side for the application to a real cylinder head. Moreover, the state variables on the valve side

are not controllable at the ends of the stroke if the slope of the NTF is flat. Therefore, a rotary sensor on the actuator side is preferred as the position feedback sensor. In the experimental apparatus, a linear position sensor is added to investigate the compliance between the z and θ domains and to measure the seating velocity. In conventional valvetrains, the ramp slope of the valve position determines the seating velocity. In the proposed system, however, the speed of the actuator at the end of the stroke and the instantaneous gear ratio of the NTF determine the seating velocity. If the slope of the NTF characteristic is almost flat at both ends of the stroke, then the seating velocity – even with finite actuator angular velocity – is almost zero. To avoid bypassing the flat NTF characteristic at stroke extremes, the mechanical compliance between the z and θ domains must be minimized: all relevant mechanical components should be as rigid as possible, and valve kinematics should be as smooth as possible. In practice, this compliance issue is not as critical for the proposed EMVD system as for conventional valvetrains.

5.2 Simulation of the Proposed EMVD

The objective of the simulation is to confirm the benefits of the proposed system. The proposed EMVD control system is simulated using the mathematical model of (4.11) with realistic values. See Appendix A.2 for the Matlab simulation program and parameters.

For fast acceleration, a feedforward current injection technique plus linear controller (such as a PD controller) is used near both ends of the stroke during the transition. The dynamics of the EMVD system vary significantly with valve and rotor position. A PD controller with constant controller gains does not perform well during the transition mode. A nonlinear controller designed by the feedback-linearization technique is therefore considered during the transition except for the period when the valve is near both ends, in other words, except for the current injection period. Therefore, for the whole transition, a switched-mode controller is designed, comprising two control laws: the feedforward current injection plus PD controller for the current injection period and the feedback

linearization controller during the remainder of the transition. For the holding mode, another PD controller with appropriate controller gains is used. Details of controller designs will be discussed in Chapter 8.

Fig. 5.4 shows the time response of the proposed EMVD for an exhaust valve with the controllers mentioned above. In this simulation, the calculated position response, computed for the case with current injection and without disturbance or system losses, is used as the reference input. Gas force and energy losses due to friction and electrical resistance are included. As can be seen from the figure, the acceleration is smooth, so the jerk remains small. Further, the system shows small driving and holding currents and no deterioration of the free-flight travel time. Position and velocity errors are negligibly small. The peak power input is about 2 kW per exhaust valve in the presence of the gas force profile based on full load and engine speed. The peak motor current can be greatly reduced with an NTF optimized to minimize motor size, as will be described in Chapter 10. The spikes in Fig. 5.4 are computational artifacts due to the switching of control laws, and can be ignored. They can be effectively eliminated in the hardware system.

Without losses, the average power required over a cycle to compensate for gas forces is approximately 60 W per exhaust valve at full load and the maximum engine speed of 6000 rpm. Simulations show that the average power required to compensate for gas force and electrical and mechanical power losses is about 1 to 2 kW, depending on friction modeling values, for 16 valves (4 cylinders) at maximum engine speed and full load. This power requirement is comparable to that of a conventional valvetrain with roller cam, i.e., 1.5 kW, as mentioned in Chapter 2.

Fig. 5.5 shows, for contrast with the NTF system, a simulation of a controlled EMVD with a rotary motor, linear spring, linear inertia, linear mechanical transformer, and a smooth kinematic reference input. See Appendix A.3 for the Matlab simulation program and parameters. Jerk is reduced by the smooth kinematic reference inputs, and gas-force disturbances are reduced by feedback. As expected, however, this system suffers from two crucial drawbacks: the current required to hold the valve at either end of the stroke (and the corresponding power loss) is undesirably high, and the driving current required

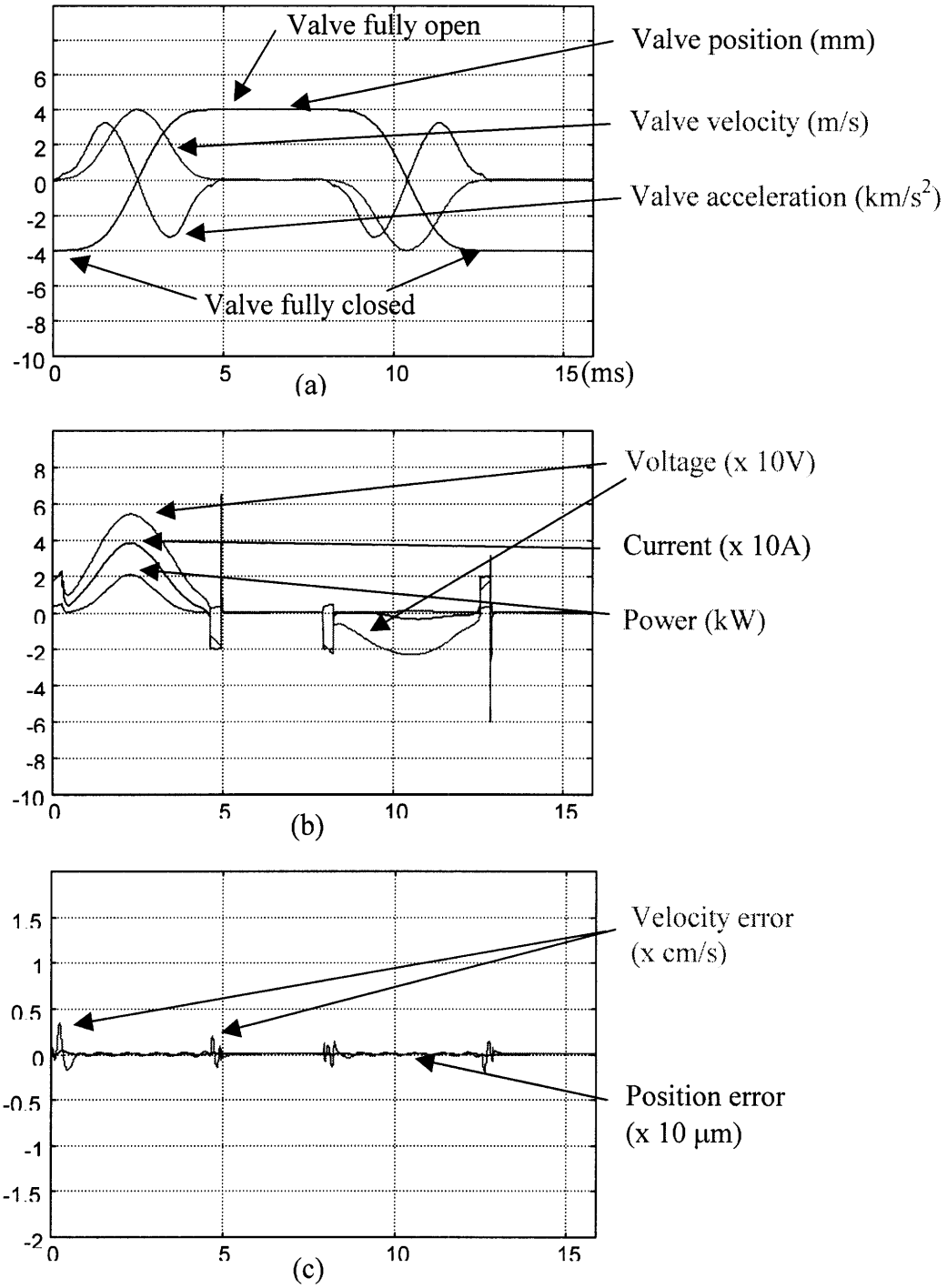

Fig. 5.4. (a) Simulated time response of the proposed EMVD; (b) Associated voltage, current and power; (c) Associated position and velocity errors.

for the valve to follow smooth reference inputs is unacceptably large. These simulation results, with those of Fig. 5.4, confirm the performance and low power requirements of the NTF-based EMVD.

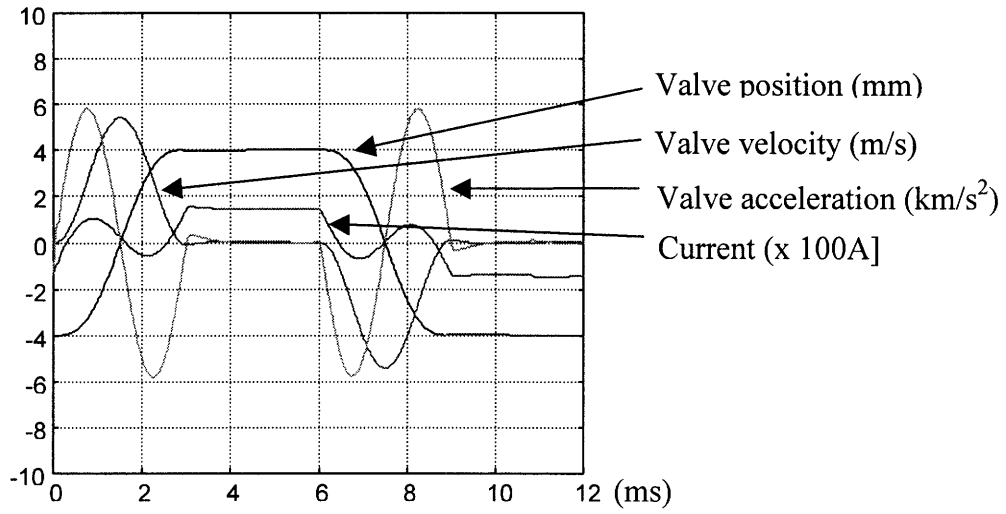

Fig. 5.5. Time response of a feedback-controlled EMVD incorporating a shear-force actuator and a linear mechanical transformer.

6 Electrical Components and Subsystems

An experimental apparatus was built to demonstrate the feasibility and performance of the NTF-based EMVD. This chapter details the design of the electrical components and subsystems necessary to meet the system specifications discussed in Chapter 5.

6.1 Motor

A rotary shear-force actuator is preferable to a normal-force actuator in the proposed EMVD, as explained in Chapter 4. After a detailed consideration of motors, a moving-coil brushed dc motor (Pacific Scientific 4N63-100-1, shown in Fig. 6.1) was selected for its following features:

- Large torque/inertia ratio (i.e., sufficient maximum torque developed with the lowest possible rotor inertia at the required power)
- Small winding resistance and inductance
- Adequate power rating at 42 V nominal voltage

Table 6.1 shows key specifications for the 4N63-100-1. Simulation confirmed that the choice was appropriate to prove the proposed concept in an experimental apparatus.

The Pacific Scientific motor is too large to fit in an engine head. However, it is believed that much of the volume of the motor could be removed by redesign without substantial loss of function. Furthermore, actuator torque requirements and size can be reduced by optimization of the NTF. Details of the NTF optimization will be described in Chapter 10, and further ideas to reduce the motor size will be discussed briefly in Chapter 11.

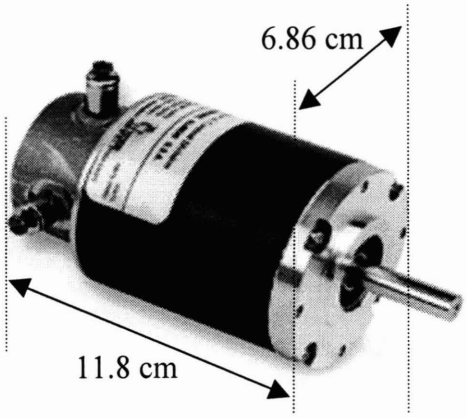

Fig. 6.1. The motor used for the EMVD apparatus (Pacific Scientific 4N63-100-1).

Table 6.1. Key specifications of Pacific Scientific 4N63-100-1.

Parameters	Values
Rated torque	0.89 N-m
Rotor inertia	3.5×10^{-6} kg-m^2
Motor terminal resistance	0.89 Ω at 25° C, 1.31 Ω at 155° C
Winding inductance	0.1 mH
Rated power output	321 W
Rated voltage	42 V
Rated current	14.2 A
Rated speed	3440 rpm
Torque constant	0.07 N-m/A
Viscous damping coefficient	0.008 N-m/krpm

6.2 Motor Drive

A current drive – in which rotor torque is commanded regardless of dynamics – is preferable to a voltage drive in an EMVD application. Current drive enforces motor current regardless of back emf, winding inductance, and mechanical dynamics, reducing the system order and extending actuator bandwidth.

A hysteretic current drive [39], [40] was chosen which follows a commanded current within a ±1 A hysteresis band. Fig. 6.2 shows the Simulink model of the motor drive and

motor [35]. The hysteretic controller properly provides the motor with positive or negative bus voltage (whose magnitudes are determined by the positive and negative amplitudes of the hysteresis curve), based on the current error information (the difference between the desired motor current and the actual motor current) so that the actual motor current may follow the (desired) motor current command within the upper and lower hysteresis bands, which are determined by the width of the hysteresis curve. Note that electrical and mechanical dynamics of the motor are also included in the mathematical model of Fig. 6.2.

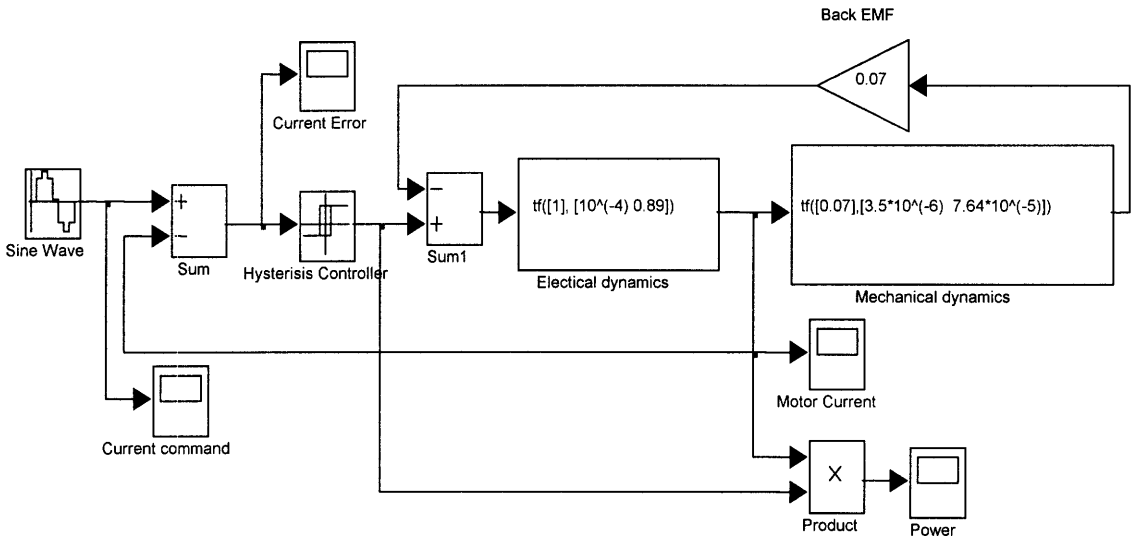

Fig. 6.2. The Simulink model of a hysteretic motor drive and a motor.

Fig. 6.3 shows the schematic implementation of the motor drive and motor [35], [41], [42]. The hysteretic current control is performed by three stages: the hysterisis band set, the current comparator, and the PWM/logic. In the stage of the hysterisis band set, upper and lower hysteresis bands around the current command (input to the motor drive circuit) are generated by adding/subtracting the ripple current reference to/from the current command input. In the stage of the current comparator, the sensed (actual) motor current is compared with the upper and lower hysteresis bands. The logic gate of the last stage processes the outputs of the comparators and controls the gate drivers for the MOSFETs so that the actual motor current follows the current command within the upper and lower hysteresis bands. For example, if the actual motor current is larger than the upper

hysteresis band, the state is changed such that one pair (pair A) of MOSFETs is turned on and the other pair (pair B) of MOSFETs is turned off, applying the negative of the bus voltage to the motor, reducing the actual motor current. Similarly, if the actual motor current is smaller than the lower hysteresis band, the state of the switches is set such that pair A of MOSFETs is turned off and pair B of MOSFETs is turned on, applying the bus voltage positively to the motor, increasing the actual motor current. If the actual motor current is between the upper and lower hysteresis bands, the MOSFETs in the bridge maintain their previous states. Therefore, the motor drive can provide the motor with the desired motor current (current command) within the hysteresis bands.

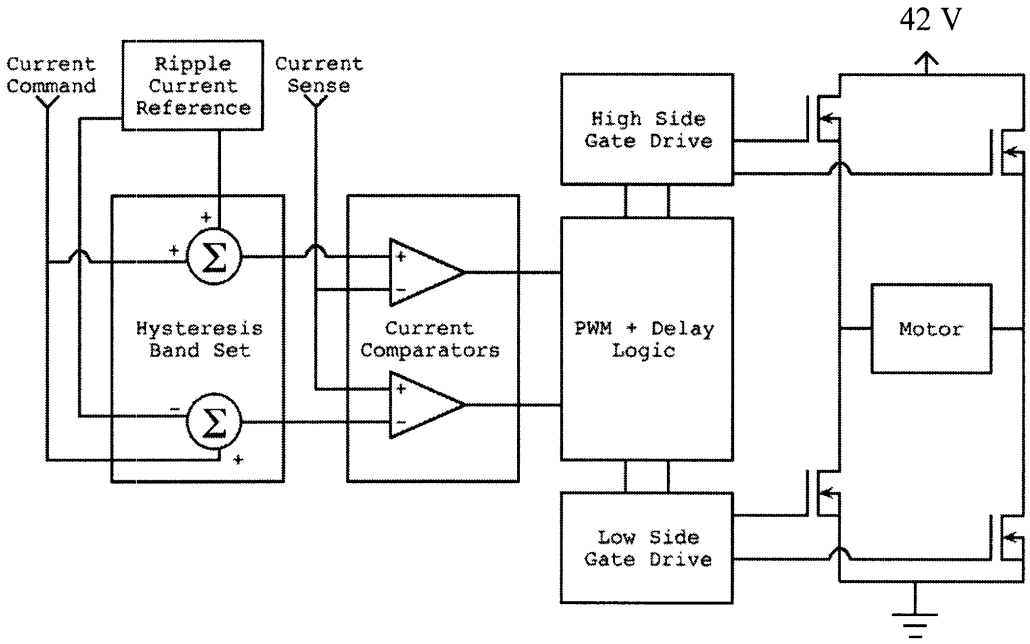

Fig. 6.3. The schematic implementation of the hysteretic motor drive [35].

The control loop of the constructed drive is simple and fast, but has non-zero current-tracking error due to inherent characteristics of the hysteretic drive. Since the maximum error (a peak-to-peak ripple current of 2 A between the hysteresis bands) is small relative to the motor current required to overcome static friction near both ends of the stroke, the tracking error is negligible.

Simulation results in Fig. 5.4 were used to determine motor-drive specifications: 70 A/ms slew rate, 10 kHz bandwidth, 1 kW average power, and +/- 40 A maximum current when operated on a 42 V bus. Fig. 6.4 shows a photograph of the constructed motor drive [35]. See Appendix B for the circuit. The constructed drive has 69 A/ms slew rate, 9.5 kHz bandwidth, and average power capability greater than 1 kW. Fig. 6.5 shows simulated and actual responses to a 7 A step with a 42 V bus voltage. Fig. 6.6 shows simulated and actual responses to a 7 A, 3 kHz sinusoid with a 42 V bus voltage. The frequency of 3 kHz is approximately 20 times the operating frequency, which is appropriate, and the amplitude of 7 A, which is about half of the rated current in the apparatus, was chosen arbitrarily. The measured motor current agrees well with the simulation. The specifications were confirmed with various amplitudes and frequencies.

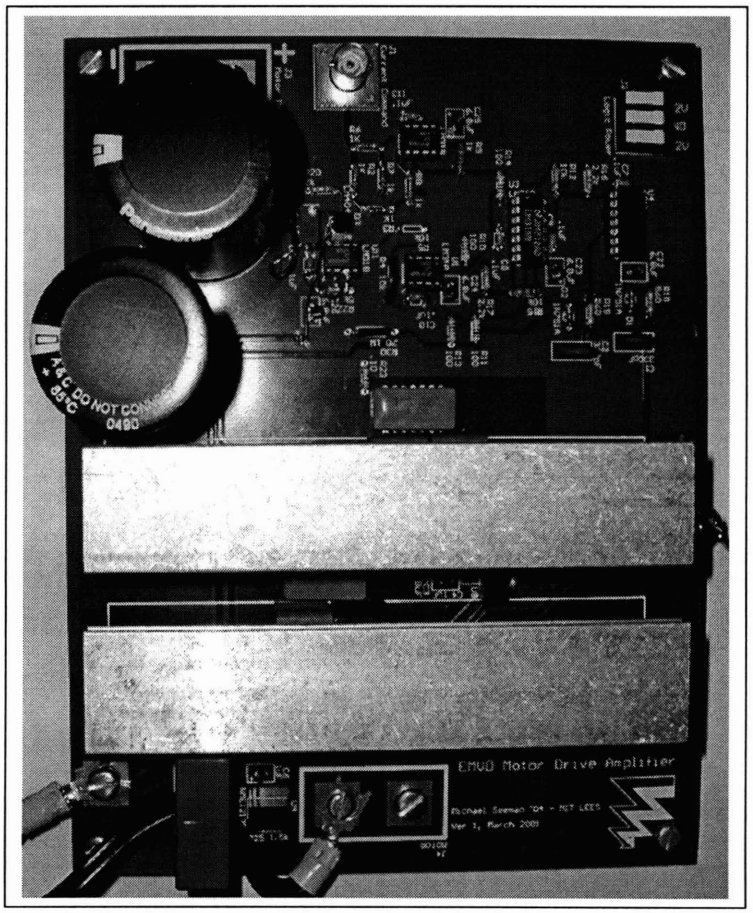

Fig. 6.4. The completed motor drive circuit used for the apparatus [35].

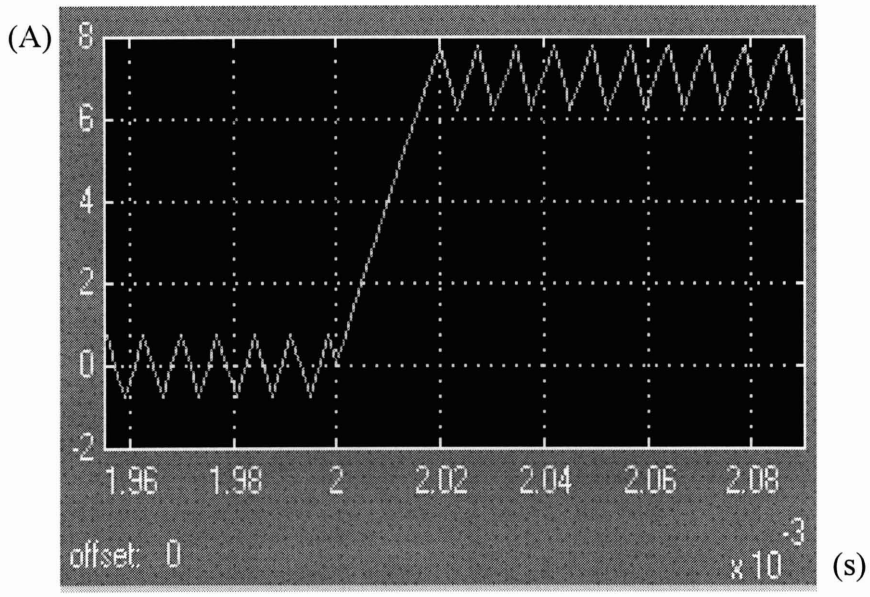

(a)

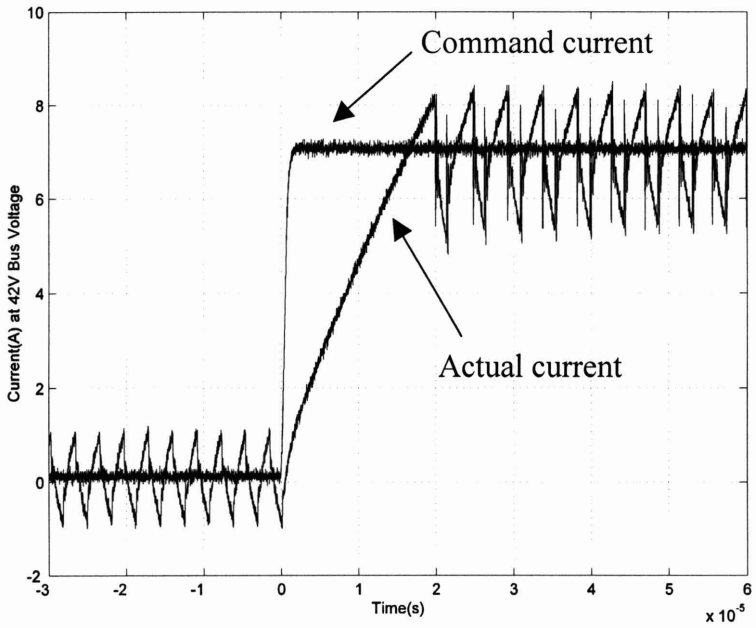

(b)

Fig. 6.5. (a) Simulated and (b) actual step response of the motor drive plus the motor with a 7 A step input.

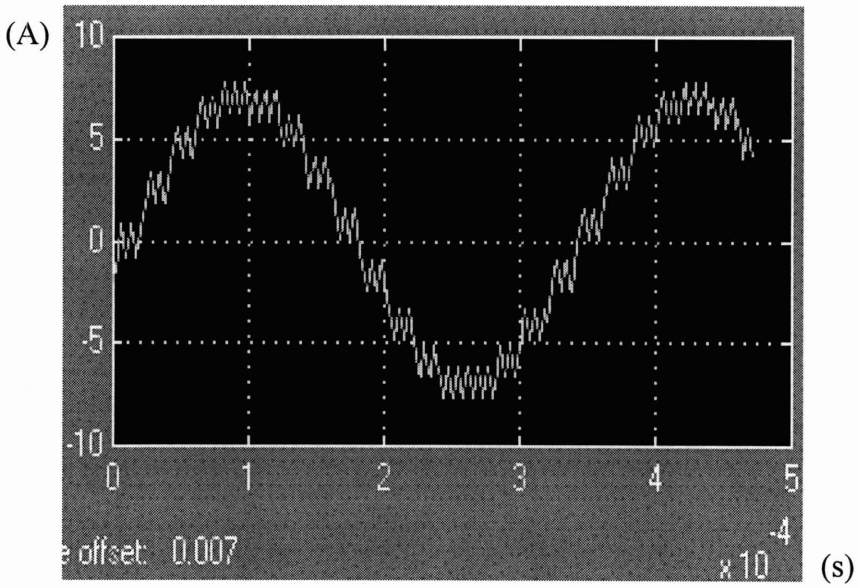

(a)

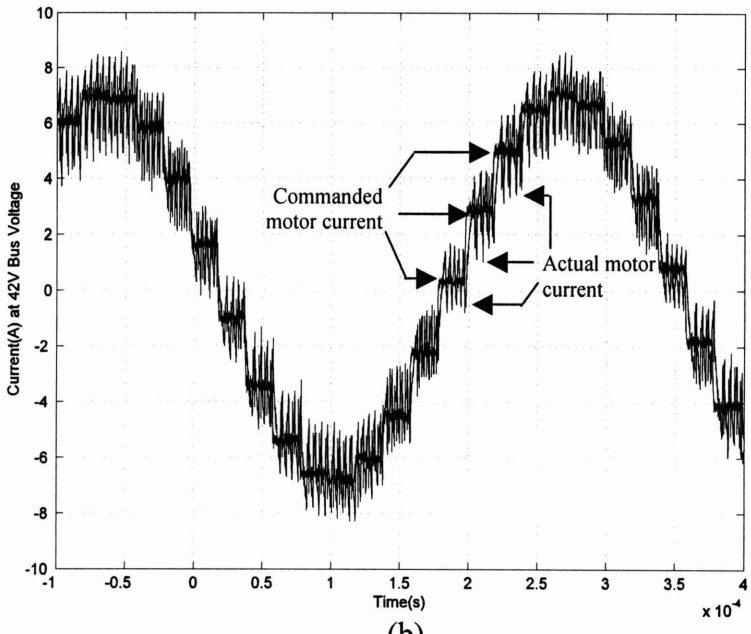

(b)

Fig. 6.6. (a) Simulated and (b) actual response of the motor drive plus the motor with a 7 A, 3 kHz sinusoidal input.

6.3 Sensor

As discussed in Chapter 5, a rotary optical encoder is the best choice for the position feedback sensor. A rotary optical incremental encoder (US Digital E6D, with 8192 signal cycles per revolution) was chosen as a position feedback sensor for its low inertia and high resolution. The resolution of the rotary optical encoder ($\delta\theta$) is 360°/8192 = 0.044° = $7.7 \cdot 10^{-4}$ rad. The nominal equivalent resolution of the rotary encoder in the valve domain (δz) is:

$$\delta z = r_n \delta\theta , \tag{6.1}$$

where r_n is the nominal modulus of the NTF, the full lift of the valve divided by the full rotation angle of the rotor. For $r_n = 8.8 \times 10^{-3}$ m/rad, as will be determined in the next chapter, δz = 6.7 μm. Because of the nonlinear transformer modulus, the reflected resolution of the rotary position sensor (viewed in the z domain) becomes higher as the valve approaches the end of a stroke. This higher effective resolution near stroke extremes is desirable, since it coincides with the need for high-precision position control during valve landing.

A variable-reluctance, linear-position sensing system (Sentech's Fastar FS380 sensor and a SP300A signal processor) measured valve position for performance evaluation, but not for control. The linear sensor has a 15 kHz bandwidth, 4.8 g mass, 0.17 μm repeatability, and 19 mm linear range. The resolution of the sensor was limited by the number of bits in the ADC channel: with a 12 bit channel and 8 mm stroke, the resolution was 8 mm/2^{12} = 2 μm. The sensor was used to investigate the effects of the compliance between the rotor position and the valve position, and provided a direct measure of seating velocity.

6.4 System Integration with a DSP Board

A DSP board, the dSpace 1104, was used for signal conditioning and control in the prototype EMVD apparatus. The dSpace 1104, shown in Fig. 6.7, has a 250 MHz Power PC 603e, TI's TMS320F240 DSP, 4 ADC channels with 12 bits and 50 kHz sampling frequency, 8 DAC channels with 16 bits, and 2 digital inputs for the incremental encoder interface.

Rotor- and valve-position information from the prototype are transferred through the incremental encoder interface and ADC channel, respectively, on the dSPACE 1104 board to a software controller implemented in Simulink on the PC. The calculated control input (determined by a control law, the measured position information, and the reference input) is transferred to the motor-drive board through a DAC channel. The motor drive enforces the commanded current into the motor terminals.

To measure motor current and voltage, a high-bandwidth hall-effect current probe and a high-bandwidth differential voltage probe were used. A high-sampling-rate digital oscilloscope with a GPIB card and LabView measured and recorded electrical power.

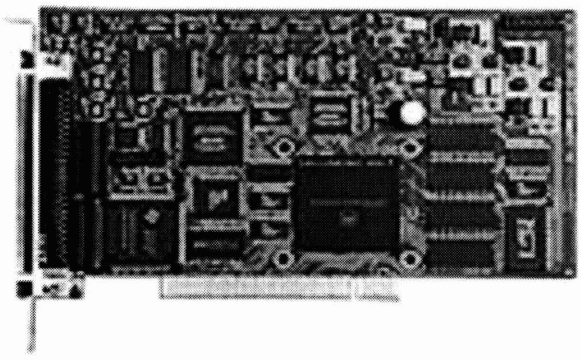

Fig. 6.7. A DSP board used for the apparatus (dSpace 1104).

7 Mechanical Components and Subsystems

This chapter describes the design guidelines, specifications, and construction of the mechanical components for the proposed EMVD.

7.1 Structure Design for the Experimental Apparatus

Fig. 7.1 shows the conceptual design of the prototype EMVD, and Fig. 7.2 shows the 2-D mechanical design of the apparatus based on the conceptual design after the dimensioning of key mechanical components – such as the motor and valve – were determined. The motor is held by front and rear brackets; the brackets are attached to column I; the column is connected to the table (mechanical ground). The bearing is supported by the bearing housing; the housing is held by the housing holder; the housing holder is attached to column II. The disk cam has a hole through which the rotor shaft is rigidly connected. The valve holder connects the roller shaft with the top of the valve stem. The spring divider is rigidly attached to the valve stem at a pre-determined position. One spring is placed between the top plate and the spring divider, and the other spring is placed between the bottom plate and the spring divider. Long bolts connect the two plates rigidly, and the top plate is attached to the two columns so that the springs are retained between the valve stem and mechanical ground. Each plate has a hole in its center, in which a bushing is placed so that the valve is guided vertically. The valve-seat plate is bolted to the columns, and has a recess on its lower surface into which the valve head fits. The rotary optical encoder is attached to the rear of the motor, and the spring divider holds the linear position sensor.

The dimensions of the mechanical components need to be designed with consideration for two important horizontal and vertical constraints. The rotor-shaft length of the stock

motor limits the thicknesses of the roller/disk cam, bearing, and valve holder. The length of the valve stem constrains the length of springs and the thicknesses of the spring divider, top/bottom plates, and valve seat plate. Fit conditions (dimensions and tolerances) for press-fits were carefully specified wherever necessary, and all components and subsystems were designed to be assembled, aligned, disassembled, and replaced as easily as possible.

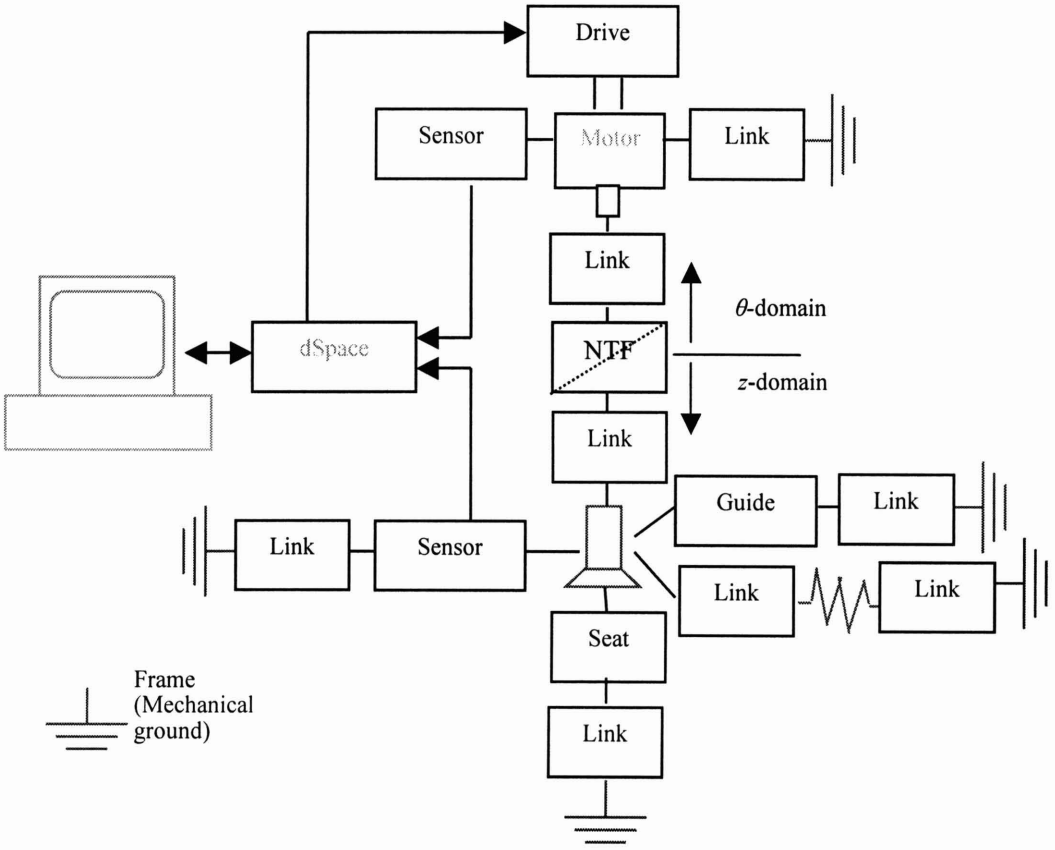

Fig. 7.1. The conceptual design of the proposed EMVD apparatus.

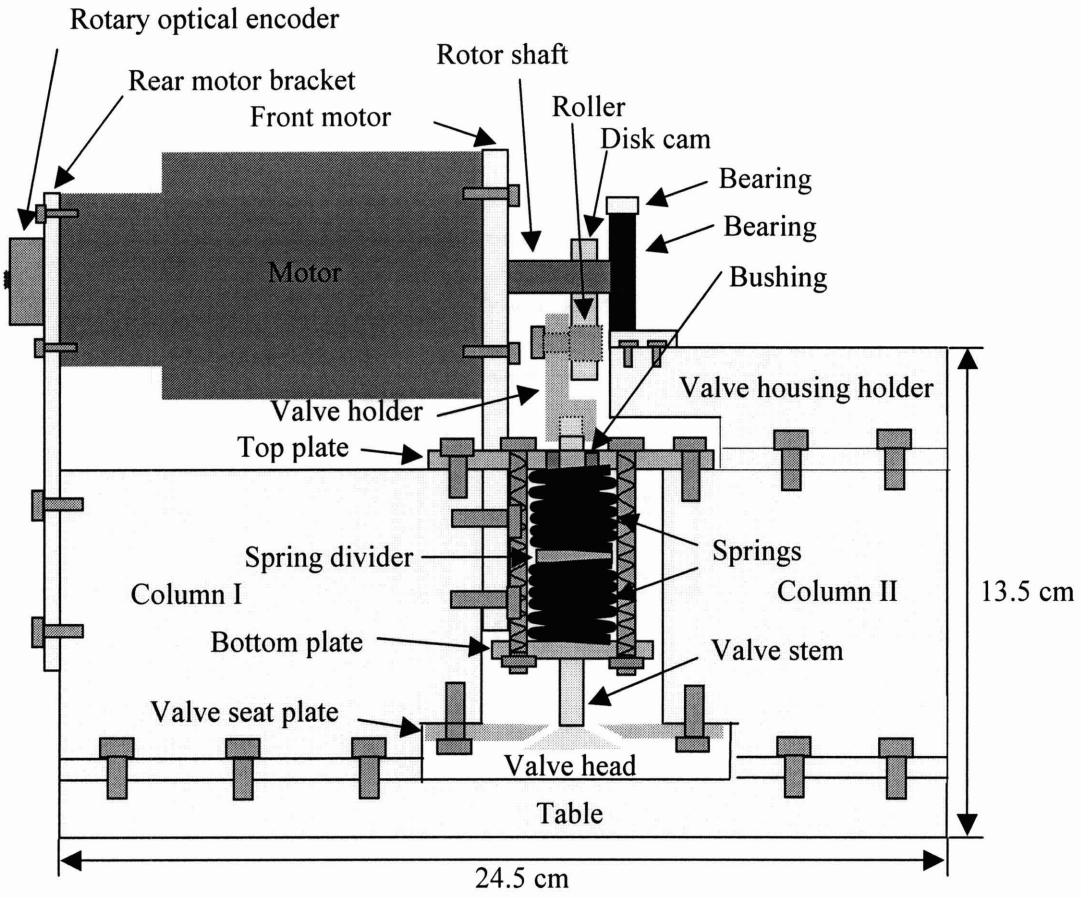

Fig. 7.2 The 2-D design of the proposed EMVD apparatus.

7.2 Valve

An exhaust valve from a Ford Zetec engine head (16 valves, 4 cylinders, and 2.0 L) was used in the EMVD prototype. The valve has a mass of 40 g, length of 90 mm, 6 mm stem diameter, and 28 mm head diameter.

A smaller valve mass could increase the system response speed. Eaton Corporation's ultra-light engine valves (ULVs) may be considered for a future version of the apparatus. The masses of the ULVs are 22 g and 26 g for exhaust valve and intake valve, respectively.

7.3 Nonlinear Mechanical Transformer

The design of the NTF is the most important procedure in the development of the prototype EMVD apparatus. Among the design alternatives introduced in Chapter 4, an NTF comprising a disk cam and a roller (see Fig. 4.9) was chosen because of its simple construction.

The transformer modulus of the NTF, a function of valve position, should be very small at both ends of the stroke and large in the middle of the stroke. For simplicity, a sinusoidal NTF characteristic (z vs. θ) was chosen to implement the following transformation:

$$z = g(\theta) = \frac{L/2}{\sin(\pi a_1 / 2)} \sin(\theta \cdot a_2), \tag{7.1}$$

where

$$0 < a_1 \leq 1,$$

$$|\theta| \leq \pi\, a_1/(2\, a_2) = \theta_{max}/2,$$

$$|z| \leq L/2,$$

and L and θ_{max} are full lift and full rotation angle, respectively. The constants a_1 and a_2 determine the slot end slope and transformer gear ratio, respectively. The larger the value of a_1, the flatter is the slope of the NTF at both ends of the stroke (an a_1 of 0.999, for instance, produces a flat characteristic and soft valve landing). For a given L and a_1, the nominal gear ratio of the NTF is given by

$$r_n \equiv L/\theta_{max} = La_2/(\pi\, a_1).$$

As seen from the simulation results in Fig. 5.4, maximum motor power is required in the approximate middle of the stroke. Maximum power is delivered when the inertia (J) on

the actuator side is matched with the mass (m) on the valve side with the following transformer modulus (r):

$$r = \sqrt{\frac{J}{m}}. \tag{7.2}$$

In the experimental apparatus, the estimated inertia on the actuator side and the estimated mass on the valve side are approximately $6.9\text{x}10^{-6}$ kg-m^2 and 90 g, respectively, and the impedance-matched modulus, r, is $8.8\text{x}10^{-3}$ m/rad. For simplicity in the first design iteration, setting the nominal NTF modulus r_n to $8.8\text{x}10^{-3}$ m/rad and a_1 to 0.999, for a valve lift L = 8 mm, the constants a_2 and θ_{max} are 3.46 and 52°, respectively. The nominal gear ratio can be optimized to minimize motor size. This optimization will be discussed later in this chapter.

Implementation of the NTF characteristic of (7.1), beyond the choice of nominal modulus, reduces to the design of the top and bottom surfaces of the NTF disc-cam slot. Given h_0 — the distance between the center of the motor shaft and the center of the roller shaft in the middle of the stroke — the profile of the center of the roller is obtained from z, θ pairs in the NTF characteristic by rotating $(0, z - h_0)$ by θ as follows:

$$\begin{pmatrix} x_0(\theta) \\ y_0(\theta) \end{pmatrix} = \begin{pmatrix} \cos\theta & -\sin\theta \\ \sin\theta & \cos\theta \end{pmatrix} \begin{pmatrix} 0 \\ z - h_0 \end{pmatrix}, \tag{7.3}$$

where $x_0(\theta)$ and $y_0(\theta)$ are x and y components of the roller center profile in x-y coordinates (i.e., in the coordinates of the cam face, referred to the motor-shaft center). Assuming that the tangential lines of the top and bottom surfaces are parallel to the dy_0/dx_0 line as illustrated in Fig. 7.3, the top and bottom surface profiles can be expressed as follows:

$$\begin{pmatrix} x_1(\theta) \\ y_1(\theta) \end{pmatrix} = \begin{pmatrix} \cos\beta & -\sin\beta \\ \sin\beta & \cos\beta \end{pmatrix} \begin{pmatrix} r_0 \\ 0 \end{pmatrix} + \begin{pmatrix} x_0(\theta) \\ y_0(\theta) \end{pmatrix}, \tag{7.4}$$

$$\begin{pmatrix} x_2(\theta) \\ y_2(\theta) \end{pmatrix} = \begin{pmatrix} \cos\beta & -\sin\beta \\ \sin\beta & \cos\beta \end{pmatrix} \begin{pmatrix} -r_0 \\ 0 \end{pmatrix} + \begin{pmatrix} x_0(\theta) \\ y_0(\theta) \end{pmatrix}, \tag{7.5}$$

where r_0 is the radius of the roller, and $x_1(\theta)$ and $y_1(\theta)$ and $x_2(\theta)$ and $y_2(\theta)$ are the x and y components of the top and bottom surface profiles, respectively, and

$$\beta = \tan^{-1}\left(\frac{-1}{\tan(\alpha)}\right),$$

where

$$\tan(\alpha) = \frac{dy_0}{dx_0}.$$

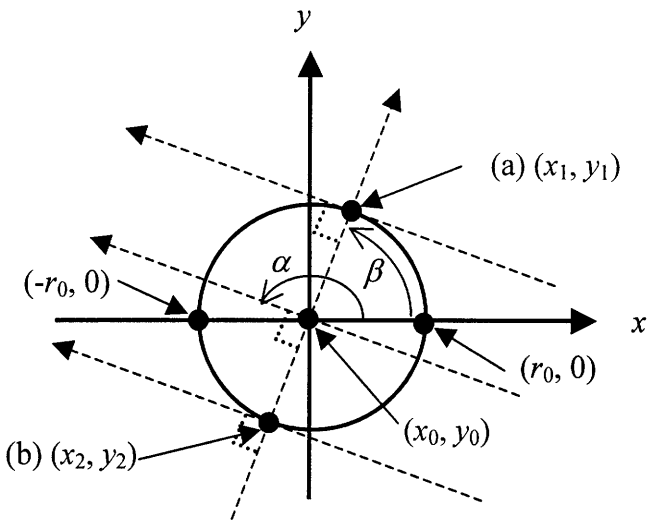

Fig. 7.3. A drawing to find the (a) top and (b) bottom contact surfaces from a position (x_0, y_0) on the profile of the center of the roller.

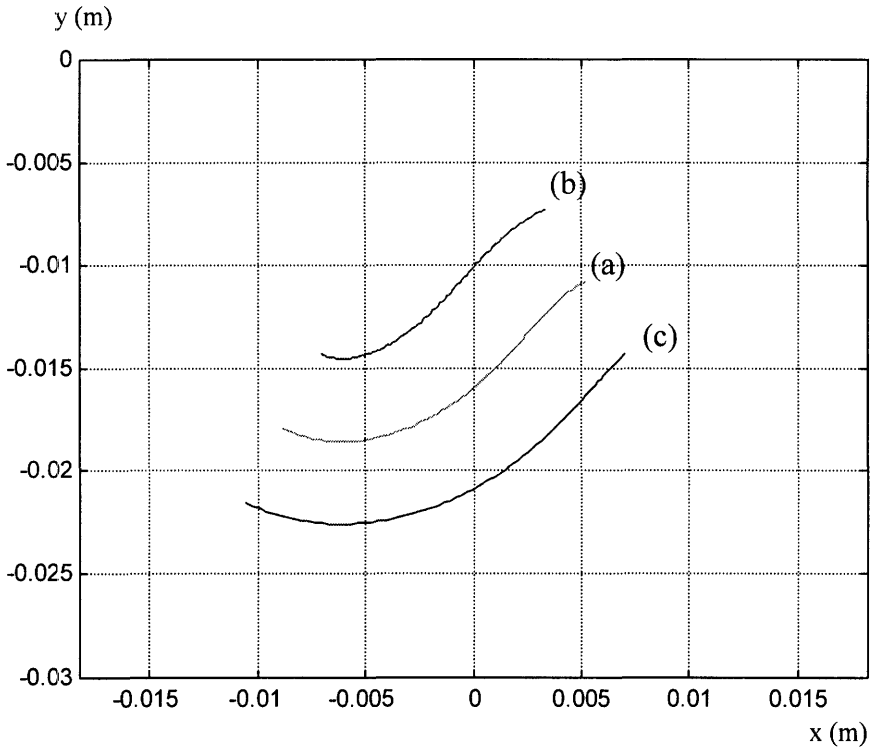

Fig. 7.4. The calculated profiles of (a) the center of the roller, (b) the top and (c) bottom surfaces of the disk cam.

Fig. 7.4 shows the calculated profile designs of the center of the roller and the surfaces of the disc-cam slot, where the origin (0, 0) is the center of the motor shaft. See Appendix A.4 for the Matlab simulation code to generate the profiles. At both ends of the stroke, an extended flat region allows overshoot in the motor kinematics. The clearance between the roller diameter and the disc-cam slot is approximately 75 μm. This gap prevents contact between the roller and the non-active surface, and has proven effective. We know that there is at least one transfer of roller-cam contact (from cam top to bottom or vice versa) in each stroke. This non-ideality has not caused operating problems.

IKO's CFS-5-V was chosen as the roller. It has a 10 mm diameter, 6 mm width, 18 mm total length, 7 g mass, 3.1 kN basic dynamic-load capability (a constant radial or axial load allowing a basic rating life of 10^6 revolutions), and 4.7 kN basic static-load capability (the maximum allowable load at rest without permanent deformation). These

ratings are sufficient for the experimental apparatus, though not, perhaps, for engine service. Fig. 7.5 shows a photo of the NTF (the disc cam and roller) used in the prototype. As mentioned in Chapter 4, the NTF, consisting of disk cam with the roller, experiences slip in mid-stroke during the transition from top to bottom and vice versa because the rotational direction of the roller reverses in the middle of the stroke, resulting in noise and wear. The conjugate disk cam of Fig. 4.10 can reduce the slip loss and reduce the noise and wear because there is no reversal of the roller rotational direction in the middle of the stroke.

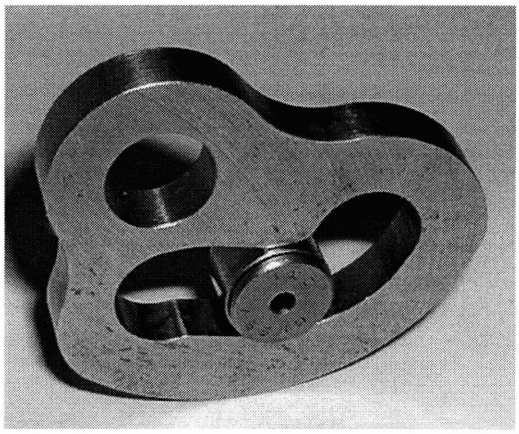

Fig. 7.5. The disk cam and roller.

7.4 Spring

The spring stiffness was selected to meet the required transition time of 3-4 ms in conjunction with the effective z-domain inertia. The effective inertia comprises the valve mass, spring-divider mass, roller mass, effective spring mass, and the reflected mass of the θ–domain inertia. The effective mass is not constant, but varies with respect to valve position, and it is difficult to determine the desired spring stiffness analytically with precision. An alternative and practical approach, given the NTF design, is summarized here:

- Calculate the effective moving mass at the nominal NTF modulus.
- Determine tentatively the spring stiffness necessary to meet the minimum natural mechanical frequency (150 Hz in the prototype).
- Check if the system meets the transition requirement using simulation.
- Adjust the stiffness until the system satisfies the transition-time requirement.

The prototype springs, Danly IEM's 075x1.00 green spring (part #: 9-124-11), produce a valve-suspension stiffness of 112 N/mm, i.e., each spring has 56 N/mm stiffness. The mass of each spring is 14.7 g, and the effective mass of the two springs is 14.7 x 2 / 3 = 9.8 g. The maximum deflection of the springs is 10.2 mm, greater than the full lift of 8 mm. Each spring must be pre-compressed by at least 4mm (half of the full lift) so that they are always under compression within the maximum valve deflection during operation. The length and inner diameters of the spring are 1 in and 3/8 in, respectively, dimensions compatible with the length and diameter of the valve stem.

For preliminary test of the apparatus at a mild operating condition (e.g., compatible with 1500 rpm engine speed), we prepared another assembly incorporating soft springs (McMaster-Carr part #: 94350K149) instead of the above springs. The soft spring has a stiffness of 10 N/mm. The inner and outer diameters of the spring are 0.576 in and 0.72 inch.

7.5 Other Mechanical Components

The spring divider transfers spring forces to the valve stem, and serves as a mount for the linear position sensor. The divider is small and light to minimize effective z-domain inertia and meet valve transition times. The diameter of its though-hole is smaller than the diameter of the valve stem so that Coulomb friction — after press-fit — is large enough to overcome the maximum spring force. The hole is not so small, however, that press-fit parts exceed the allowable deformation limits. The divider itself is stiff enough to avoid deformation due to the spring load.

The valve holder has the same design requirements as the spring divider. In the apparatus, due to the length of the valve stem, the contact surface between the valve stem and the valve holder after press-fit is not large enough to overcome the maximum spring force. Pins placed in through-holes on the valve stem and valve holder prevent slip.

The top and bottom plates are thick enough to resist deformation due to the spring force. Three sets of nuts and bolts rigidly connect the top and bottom plates through three sets of aligned holes. To assure the alignment between the plates, two precision bars are inserted into two additional sets of holes. The central hole of the valve-seat plate is recessed to accommodate the valve head.

Two bushings (McMaster Carr's 6381K422) guide the valve stem through the top and bottom plates, into which they are press fit. The bushings can accommodate a ¼ in-diameter shaft, a little larger than the valve-stem diameter (6 mm). The bushings' 3/8 in outer diameter ensures that the springs are retained by the top and bottom plates.

The front and rear motor brackets are thick enough to hold the motor but thin enough to allow adequate axial space to assemble the NTF, the bearing, and the rotary optical encoder on the rotor shaft. The holders are stiff vertically but compliant horizontally. This mass-spring system in the horizontal direction, comprising the motor and the motor brackets, has a natural frequency not far separated from the frequency of valve operation. Coupling to an undesirable mounting resonance is low, however, because the valve motion is orthogonal to the horizontal motor vibration.

Columns I and II are simple and bulky to provide a low-compliance connection to mechanical ground. They are large enough to hold the top plate, the valve seat plate, the front and rear motor brackets, and the bearing-housing holder.

A deep-groove ball bearing (SKF's 61901) was chosen to support the rotor shaft vertically. The bearing has a 6 mm width, 12 mm shaft diameter, 24 mm outer diameter, 11 g mass, 2.2 kN basic dynamic-load capability, and 1 kN basic static-load capability. These ratings are sufficient for the experimental apparatus, though not, perhaps, for

engine service. The bearing is press-fitted into the bearing housing, and is press-fitted over the motor shaft.

A high-load-capacity table, McMaster Carr's 4769T44 (steel, 36 in width x 24 in depth x 36 in height), was chosen as the mechanical ground. The table has 0.002 in/ft flatness, ¾ in thickness, and a 35000 lb static-load rating.

7.6 Assembly of Mechanical Components and Subsystems

Assembly of the complete mechanical apparatus is a delicate process. The motor assembly (the motor, front and rear motor brackets, disc cam, and bearing housing) and the valve assembly (the valve, valve holder, two springs, spring divider, top and bottom plates, valve seat, and bushings) are constructed separately, and then connected through the roller of the NTF. This sequence enables easy alignment among the components and subsystems.

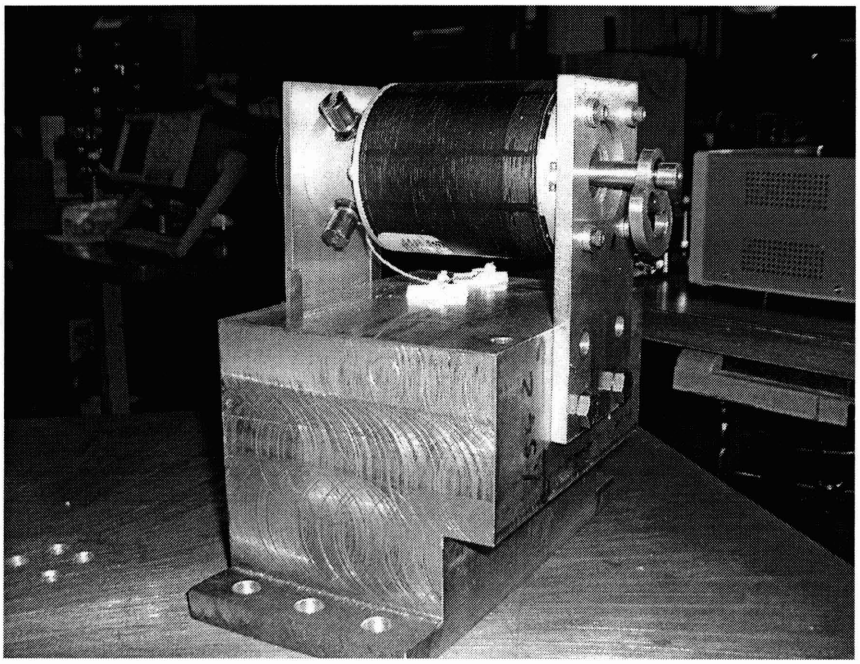

Fig. 7.6. The motor assembly with column I.

The first step in motor-assembly is to pass the front motor bracket over the motor shaft. Next, the disc cam and the bearing assembly (the bearing plus the bearing housing) are press-fit onto the motor shaft to pre-determined positions. In fact, in the first experiment, we did not assemble the bearing assembly, so that we could test, assemble, and disassemble the apparatus easily. Last, the front and rear motor brackets are carefully attached to the front and back mounting surfaces of the motor, using screws. Shims between the bracket surfaces and the column surface are added for alignment. Fig. 7.6 shows the motor assembly mounted on column I.

The valve assembly is constructed by first press-fitting the top and bottom bushings into the top and bottom plates, respectively. Next, the valve-seat plate, the bottom plate, and the bottom spring are passed over the valve stem. After the spring divider is press-fit onto the valve stem to the pre-determined location, the top spring and top plate are passed over the valve stem. After inserting the two precision bars to align the top and bottom plates, both springs are carefully pre-compressed using the three sets of nuts and bolts. Fig. 7.7 shows the completed valve assembly. The valve holder is press-fit onto the top of the valve stem. After the top plate of the valve assembly is bolted onto the top of columns I and II, the roller of the NTF is inserted between the valve assembly and the motor assembly. Only then is the valve seat bolted to the underside of columns I and II. Shims are inserted to align the valve assembly relative to the motor assembly and to adjust the height of the valve seat relative to the valve's landing height. The bearing housing is bolted to the bearing-housing holder, which is in turn bolted into the top of the column II. Component dimensions and tolerances are specified precisely for press-fits and key alignment features of the assembled apparatus. Fig. 7.8 shows the front view of the EMVD apparatus, and Fig. 7.9 shows the integrated mechanical system. Appendix C shows detailed drawings of all mechanical components and subsystems with their dimensions and tolerances.

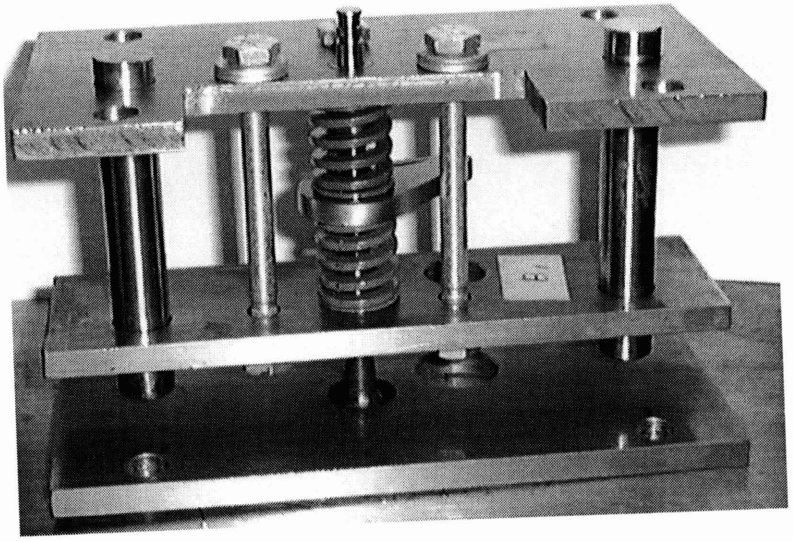

Fig. 7.7. The valve assembly.

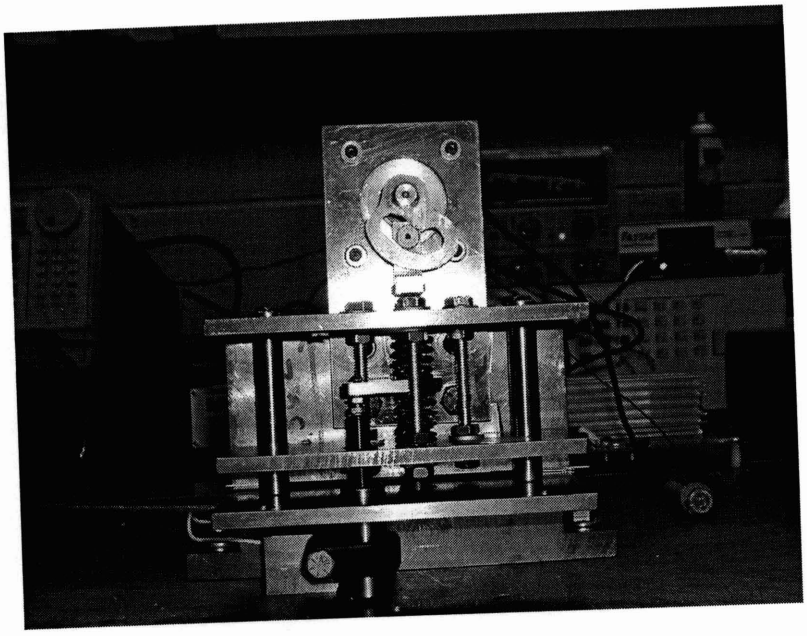

Fig. 7.8. Front view of the EMVD apparatus without column II.

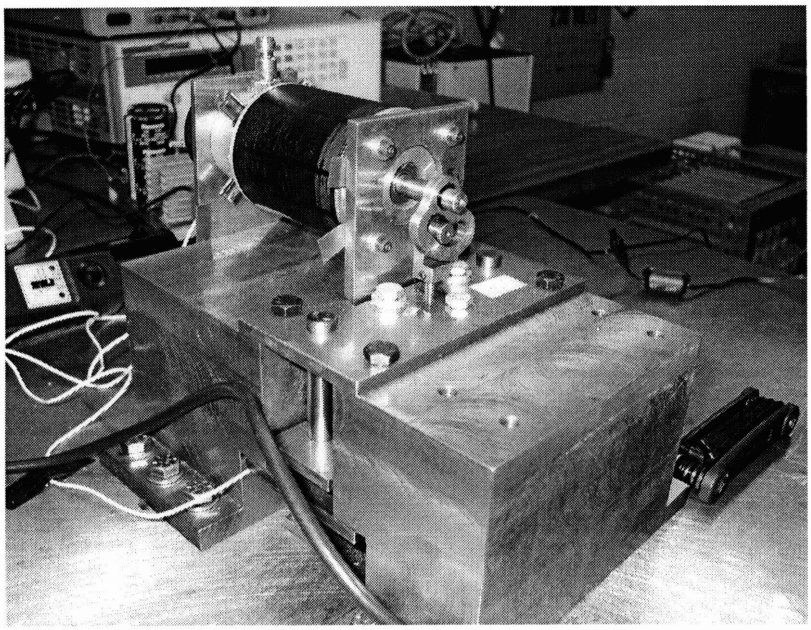

Fig. 7.9. The integrated mechanical system of the EMVD apparatus.

8 Design of Controllers

This chapter describes the design of controllers for the three EMVD operating modes-initial, holding, and transition modes. Though the operating modes are the same as in the NFEMVD, as explained in Chapter 3, the proposed EMVD requires controllers designed with consideration for its nonlinear characteristics. Fig. 8.1 shows the valve profile of the EMVD with the three operating modes labeled.

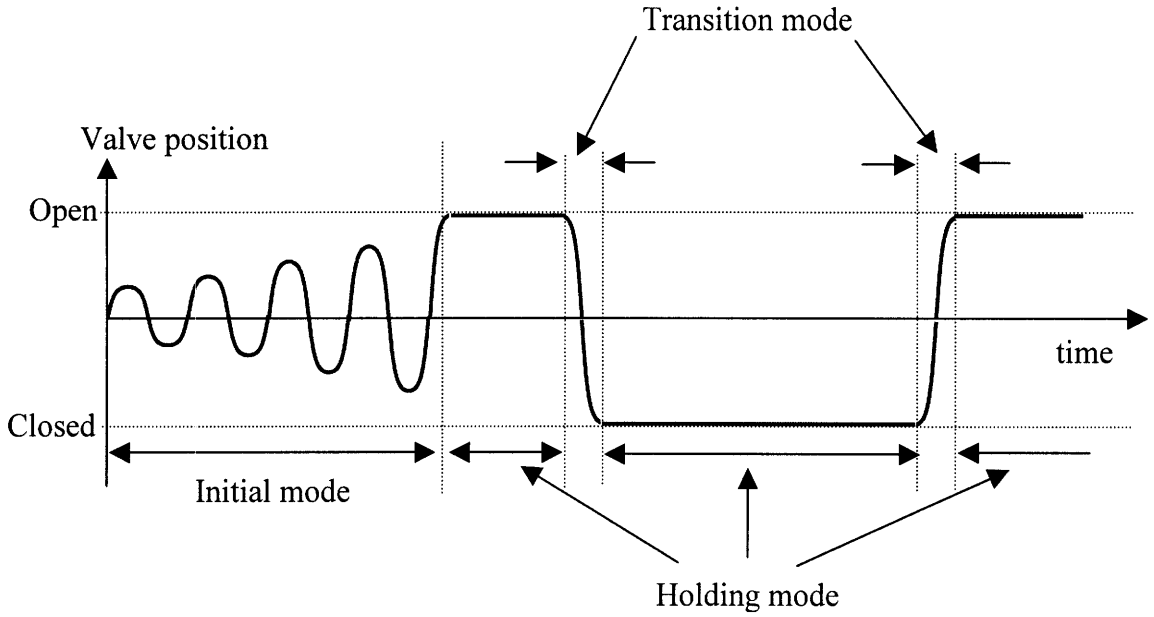

Fig. 8.1. A valve position profile showing the three basic operating modes: initial, holding, and transition.

8.1 Initial-Mode Control

Upon system startup, the valve is moved from the rest position (the middle of the stroke) to the open or closed position quickly and within acceptable current limits. An efficient strategy for initial-mode actuation is to apply torque pulses whose frequency is close to

the natural frequency of the EMVD. The time necessary to open or close the valve depends on the natural mechanical frequency, the quality factor (i.e., damping ratio) of the EMVD, and the magnitude of the applied torque pulses.

A feedback control law for the initial mode control is given by:

$$i = \frac{\alpha \cdot \omega}{|\omega|}, \quad \omega \neq 0 \tag{8.1}$$

where ω and α are the angular velocity of the motor and a pre-determined constant value (for example, 7 A), respectively. In a discrete implementation, i keeps its previous value whenever $\omega = 0$. Assuming that the NTF has the nominal modulus, the simplified equation of motion for the EMVD is:

$$J\frac{d^2\theta}{dt^2} + b\frac{d\theta}{dt} + k\theta = K_T i, \tag{8.2}$$

where K_T is the torque constant of the motor.

To understand the response of the mechanical model to a train of current pulses based on (8.1), assume that $i = \alpha > 0$, $0 < \zeta$ (the damping ratio) < 1, and zero state initial conditions. The first peak in valve position (θ_1) is:

$$\theta_1 = (1 + e^{-\frac{\zeta\pi}{\sqrt{1-\zeta^2}}}) \cdot K_T \cdot \alpha > 0, \tag{8.3}$$

at $t = t_0 \equiv \pi/\omega_d$, where ω_d is the damped natural frequency. As soon as the rotor reaches the first peak, $i = -\alpha$ is applied to the EMVD according to (8.1), and the next peak position, θ_2, is

$$\theta_2 = \theta_1 \cdot \gamma < 0, \tag{8.4}$$

at $t_n = t_0 \cdot 2$, where

$$\gamma = -(1 + e^{-\frac{\zeta\pi}{\sqrt{1-\zeta^2}}}). \tag{8.5}$$

Similarly, θ_n, the n^{th} peak position is obtained by

$$\theta_n = \theta_1 \gamma^{n-1}, \tag{8.6}$$

at $t_n = t_0 \cdot n$. When a peak value is close enough to an end of the stroke, control is switched from the initial-mode controller to the transition-mode controller to ensure a soft valve landing.

With the controller described above, the initial-mode control phase ends quickly after a few, small-magnitude current pulses. Experimental results of initial-mode control will be discussed in Chapter 9.

8.2 Holding-Mode Control

The holding mode is characterized by two parameters: holding time and lift. A second nonlinear mechanical transformer could enable variable lift control in the proposed EMVD, as described in Chapter 10, but the prototype constructed for this thesis research can only alter holding time by shaping the reference input. Note that during the holding period, actuator power is negligible if the slope of the NTF characteristic is almost flat at stroke extremes and disturbances are not large enough to perturb the valve from its equilibrium in the open or closed position, as explained in Chapter 5.

8.3 Transition-Mode Control

As mentioned in Chapter 5, the ideal free-flight valve profile (i.e., the valve kinematics in the absence of friction, disturbances or gas forces) minimizes actuator effort when used as a reference input. The ideal free-flight valve position profile is generated by simulation.

Simple linear controllers such as PD controllers or lead-lag compensators are simple to design, but do not guarantee the best performance. Linear controllers should be designed to meet the desired system bandwidth, and can be based on a linear model, which assumes that the NTF has the nominal modulus over the whole stroke. Chapter 9 will describe the details of the characterization (system identification) of the proposed EMVD, the design of the lead compensator based on the characterization, and the experimental results of the controlled EMVD system.

The dynamic characteristics of the proposed EMVD change significantly as a function of valve or rotor position because of the nonlinear transformer characteristic, and high-performance controller designs must account for this nonlinearity. The effective inertia and stiffness of the EMVD on the actuator side become small near both ends of the stroke and large near the middle of the stroke, so that the system gain changes according to valve or rotor position. One solution is to design a linear controller, such as a proportional-derivative (PD) controller or lead-lag compensator with adjusting gains to compensate a piece-wise linear set of system models. In other words, the z vs. θ characteristic of the NTF is divided into several pieces and modeled linearly for each piece of the region, and the gains of the controller are adjusted based on each piece-wise set of the linear models. The gain sets can be implemented with a look-up table in practice. However, the gain-scheduling technique [43] – adjusting controller gains based on the local linearization – cannot be applied effectively to the proposed EMVD because the operating point of the locally linearized system moves as fast as the EMVD dynamics themselves.

A nonlinear controller based on the feedback-linearization technique is an alternative to the PD controller [38]. This technique generates control inputs to the nonlinear plant in full consideration of the nonlinear model. The motor-current command obtained for the system in (4.14) in conjunction with (4.15) and (4.16), based on the technique, is:

$$i = \frac{1}{B(y_1, y_2)}\left(\frac{\mathrm{d}^2\theta_d}{\mathrm{d}t^2} - A(y_1, y_2) - \mathrm{k}_0 e - \mathrm{k}_1 \frac{\mathrm{d}e}{\mathrm{d}t}\right), \tag{8.7}$$

where y_1, y_2, θ_d, and e represent rotor position, rotor velocity, desired rotor position, and position error (y_1-θ_d), respectively, and k_0 and k_1 are controller gains.

Substituting (8.7) into (4.14), we can obtain the resultant error equation for the system of (4.14) with the nonlinear control input i in (8.7) as follows:

$$\frac{\mathrm{d}^2 e}{\mathrm{d}t^2} + \mathrm{k}_1 \frac{\mathrm{d}e}{\mathrm{d}t} + \mathrm{k}_0 e = 0, \tag{8.8}$$

where the constants k_0 and k_1 are determined so that the bandwidth of the controlled system can be specified.

A position-velocity controller, depicted schematically in Fig. 8.2, is another candidate for transition-mode control. Before explaining the controller operation, consider the position-velocity trajectories of the rotor during a valve transition, as shown in Fig. 8.3. The figure shows the transition-mode trajectories to the target state (origin), without driving input, for cases with and without friction. In other words, Fig. 8.3 (a) shows the state trajectory of the free-flight (without driving input) kinematics for an ideal (without friction) EMVD system, and Fig. 8.3 (b) is the state trajectory to the target state without driving input in the case that the EMVD system is not ideal but has friction. The starting state of the non-ideal system free flight trajectory of Fig. 8.3 (b), state (ii), is different from the actual initial state of the non-ideal system in the transition mode, for example, state (i) having zero starting velocity. If we apply an appropriate driving input so that the state of the system moves from the state (i) to a state on the trajectory of Fig. 8.3 (b), then, after that,

the system inherently follows the trajectory of Fig. 8.3 (b) without electrical power input, and finally reaches the target state. This relieves the motor of effort during the rest of the transition. Since the system model is not perfect in practice, the system is feedback controlled to follow the desired free flight velocity trajectory. Fig. 8.2 shows a schematic view of the control system. In the position-velocity feedback control system, the reference input is a train of rectangular pulses commanding the final rotor position. Once the target position is set, the controller drives the plant along a natural, pre-determined trajectory as in Fig. 8.3 (b).

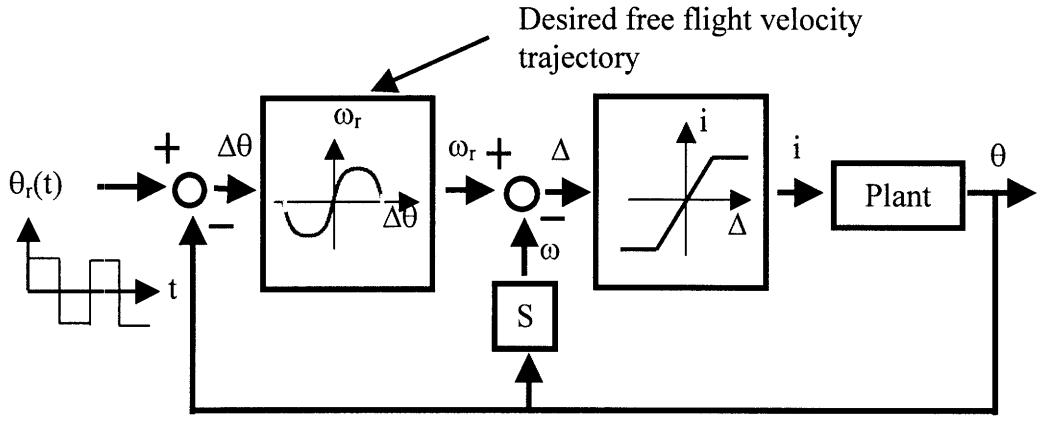

Fig. 8.2. Position-velocity feedback control system with a desired trajectory in the phase plane.

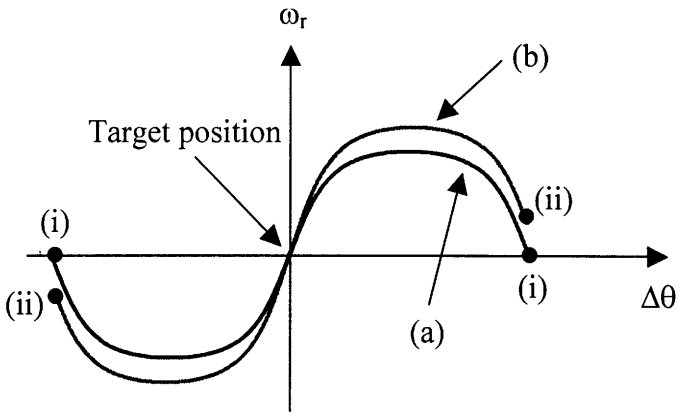

Fig. 8.3. Position-velocity phase plane trajectory to the target without electrical input for the EMVD apparatus for cases (a) with and (b) without friction force.

9 Experiments

This chapter presents the experimental results of the proposed EMVD design. The valve assembly and apparatus are characterized, and the performance of the controlled system is measured. The beneficial features of the design are confirmed.

9.1 Characterization of the Apparatus

The valve assembly (consisting of the valve, valve holder, two springs, spring divider, top and bottom plates, valve seat, and bushings in Fig. 7.7) and the EMVD assembly (consisting of the NTF, motor, and the valve assembly in Fig. 7.9) must be characterized before designing effective controllers. System identification can proceed from measured time response. Fig. 9.1 shows the time response of the free oscillation of the valve assembly. The measured damped natural frequency (ω_d) and time constant τ, given by

$$\tau = \frac{1}{\zeta\omega_n} = \frac{b}{m}, \tag{9.1}$$

where ω_n, m, and b are the natural frequency, moving mass, and viscous friction coefficient, respectively, provide estimates of the quality factor (Q) or damping ratio (ζ):

$$Q = \omega_n \frac{m}{b} = \frac{1}{2\zeta}. \tag{9.2}$$

The measured ω_d and the Q calculated by (9.1) and (9.2) are 1162 rad/s and 16, respectively, from the data of Fig. 9.1. With a Q of 16, $\omega_n \sim \omega_d$, so that the undamped

natural frequency $\omega_n = \sqrt{\frac{k}{m}}$ and the combined spring stiffness (k) of 112 N/mm (from the data sheet of the springs) yield an estimate of the moving mass on the valve side as follows:

$$m = \frac{k}{\omega_n^{\,2}} = \frac{1.2 \cdot 10^5}{1162^2} \cong 0.083\,\text{kg}, \tag{9.3}$$

which is close to the expected value of 90 g. Given the mass, quality factor, and stiffness, the viscous-friction coefficient for the valve assembly is obtained as

$$b = \frac{\omega_n m}{Q} = \frac{1162 \cdot 0.083}{16} \cong 6\ \text{kg/s}. \tag{9.4}$$

In conclusion, the characteristic equation for the valve assembly on the valve side is:

$$ms^2 + bs + k \cong 0.083s^2 + 6s + 1.12 \cdot 10^5 = 0. \tag{9.5}$$

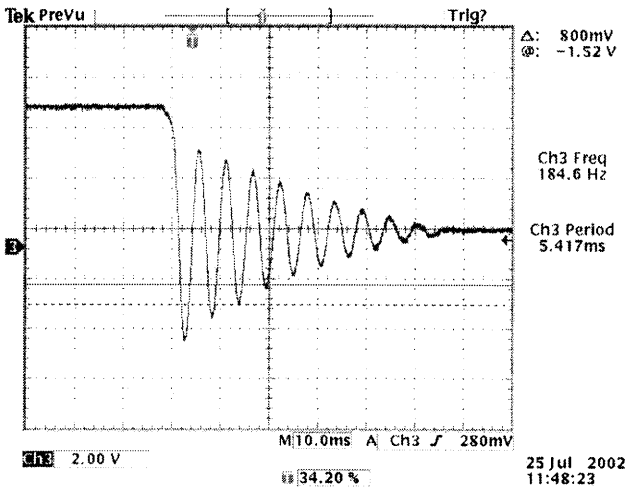

Fig. 9.1. The time response (valve position vs. time) of the free oscillation of the valve assembly.

Fig. 9.2 shows the time response of the free oscillation of the EMVD assembly. Assuming that the NTF has the nominal modulus over the whole stroke, the measured ω_d and the Q, calculated by (9.1) and (9.2), are 659 rad/s and 6, respectively. The total inertia in the actuator side, J_t, is $1.2 \cdot 10^{-5}$ kg-m^2 (the sum of the measured rotor inertia of $5.2 \cdot 10^{-6}$ kg-m^2 [42], disk cam inertia of $7.3 \cdot 10^{-7}$ kg-m^2 [42], and reflected inertia of the moving mass on the valve side of $6.4 \cdot 10^{-6}$ kg-m^2, obtained by $m \cdot (r)^2$, where m is 0.083 kg from (9.3) and r was chosen as $8.8 \cdot 10^{-3}$ m/rad in Chapter 7). The stiffness (k_θ = 5.4 N-m/rad) in the actuator side is obtained as follows:

$$k_\theta = J_t \cdot \omega_n^2, \tag{9.6}$$

where $J_t = 1.2 \cdot 10^{-5}$ kg-m^2, and $\omega_n = \omega_d / \sqrt{1-\zeta^2}$, with ω_d = 659 rad/s, $\zeta = (2Q)^{-1}$, and Q = 6. The viscous friction coefficient (b_θ) for the EMVD assembly is approximately $1.3 \cdot 10^{-3}$ kg-m^2/s, calculated by

$$b_\theta = \frac{\omega_n J_t}{Q} = \frac{664 \cdot 1.2 \cdot 10^{-5}}{6} \cong 1.3 \cdot 10^{-3} \text{ kg-m}^2/\text{s}. \tag{9.7}$$

In conclusion, the transfer function of the EMVD assembly is:

$$\frac{\theta(s)}{I(s)} = \frac{K_T}{J_t s^2 + b_\theta s + k_\theta}, \tag{9.8}$$

where $I(s)$ is input current, and $\theta(s)$ is rotor displacement, and K_T is the torque constant of the motor (0.07 N-m/A). Fig. 9.3 shows the Bode plot for (9.8). The measured friction coefficient of the motor, $b_{\theta m}$, is $2.1 \cdot 10^{-4}$ kg-m^2/s [42], and the reflected friction coefficient of the valve assembly, $b_{\theta v}$, is $4.6 \cdot 10^{-4}$ kg-m^2/s, calculated by $b_{\theta v} = b \cdot (r)^2$, where b is 6 kg/s from (9.4) and r was chosen as $8.8 \cdot 10^{-3}$ m/rad in Chapter 7. Therefore, the friction coefficient due to the NTF alone, $b_{\theta NTF}$ is $6.3 \cdot 10^{-4}$ kg-m^2/s – approximately half of the entire friction coefficient – calculated by $b_{\theta NTF} = b_\theta - b_{\theta m} - b_{\theta v}$, assuming that the motor friction does not change significantly after the valve assembly is attached.

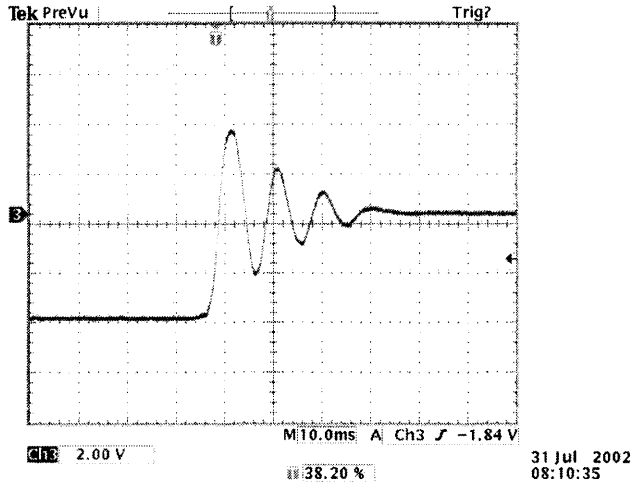

Fig. 9.2. The time response (valve position vs. time) of the free oscillation of the EMVD assembly.

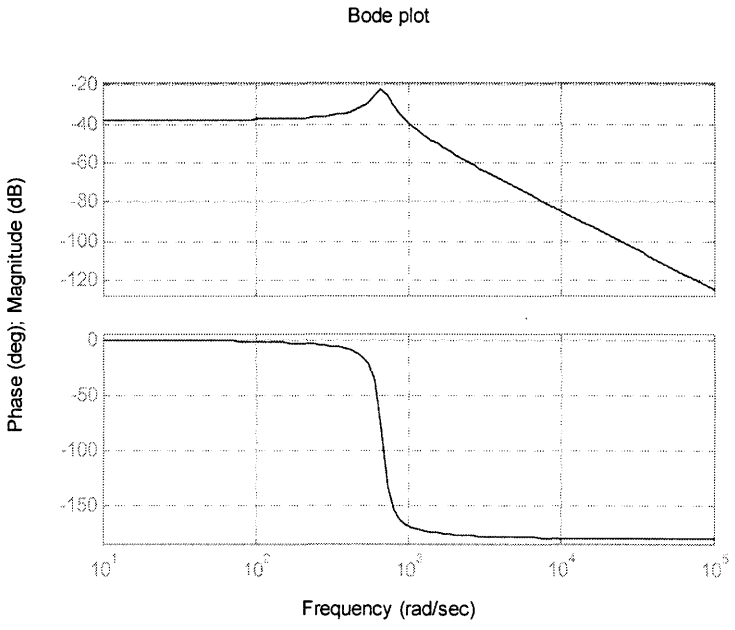

Fig. 9.3. The Bode plot for (9.8).

Based on the above system identification, we can approximately estimate the coefficients of the mathematical model of (4.14) through (4.16). For convenience, the equations are repeated:

$$\begin{aligned} \frac{dy_1}{dt} &= y_2, \\ \frac{dy_2}{dt} &= A(y_1, y_2) + B(y_1, y_2)i, \end{aligned} \tag{9.9}$$

where

$$\begin{aligned} A(y_1, y_2) &= \frac{-1}{\mathrm{J} + \mathrm{m_v}\left(\frac{dg}{d\theta}\right)^2}\left\{\left(\mathrm{b} + \mathrm{b_v}\left(\frac{dg}{d\theta}\right)^2\right)y_2 + \mathrm{m_v}\frac{d^2g}{d\theta^2}\frac{dg}{d\theta}{y_2}^2 + \mathrm{k}g(\theta)\frac{dg}{d\theta}\right\}, \\ B(y_1, y_2) &= \frac{1}{\mathrm{J} + \mathrm{m_v}\left(\frac{dg}{d\theta}\right)^2}\mathrm{K_T}, \end{aligned} \tag{9.10}$$

where the state variables y_1 and y_2 represent rotor position and velocity, respectively, and $z = g(\theta)$ is given by (7.1).

The parameter J (inertia on the actuator side) is $5.9 \cdot 10^{-6}$ kg-m^2, obtained by the sum of the measured rotor inertia of $5.2 \cdot 10^{-6}$ kg-m^2 and the calculated disk cam inertia of $7.3 \cdot 10^{-7}$ kg-m^2. The moving mass on the valve side m_v is 0.083 kg from (9.5). The viscous friction coefficient on the actuator side b is $8.4 \cdot 10^{-4}$ kg-m^2/s, obtained by the sum of the motor friction coefficient of $2.1 \cdot 10^{-4}$ kg-m^2/s and the estimated NTF friction coefficient of $6.3 \cdot 10^{-4}$ kg-m^2/s. The viscous friction coefficient on the valve side b_v is 6 kg/s from (9.5). The stiffness of the springs on the valve side k is $1.12 \cdot 10^5$ N/m from (9.5), and the torque constant K_T is 0.07 Nm/A.

The transfer functions for two extreme cases –the middle of the stroke and stroke ends – can be determined directly from the state-space formulation of (9.9) and (9.10) in conjunction with the estimated parameters.

In the middle of the stroke, the linearized modulus of the NTF is $\pi r_n/2$, where r_n is the nominal modulus. At the middle of the stroke, then, the transfer function for the apparatus becomes

$$\frac{\theta(s)}{I(s)} = \frac{0.07}{2.2 \cdot 10^{-5} s^2 + 2.0 \cdot 10^{-3} s + 13}. \tag{9.11}$$

Fig. 9.4 shows the Bode plot of (9.11).

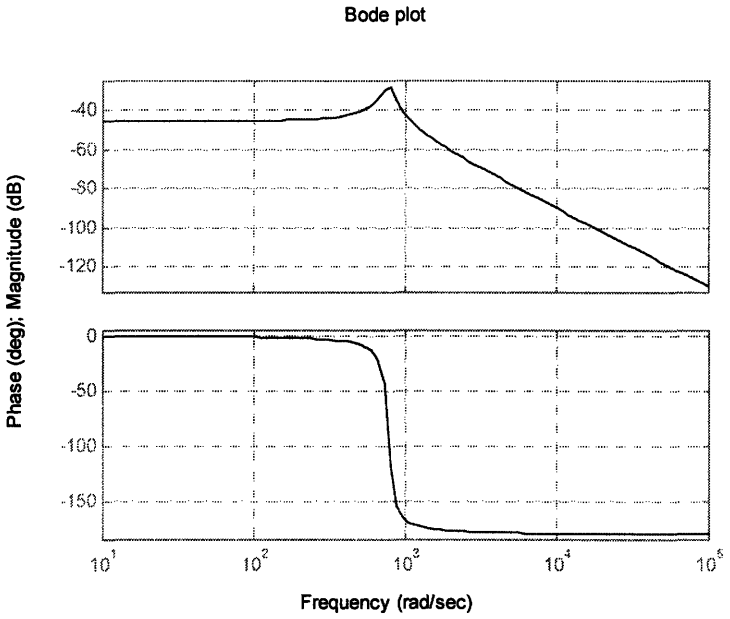

Fig. 9.4. The Bode plot for (9.11).

At the ends of the stroke, assuming that the NTF has perfectly flat ends, the transfer function is

$$\frac{\theta(s)}{I(s)} = \frac{0.07}{5.9 \cdot 10^{-6} s^2 + 8.6 \cdot 10^{-4} s}. \tag{9.12}$$

Fig. 9.5 shows the Bode plot of (9.12).

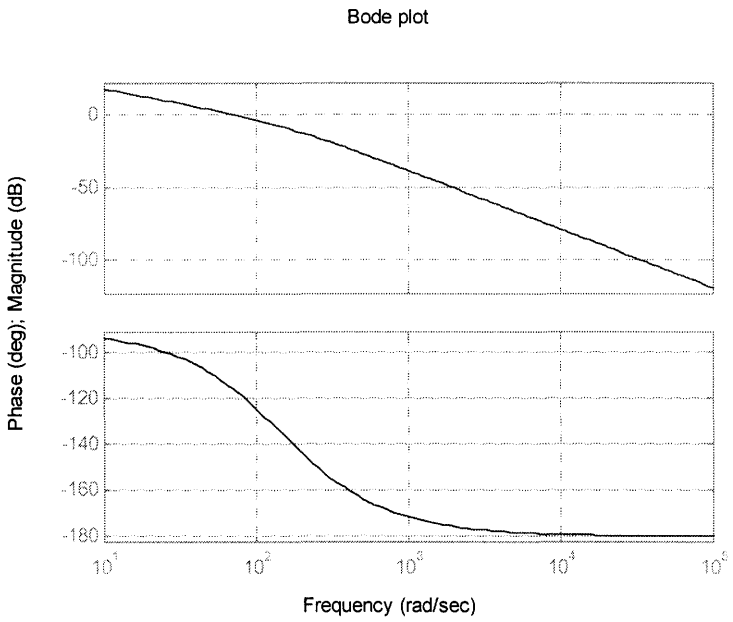

Fig. 9.5. The Bode plot for (9.12).

9.2 Implementation of Controllers

For the system of (9.8) with the nominal transformer modulus, a simple lead controller [44] for the transition mode was designed in the experiment:

$$G_c(s) = G_{DC} \frac{\frac{s}{p}+1}{\frac{s}{z}+1}, \tag{9.13}$$

where G_{DC} (dc gain of the controller) = 250, p (pole frequency) = 1250 rad/s, z (zero frequency) = 5000 rad/s. To explain how to determine the three parameters (G_{DC}, p, and z), consider Fig. 9.6, a general Bode plot for (9.13). Given p and z, we can determine ω_m (geometric center frequency) $\equiv \sqrt{p \cdot z}$ and φ_m (peak phase lead) $\equiv \sin^{-1}(\frac{\alpha-1}{\alpha+1})$, where α (pole zero ratio) $\equiv p/z$. The EMVD plant of (9.8) has a dc gain of –38 dB, as shown in Fig.

9.3. In order to achieve a dc gain of –2.4 dB (greater than -3 dB) of the overall feedback controlled system, the dc gain of the open transfer function, consisting of the EMVD plant and the controller, should be 10 dB. Therefore, the dc gain of the controller, G_{DC} should be 38 dB + 10 dB = 48 dB = 250. With G_{DC} = 48 dB, the phase margin might be very small unless the controller of (9.13), whose Bode plot is shown in Fig. 9.7, increases the phase of the open loop transfer function, consisting of (9.8) and (9.13), as shown in Fig. 9.8. To obtain a phase margin of 30-40° at the desired bandwidth frequency of the overall controlled system, which is between 2000 and 3000 rad/s (several times the valve operation frequency), we tentatively specify $\varphi_m = 37°$ at $\omega_m = 2500$ rad/s. The specified values determine $\alpha = 4$, p = 5000 rad/s, and z = 1250 rad/s. Fig. 9.9 shows the Bode plot of the closed-loop system. The bandwidth is approximately 300-400 Hz, which is about two to three times the valve operating frequency, as desired.

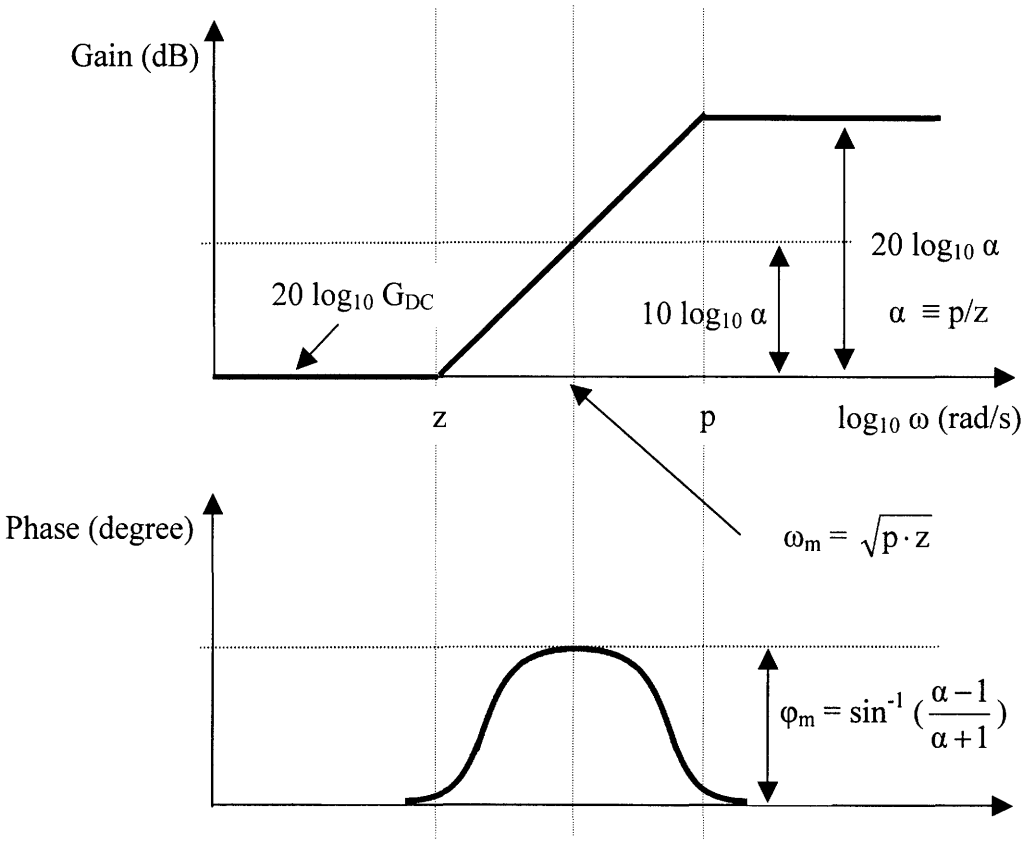

Fig. 9.6. Bode plot of a general lead compensator.

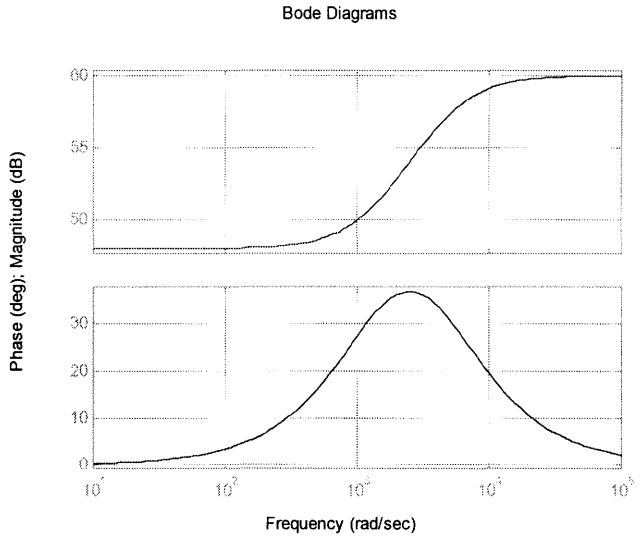

Fig. 9.7. Bode plot for the lead compensator of (9.13).

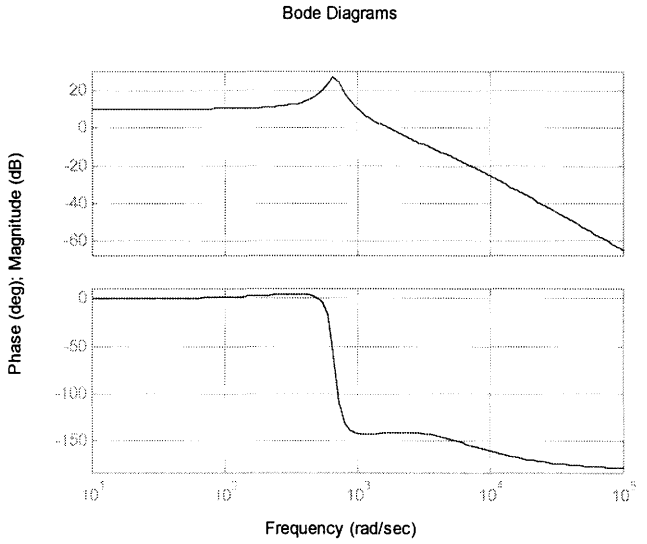

Fig. 9.8. Bode plot for the open loop transfer function, consisting of (9.8) and (9.13).

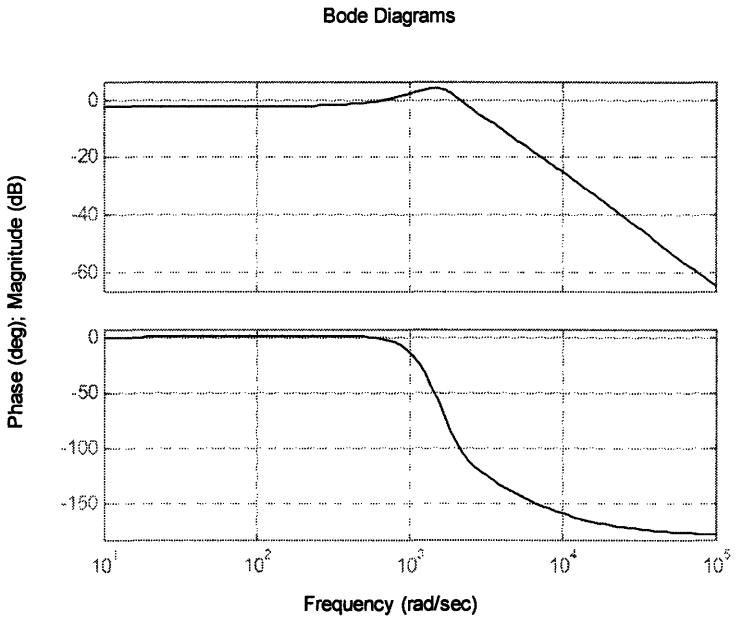

Fig. 9.9. The Bode plot for the overall closed loop transfer function.

9.3 Performance Measurements of the EMVD Apparatus

The EMVD apparatus, shown in Fig. 9.10, is operated in three modes – initial, transition, and holding – as mentioned in Chapter 8. The control law of (8.1) with $\alpha = 7$ A was used for the initial mode, and for simplicity, the control law of (9.13) was used for both the transition and holding modes in the experiment. Fig. 9.11 shows the rotor- and valve-position profiles during the initial mode and the corresponding motor current. As the valve nears the fully open or closed position, the controller is changed to the transition-mode law. The initial mode was completed within 35 ms with +/- 7 A. The average power during the initial mode is approximately 150 W.

After the initial mode, the valve is retained at one end of the stroke in the holding mode. The non-zero holding current in the holding mode in Fig. 9.11 results from non-zero steady state position errors. However, we observed that the valve was held at the end of the stroke even after the electrical power was cut off. Therefore, the required holding current is zero, as expected.

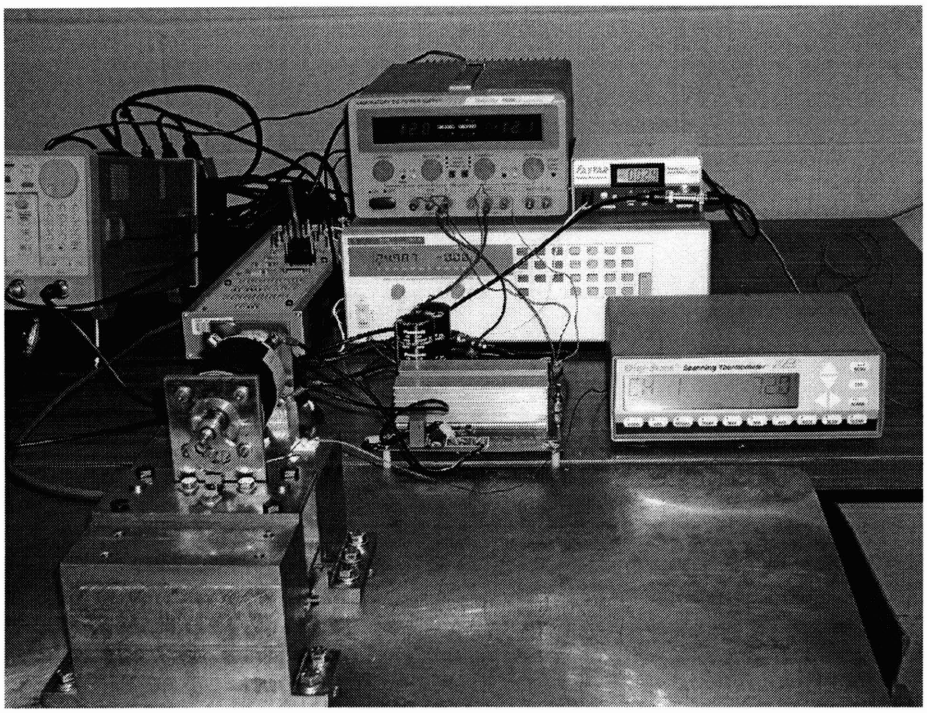

Fig. 9.10. The constructed EMVD apparatus.

The key performance measures of the transition-mode controller are transition time, seating velocity, and power. Fig. 9.12 shows the valve and rotor position profiles, and the corresponding current during the transition mode. In the experiment, we limited the maximum current level to 18 A to relieve the motor drive and motor of thermal stresses. For simplicity we employed the lead compensator of (9.13). The transition time was approximately 3.5 ms, which can support engine operation at 6000 rpm. The consumed energy was approximately 1.4 J per transition. Since there are two transitions per cycle, 2.8 J per cycle is consumed for the apparatus. At 6000 rpm engine speed, the crankshaft rotates at 100 (rev/s), and the camshaft rotates at 50 (rev/s). Therefore, the nominal period of the valve profile at 6000 rpm engine speed is 20 ms, giving an average power of 140 W per valve at 6000 rpm, assuming the holding power is negligible. In general, the average power per valve, P (W), for the proposed apparatus is obtained as

$$P = \frac{1.4 \cdot N}{60}, \tag{9.14}$$

where N = engine speed (rpm).

The experimental apparatus did not include gas force. Therefore, the estimated power of (9.14) is for the case of an intake valve. As described in Chapter 2, an exhaust valve requires an additional 0.7 J per cycle at full engine speed and load to compensate for the gas force, giving an average power of 35 W per exhaust valve. Therefore, the apparatus is expected to require 140 W per intake valve and 175 W (140 + 35 W) per exhaust valve at 6000 rpm engine speed and full load. Note that the required gas work depends on engine speed and load. The proposed apparatus is expected to require 2.5 kW at full engine speed and load for a 4 cylinder, 8 intake valve and 8 exhaust valve engine, which is comparable to the power required to compensate for friction in a conventional valvetrain for the same engine and conditions without roller followers, approximately 3 kW, as described in Chapter 2. A conjugate disk cam (Fig. 4.10), however, can reduce the required power of the proposed EMVD because there is no reversal of the roller rotational direction in the middle of the stroke, as described in Chapter 7. The transition-mode controller allows overshoot in the rotor displacement, as seen in Fig. 9.12.

The NTF-based EMVD achieved a 3.5 ms transition time with acceptable power consumption using a rotary motor, and is a strong candidate for future VVA systems.

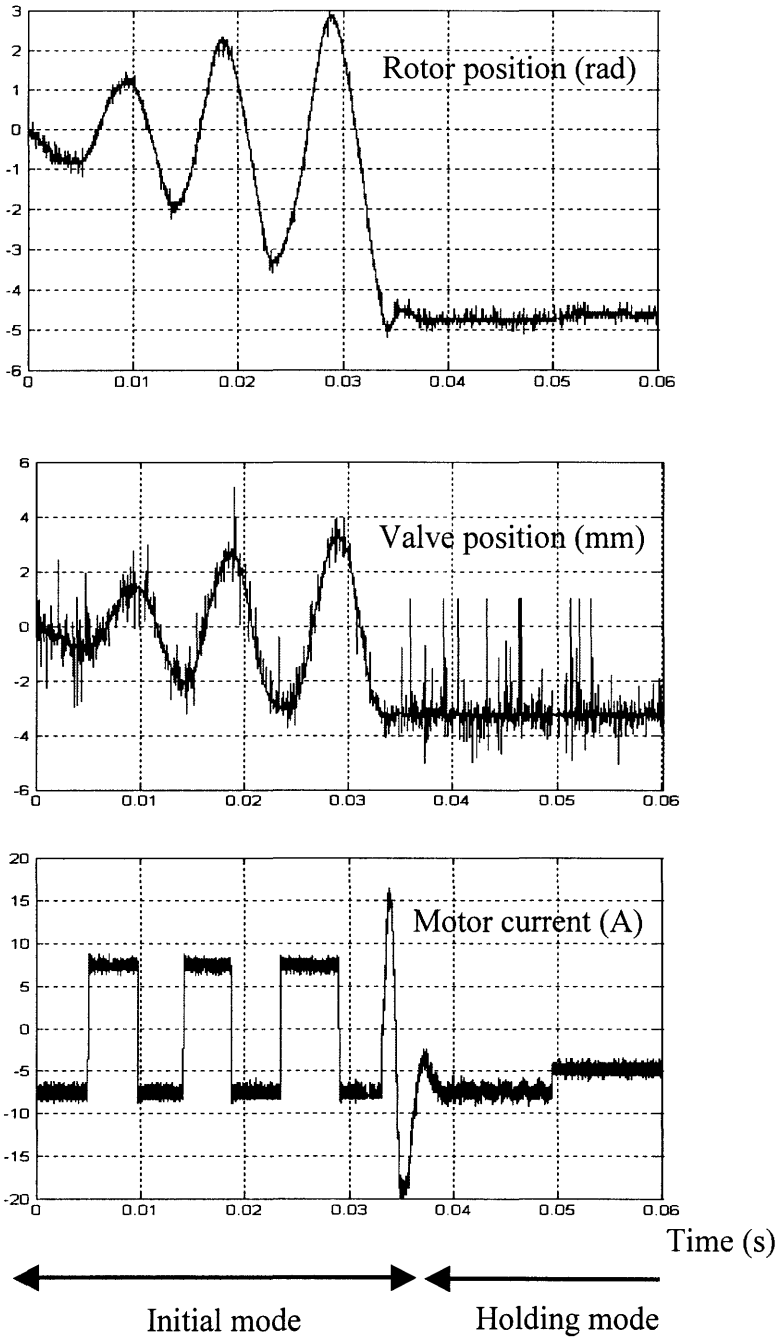

Fig. 9.11. Valve and rotor positions and corresponding current with respect to time during the initial and holding modes.

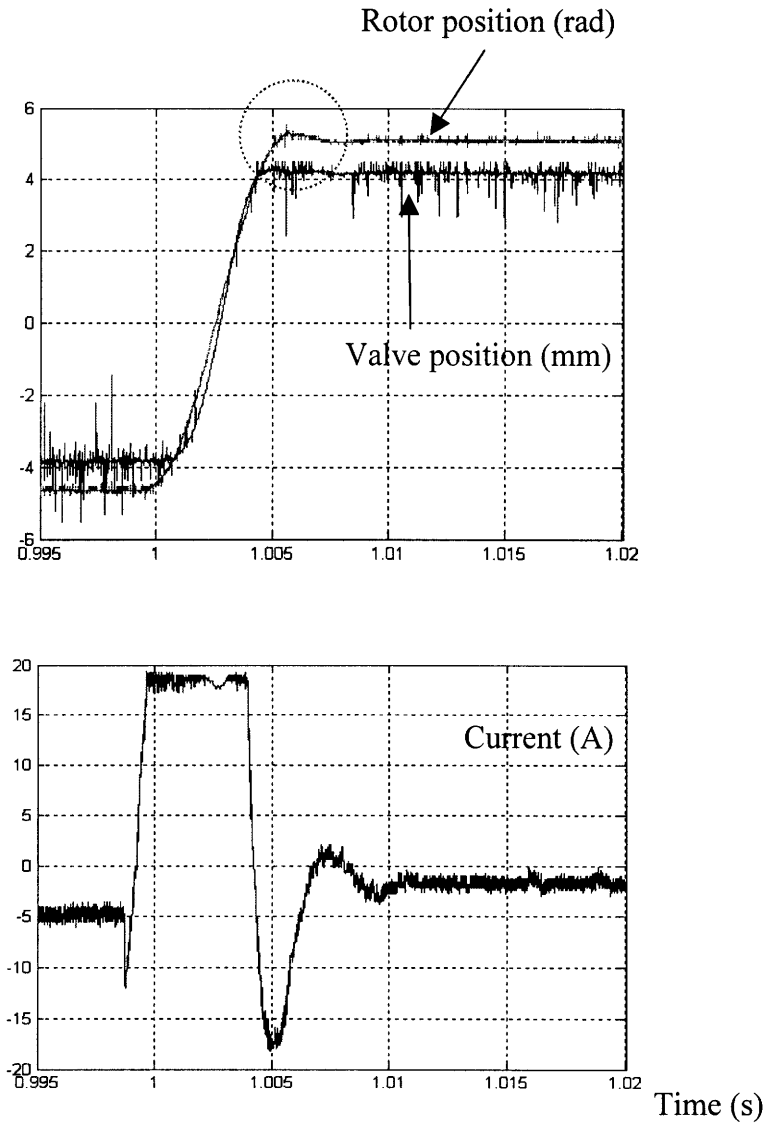

Fig. 9.12. Valve and rotor positions and corresponding current with respect to time during the transition mode.

10 Design Refinements

This chapter describes the conceptual design of a lash-adjustment device and a lift-control mechanism, and the optimization of the NTF for minimized actuator torque

10.1 Proposal for a Lift Control Mechanism

Variable lift control in the proposed EMVD can be accomplished with a second nonlinear mechanical transformer (NTF 2) in combination with the original NTF (NTF 1), as illustrated in Fig. 10.1 (a). NTF 2 controls the amplitude of the modulus of the NTF 1, generating a transformer characteristic (between x_2 and x_3) with an extra degree of freedom:

$$x_3 = a \cdot (x_2 + \frac{\mathrm{L}}{2}) - \frac{\mathrm{L}}{2}, \tag{10.1}$$

where L represents full lift, and $0 \leq a \leq 1$. A larger a, controlled by a second actuator, results in larger partial lift. The combined NTF characteristic of NTFs 1 and 2 is shown in Fig. 10.1 (b). Fig. 10.2 shows a simple sliding-fulcrum implementation of the variable transformer characteristic of (10.1). Given a, the second actuator controls the position of the pivot point of the sliding-fulcrum. Fig. 10.3 shows a conceptual design of the proposed EMVD enabling variable lift control and a desired characteristic of the combined NTF.

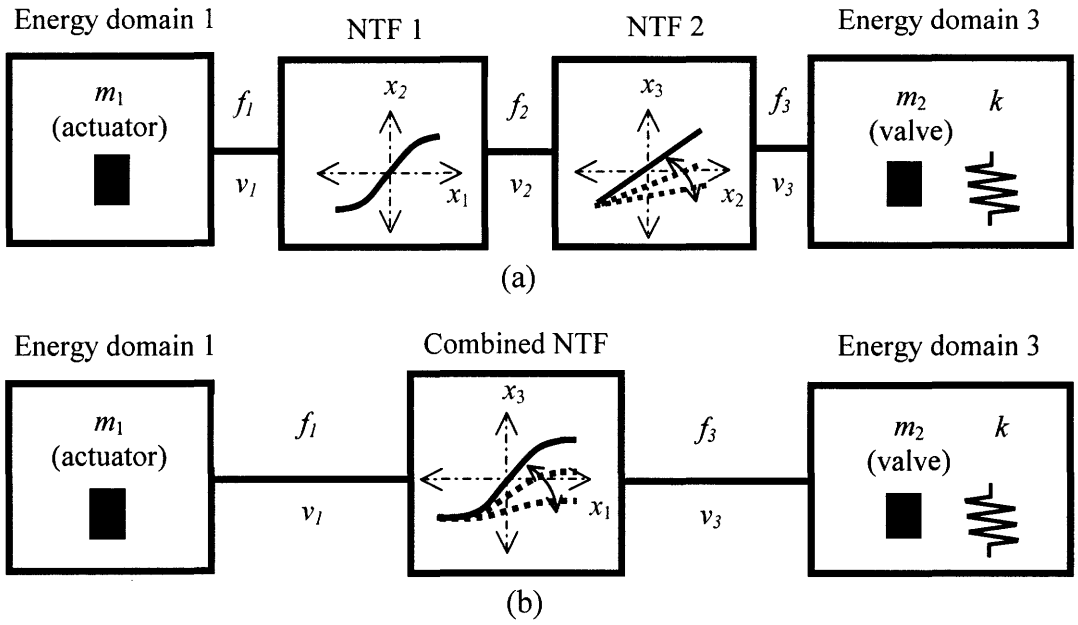

Fig. 10.1. (a) Another NTF (NTF 2) plus the original NTF (NTF 1) to offer lift control. (b) An NTF equivalent to the combination of NTFs 1 and 2.

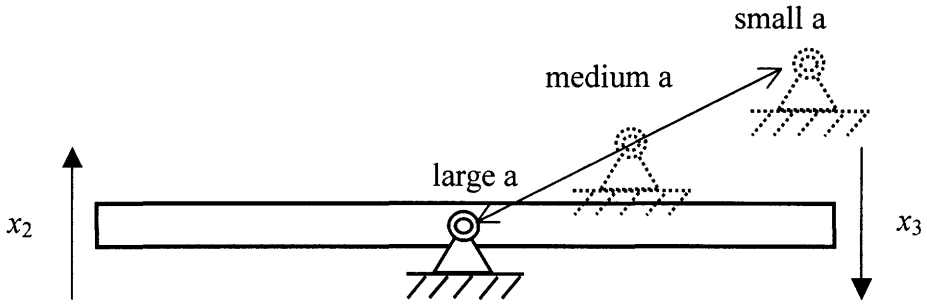

Fig. 10.2. A simple example of the NTF 2.

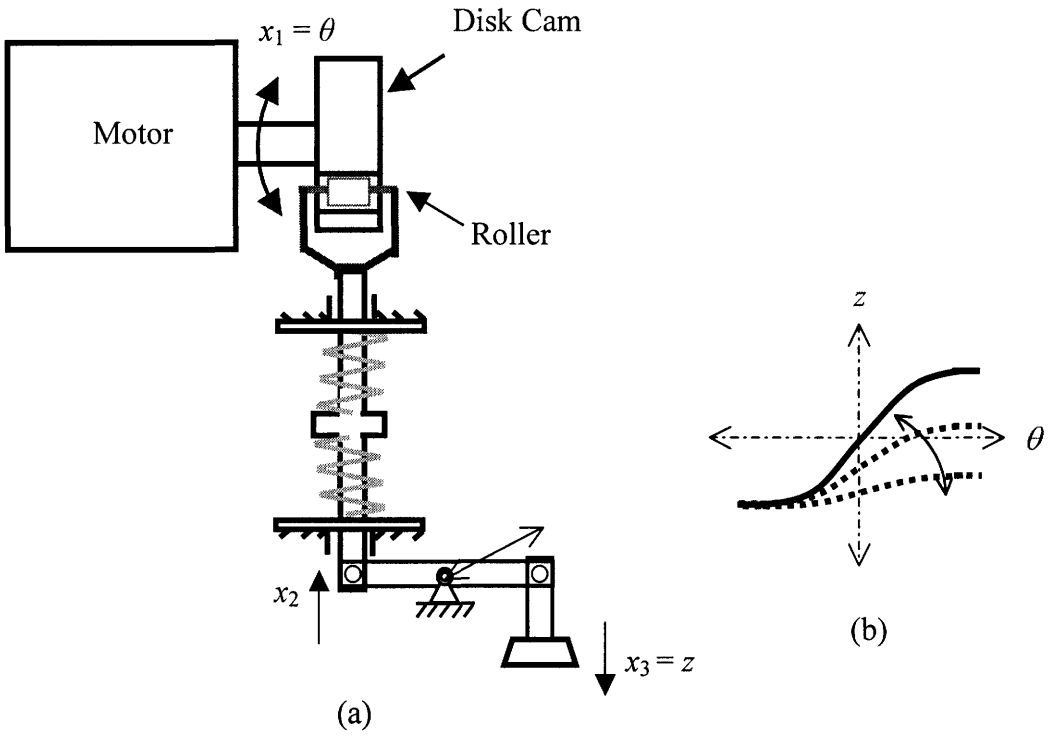

Fig. 10.3. (a) Conceptual design of the proposed EMVD with variable lift control; (b) A desired characteristic of the combined NTF.

10.2 Proposal for a Lash Adjustment Device

The proposed EMVD needs a lash adjuster to compensate for temperature change, wear, and manufacturing tolerances of the valvetrain. Unlike conventional valvetrains, in the NTF-based EMVD the spring force is zero in the middle of the stroke, and lash adjusters for conventional valvetrains do not work in this case because valve springs always under compression transmit the compressed force to the lash adjusters in conventional valvetrains.

Fig. 10.4 (a) shows a lash-adjuster design for the NTF-based EMVD, which was conceptually proposed for the first time by Dr. Thomas Keim. The lash adjuster, consisting of a spring (k_l) and a damper (b_l), is a low pass filter whose cut-off frequency is far below the operating frequency of the valve. The effective moving mass (m_1) is very

small compared to the mass of the EMVD block (m_2) so that the effect of valve dynamics on the EMVD block dynamics is negligible. The spring (k_l) is always compressed. In the case where the spring resists the action of gravity on the EMVD block, as suggested in Fig. 10.4 (a), the compression of the spring is greater than that caused by m_2. The dc component of excess spring force is balanced by an identical dc component at the valve/valve-seat interface. The lash is adjusted since the equilibrium position of the valve is determined by the position where the valve lands on the valve seat, regardless of wear, temperature change, and manufacturing tolerances in the EMVD. Fig. 10.4 (b) shows a simplified mathematical model of the adjuster. The variables x_1 and x_2 represent the displacements of the effective moving mass and the EMVD block with respect to the cylinder head, respectively. Note that the effective viscous friction, the effective force source, the effective stiffness, and the effective moving mass in Fig. 10.4 (b) are nonlinear in the NTF-based EMVD. The equation of motion for m_1 respect to the displacement of m_2 is the same as in (4.7)-(4.9).

The lash adjuster can alternatively be placed between the valve seat and the cylinder head instead of between the EMVD block and the cylinder head, as shown in Fig. 10.5. The valve seat is supported by the lash adjuster and floated relative to the cylinder head. This configuration requires the implementation of a moving seal between the valve seat and the cylinder head.

10.3 Optimization of an NTF to Minimize Motor Size

The motor must be small enough to fit the limited space available over the engine head. The required peak motor torque, indicative of motor size, can be minimized by optimizing the transformer modulus, since the peak motor torque depends on the modulus.

Assume the torque and force balance equations in (4.7) and (4.8) hold. According to the simulation result in Fig. 5.4, motor torque is maximum at approximately midstroke because the reflected gas-force torque and the viscous friction torque are maximum there.

In the middle of the stroke, the effective inertial torque and the effective spring torque are small and cancel each other if the valve follows the reference input (i.e., follows the ideal free-flight profile, as described in Chapter 5). Viscous friction is dominant near the middle of the stroke, and is greater than the Coulomb friction because the spring force is small in midstroke. The torque balance equation near the middle of the stroke becomes, approximately:

$$\tau_p = r \cdot \left(F_{gas} + F_{friction}\right), \tag{10.2}$$

where τ_p is the peak motor torque, r is the transformer modulus in the middle of the stroke, and F_{gas} and $F_{friction}$ are gas and friction forces in the middle of the stroke. For intake valves, F_{gas} is negligible, and for exhaust valves, at full engine speed and load, near the middle of the stroke,

$$F_{gas} \approx \text{constant}. \tag{10.3}$$

Assume the friction force in the NTF, depending on its design as discussed in Chapter 4, is negligible for simplicity. Then, $F_{friction}$ can be expressed as

$$F_{friction} = \left(\mathrm{b_v} + \frac{\mathrm{b}}{r^2}\right) v_{\max}, \tag{10.4}$$

where $\mathrm{b_v}$ and b represent viscous friction on the valve side and on the actuator side respectively, and b/r^2 is the reflected viscous friction of the motor, and v_{max} is the maximum velocity of the valve in the middle of the stroke. Suppose the EMVD meets the transition time requirement and has constant moving mass and stiffness in the z domain. Then,

$$\omega_n = \sqrt{\frac{\mathrm{k}}{\mathrm{m_v} + \frac{J}{r^2}}} = \text{constant}, \tag{10.5}$$

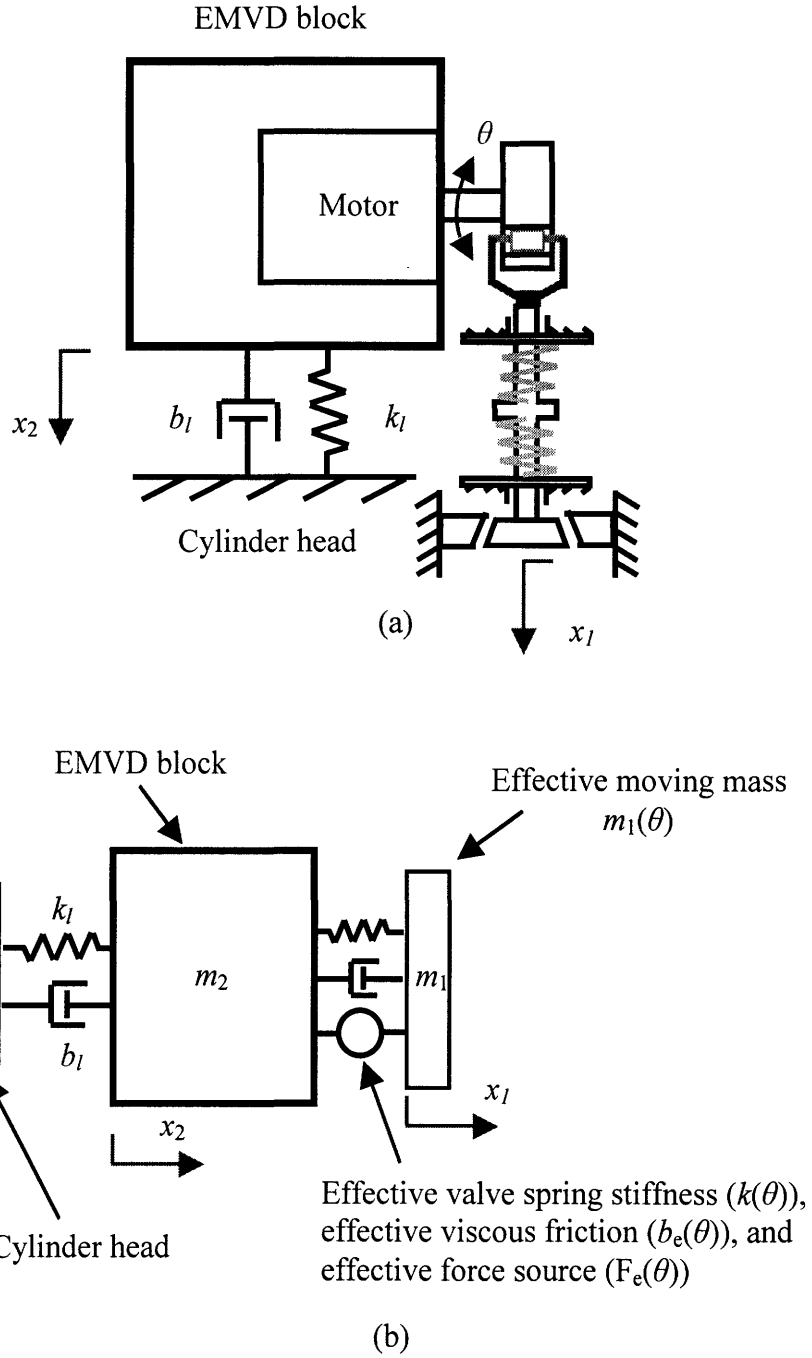

Fig. 10.4. (a) A lash adjuster for the proposed EMVD. (b) A simplified mathematical model of the adjuster.

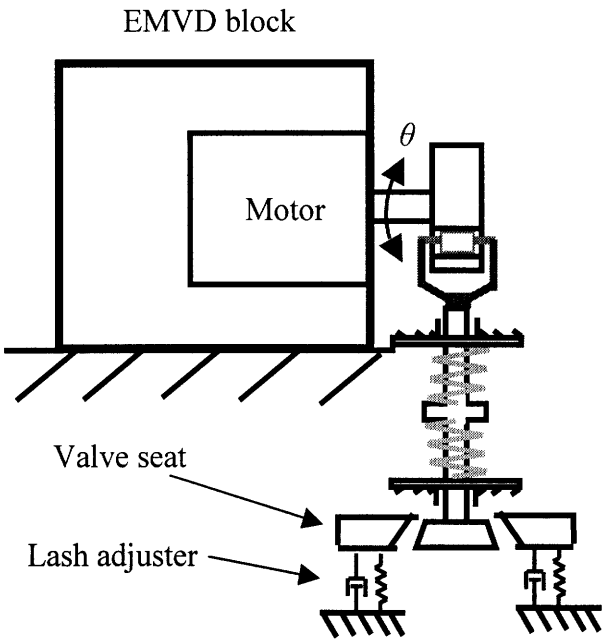

Fig. 10.5. Alternative conceptual lash adjuster design for the proposed EMVD.

where J/r^2 is also a constant. Since the proposed EMVD has a high quality factor, the maximum kinetic energy is approximately equal to the maximum stored spring energy. Therefore, v_{max} is almost a constant, namely

$$\frac{1}{2}\left(m_v + \frac{J}{r^2}\right) v_{max}^{\ 2} = \frac{1}{2} k \left(\frac{L}{2}\right)^2 = \text{constant.} \tag{10.6}$$

In other words,

$$v_{max} = \frac{L}{2}\sqrt{\frac{k}{m_v + \frac{J}{r^2}}} = \frac{L}{2}\omega_n = \text{constant.} \tag{10.7}$$

Substituting (10.3), (10.4), and (10.7) into (10.2),

$$\tau_p = c_0 \cdot r + c_1 \frac{1}{r}, \tag{10.8}$$

where the constants, $c_0 = F_{gas} + b_v \cdot v_{max}$, and $c_1 = b \cdot v_{max}$.

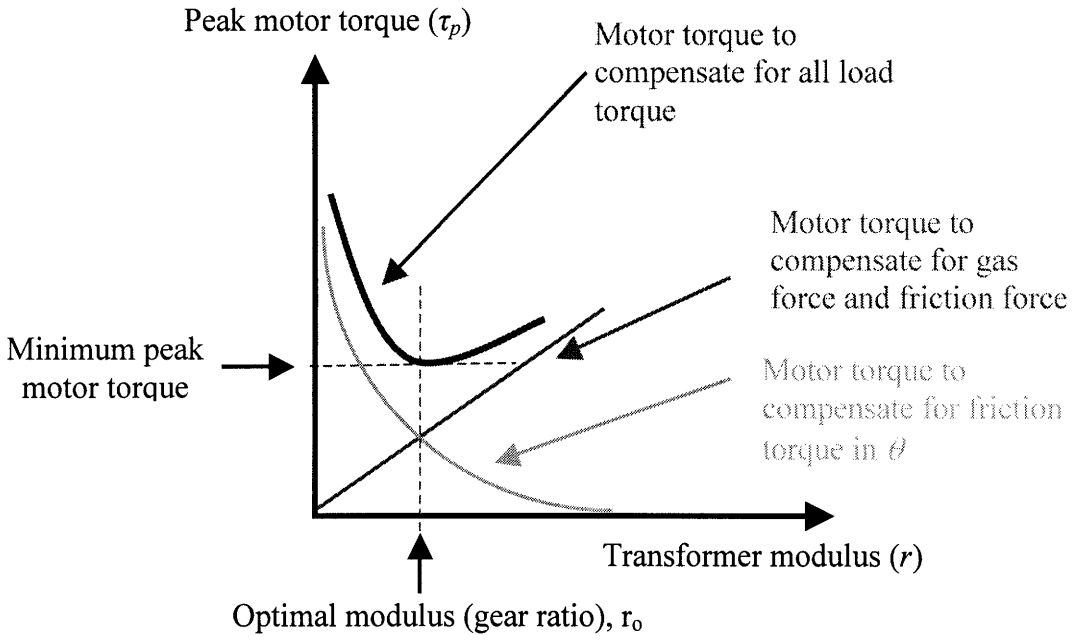

Fig. 10.6. Peak motor torque with respect to the modulus of an NTF.

Fig. 10.6 shows a representative of (10.8) plotted with respect to r. As seen, there is an optimal r, call it r_o, which minimizes the peak motor torque (τ_p) and hence the size of the motor. The optimal gear ratio, r_o, can be calculated as follows:

$$r_o = \sqrt{\frac{c_1}{c_0}}, \tag{10.9}$$

which satisfies

$$\frac{\partial \tau_p}{\partial r} = \frac{\partial (c_0 \cdot r + c_1 \frac{1}{r})}{\partial r}\Big|_{r=r_o} = 0. \qquad (10.10)$$

Note that smaller friction force (in either the z or θ domains) and smaller gas force allow lower peak motor torque. Intuitively, the contribution to torque from friction and gas forces on the valve side increases as the transformer modulus increases. The contribution to torque from friction force on the actuator side decreases as the transformer modulus increases because the angular velocity of the rotor must be smaller with a larger modulus to meet the transition time requirement, which is itself independent of modulus.

If the friction in the NTF is not negligible, that friction can be partitioned into two parts, one proportional to velocity in the θ domain, and one proportional to velocity in the z domain. The two parts can be combined with the appropriate terms in (10.8), and the method described here can be used to determine a new optimum r_o.

Once the minimum τ_p and the optimal r are determined, J is determined using (10.5). τ_p is proportional to $D_m^2 L_m$, in other words,

$$\tau_p = \alpha D_m^{\ 2} L_m, \qquad (10.11)$$

where D_m and L_m are the diameter and length of the air gap of the motor, respectively, and J is approximately proportional to $D_m^4 L_m$, in other words,

$$J = \beta D_m^{\ 4} L_m. \qquad (10.12)$$

Rotor dimensions (D_m and L_m) are therefore determined from the minimum τ_p and the computed J.

Given ω_n = 897 rad/s (corresponding to a 3.5 ms transition time) and L = 8×10^{-3} m for the built apparatus, v_{max} = 3.6 m/s by (10.7). According to characterization of the built apparatus, described in Chapter 9, b_v = 6 kg /s, b = $8.4 \cdot 10^{-4}$ kg-m^2/s. Fig. 2.6 gives $F_{gas} \sim$

100 N. Therefore, c_0 = 122 N, and $c_1 = 3.0\text{x}10^{-3}$ N-m^2, which results in $r_o = 5\text{x}10^{-3}$ m/rad, the minimum τ_p = 1.2 N-m. In conclusion, this optimization suggests that one can reduce the τ_p to less than half its value in the prototype system, J to 40% of its current value, and r to about 60% of the nominal modulus of the constructed NTF. Practical reductions, however, may depend on a range of other factors too, including loss limitations.

Since k = $1.12\text{x}10^5$ N/m, m = 0.083 kg, obtained in Chapter 9, (10.5) gives J/r^2 = 0.056 kg. For $r_o = 5\text{x}10^{-3}$, the inertia of the optimized motor, $J_o = 1.4\text{x}10^{-6}$ kg-m^2. For the chosen motor, D_m = 6.86 cm and L_m = 8.74 cm, $J = 3.5\text{x}10^{-6}$ kg-m^2, and τ_p = 3.4 N-m. Therefore, using (10.11) and (10.12), $\alpha = 1.8\text{x}10^{-10}$, $\beta = 8.2\text{x}10^{-3}$. For the optimized motor, since the minimum τ_p = 1.2 N-m and $J_o = 1.4\text{x}10^{-6}$ kg-m^2, we can find the dimensions for the optimized motor reference to the chosen motor, using (10.11) and (10.12) in conjunction with the α and β. The new D_m for the optimized motor is almost the same as that of the chosen motor, and the new L_m is approximately a third of that of the chosen motor. Different reference geometry information (D_m and L_m) of another stock motor introduces another optimized motor geometry.

11 Summary and Conclusions

11.1 Thesis Summary and Conclusions

To reduce the valve-holding current, existing electromechanical valve drive (EMVD) designs use two normal-force actuators. Such actuators have uni-directional and non-uniform force over a stroke and are not desirable from a servomechanical point of view. Moreover, they have inherently large jerk at both ends of the stroke, and require large actuator effort to achieve soft valve landings. To solve these problems, an innovative EMVD incorporating a nonlinear mechanical transformer (NTF) has been proposed. The NTF-based EMVD uses a shear-force actuator and requires zero holding current. In addition, the nonlinear dynamics of the novel EMVD are both fast and smooth, and naturally produce a near-zero seating velocity with small driving current. Moreover, it allows overshoot of the actuator kinematics, which can improve the system response speed. Therefore, this EMVD is capable of achieving fast and smooth valve kinematics and a soft landing with low power consumption.

The EMVD was mathematically modeled and simulated to investigate its dynamic behavior, and an experimental apparatus was designed and built to verify its operation and performance. Experimental results showed that the prototype achieved a 3.5 ms valve transition time, corresponding to an engine speed of 6000 rpm. Power consumption at 6000 rpm was approximately 140 W per intake valve, an already acceptable figure which can be reduced by employing a conjugate disc cam.

11.2 Recommendations for Future Work

The following topics require further research:

- Reduction of a motor size

  The motor in the apparatus is not small enough to be placed on top of a production cylinder head, but can be reduced by several strategies. The optimization of the nominal transformer modulus can reduce the size of the motor, as mentioned in Chapter 10. Furthermore, the intake valve actuator can be reduced because of the smaller gas forces it must counteract. The quality factor of the current apparatus is not very high, and employing a conjugate disc cam, as demonstrated in Chapter 4, can improve the quality factor and further reduce the size of the motor. Finally, an innovative motor cooling system can reduce the size of the motor further still.

- Design and implementation of devices

  The lash adjuster and the variable-lift-control device, proposed in Chapter 10, should be designed and implemented. Mathematical modeling of the devices is straightforward, and the devices should be designed and implemented after investigating their dynamic behaviors by simulation.

- Implementation of the apparatus in an engine

  The prototype should be tested with a gas-force simulator to investigate the effects of gas forces on EMVD dynamics before the apparatus is installed in an engine. A cooling system should be designed and employed in the apparatus.

- Control

  The limit of the motor drive current should be increased and tested before implementing the advanced controllers described in Chapter 8. Tolerance of overshoot in rotor kinematics introduces the possibility of employing open-loop control instead of feedback control. The mathematical model of the apparatus is not very precise, particular because of friction, and should be refined. Advanced system-identification techniques, such as adaptive-parameter estimation, should be carried out based on the refined mathematical model. Also, the employment of the lash adjuster, variable-lift-control device, and gas-force simulator will introduce new control issues. Measuring both motor voltage and current, we can estimate the rotor

displacement even without a position sensor by integrating its angular velocity with respect to time. Note that the performance of the feedback control system, based on this position-sensorless control, is limited to the accuracy of the system model parameters such as the terminal resistance, inductance, and torque constant of the motor. Therefore, the employment of an on-line parameter estimation technique is recommended for the position-sensorless control technique in practice.

- Refinement of the apparatus

  For simplicity, a sinusoidal NTF characteristic in (7.1) was used in the apparatus. An optimized function instead of the sinusoidal function could be considered. The minimization of jerk during the transition, or the minimization of the peak motor torque during the transition, given a nominal gear ration, can be a candidate optimization index (functional). A more extended flat region in Fig. 4.5 allows more overshoot in rotor kinematics. A U-shaped valve holder in Fig. 4.9 can make the line contact between the roller and disk cam be parallel to the axis of the roller shaft and will increase the quality factor of the apparatus and reduce the motor size further.

Appendices

A Simulation programs and parameters

A.1 Matlab simulation programs and parameters for Fig. 4.12.

```
% This is the Matlab code to investigate the effects of the current
% injection technique, resulting in Fig. 4.12.
% Run flat1.m with flatd1.m ( cfr3.m ( flat2.m with flatd2.m.

% flat1.m is the simulation program to get the time response of an
% EMVD with zero friction in case the current is injected at the
% start of the transition.

% cfr3.m is the program to select the first half of the transition
% from the result of the flat1.m.

% flat2.m is the simulation program to get the time response of an
% EMVD of (4.11) with zero friction in case the current is injected
% at the both ends of the stroke. The second current injection timing
% depends on the results of cfr3.m.


%%%%%%%%%%%%%%%%%%%%%%%%%%%%%%%%%%%%%%%%%%%%%%%%%%%%%%%%%%%%%%%%%%%%%%%%%%%%
% file name: flat1.m
% by
% Woo Sok Chang
% 3/8/2001
% EMVD project in LEES, EECS, MIT

global kp kd ki lift R L Kt J b r kv ks t1 t2 t3 t4 t5 t6 t7 tt
       h factor1 factor2 f_1 f_2
global bs bg m bsp ksp fe1 fe2 trans_time a_0 w_0 x_0
       interval_time c_2 c_1 c_0 pp pv inj_time inj_current

kp=0; kd=0; ki=0;

% fe1, fe2; external gas force values at fully closed and open
% positions, respectively.
fe1=0; fe2=0;

% trans_time is a holding time.
trans_time=3*10^-3; interval_time=trans_time;

% tt is an arbitrary number to determine the simulation ending time.
tt=1.78447*10^(-3);t1=tt*2;t2=t1+interval_time;
t3=t1*2+interval_time;t4=t1*2+2*interval_time;
```

```
lift=8*10^-3;
% -/+lift/2 represents valve fully closed/open, respectively.

factor1=0.999999; factor2=3.46;
% factor1 and factor2 represent a1 and a2 in (7.1).
% 8mm on the valve side corresponds to
% pi*factor1/factor2 on the rotor side.

h=lift/2/sin(factor1*pi/2);

%t0 & tf: simulation time
t0=0; tf=t4;

% Kt: torque constant; J: inertia on the actuator side;
% m: mass on the valve side; ksp: stiffness of valve springs
% b: viscous friction coeff on the actuator side
% ks: stiffness of valve seat; bs: viscous friction coeff of valve seat
% bg: viscous friction coeff on the valve side;
% bsp: viscous friction coeff of valve spring

Kt=7*10^-2; J=5.9*10^-6; m=0.083; ksp=1.12*10^5; b=0;
ks=0; bs=0; bg=0; bsp=0;

% x_0=-lift/2 means the valve is initially fully closed.
x_0=-lift/2; x0=[x_0 0 0]';

inj_time=0.3*10^-3; inj_current=20;

options = odeset('MaxStep',5e-6);
[t,x]=ode45('flatd1', [t0 tf], x0, options);

% Plot control input (current) u=i(t).
u=[]; a=[]; f_11=[]; f_22=[]; c_22=[];

for i=1:length(t)
x_r=0; v_r=0;f_t=0;

%u=[u;-kp*(x(i,1)-x_r)-kd*(x(i,2)-v_r)-ki*x(i,3)];
if (t(i)<=inj_time)
u=[u;inj_current];
else
u=[u;0];
end

h=lift/2/sin(factor1*pi/2);
f_11=[f_11;(1-(x(i,1)/h)^2)^(-1/2)/h/factor2];
f_22=[f_22;(1-(x(i,1)/h)^2)^(-3/2)*x(i,1)/(h^3)/factor2];
c_22=[c_22;(J*f_11(i)^2+m)];

if (x(i,1)<=(-lift/2))
   a=[a;1/c_22(i)*(-(b*f_11(i)^2+bsp+bs)*x(i,2)-ksp*x(i,1)-
ks*(x(i,1)+lift/2)+Kt*u(i)*f_11(i)...
         +f_t-J*f_22(i)*f_11(i)*x(i,2)^2)];
elseif (x(i,1)<=(lift/2))
   a=[a;1/c_22(i)*(-(b*f_11(i)^2+bsp)*x(i,2)-
ksp*x(i,1)+Kt*u(i)*f_11(i)+f_t-J*f_22(i)*f_11(i)*x(i,2)^2)];
else
```

```
   a=[a;1/c_22(i)*(-(b*f_11(i)^2+bsp+bs)*x(i,2)-ksp*x(i,1)-ks*(x(i,1)-
lift/2)+Kt*u(i)*f_11(i)+...
         f_t-J*f_22(i)*f_11(i)*x(i,2)^2)];
end
end

% x(1): valve position; x(2): valve velocity; u: motor current
figure
plot(t*10^3,x(:,1)*10^3,t*10^3,x(:,2),t*10^3,u/10,t*10^3,a/1000)
axis([0 t4*10^3 -30 30])
legend('valve displacement: X[mm]','valve velocity: V[m/s]','motor
current: i[10A]','acceleration: a[km/sec^2]')
grid

%%%%%%%%%%%%%%%%%%%%%%%%%%%%%%%%%%%%%%%%%%%%%%%%%%%%%%%%%%%%%%%%%%%%%%%%
% file name: flat2.m
% by
% Woo Sok Chang
% 3/8/2001
% FFVD project in LEES, EECS, MIT

global kp kd ki lift R L Kt J b r kv ks t1 t2 t3 t4 t5 t6 t7 tt h
       factor1 factor2 f_1 f_2 t_cross
global bs bg m bsp ksp fe1 fe2 trans_time a_0 w_0 x_0 interval_time c_2
       c_1 c_0 pp pv inj_time inj_current

kp=0; kd=0; ki=0;

fe1=0; fe2=0;

trans_time=3*10^-3; interval_time=trans_time;
w_0=2*pi/trans_time; a_0=2*pi*lift/(trans_time)^2;

tt=t_cross;

t1=tt*2; t2=t1+interval_time; t3=t1*2+interval_time;
t4=t1*2+2*interval_time;

lift=8*10^-3;

factor1=0.999999; factor2=3.46;

h=lift/2/sin(factor1*pi/2);

t0=0; tf=t4;

Kt=7*10^-2; J=5.9*10^-6; m=0.083;ksp=1.12*10^5;
b=0; ks=0; bs=0; bg=0; bsp=0;r=(J/m)^0.5;

x_0=-lift/2; x0=[x_0 0 0]';

inj_time=0.3*10^-3; inj_current=20;

options = odeset('MaxStep',5e-6);
[t,x]=ode45('flatd2', [t0 tf], x0, options);

u=[]; a=[]; f_11=[]; f_22=[]; c_22=[];
```

```
for i=1:length(t)
x_r=0; v_r=0; f_t=0;

if (t(i)<=inj_time)
u=[u;inj_current];
elseif ((t(i)>=(2*t_cross-inj_time)) & (t(i)<=(t_cross*2)))
u=[u;-inj_current];
else
u=[u;0];
end

h=lift/2/sin(factor1*pi/2);
f_11=[f_11;(1-(x(i,1)/h)^2)^(-1/2)/h/factor2];
f_22=[f_22;(1-(x(i,1)/h)^2)^(-3/2)*x(i,1)/(h^3)/factor2];
c_22=[c_22;(J*f_11(i)^2+m)];

if (x(i,1)<=(-lift/2))
   a=[a;1/c_22(i)*(-(b*f_11(i)^2+bsp+bs)*x(i,2)-ksp*x(i,1)-
ks*(x(i,1)+lift/2)+Kt*u(i)*f_11(i)...
         +f_t-J*f_22(i)*f_11(i)*x(i,2)^2)];
elseif (x(i,1)<=(lift/2))
   a=[a;1/c_22(i)*(-(b*f_11(i)^2+bsp)*x(i,2)-
ksp*x(i,1)+Kt*u(i)*f_11(i)+f_t-J*f_22(i)*f_11(i)*x(i,2)^2)];
else
   a=[a;1/c_22(i)*(-(b*f_11(i)^2+bsp+bs)*x(i,2)-ksp*x(i,1)-ks*(x(i,1)-
lift/2)+Kt*u(i)*f_11(i)+...
         f_t-J*f_22(i)*f_11(i)*x(i,2)^2)];
end
end

figure
plot(t*10^3,x(:,1)*10^3,t*10^3,x(:,2),t*10^3,u/10,t*10^3,a/1000)
axis([0 t4*10^3 -10 10])
grid


%%%%%%%%%%%%%%%%%%%%%%%%%%%%%%%%%%%%%%%%%%%%%%%%%%%%%%%%%%%%%%%%%%%%%%%%%%%%
% file name: flatd1.m
% by
% Woo Sok Chang
% 3/8/2001
% FFVD project in LEES, EECS, MIT

function xdot=flatd1(t,x)
global kp kd ki lift R L Kt J b r kv ks t1 t2 t3 t4 t5 t6 t7 tt h
       factor1 factor2 f_1 f_2
global bs bg m bsp ksp fe1 fe2 trans_time a_0 w_0 interval_time c_2 c_1
       c_0 pp pv inj_time inj_current

x_r=0; v_r=0; f_t=0;

h=lift/2/sin(factor1*pi/2);

f_1=(1-(x(1)/h)^2)^(-1/2)/h/factor2;
f_2=(1-(x(1)/h)^2)^(-3/2)*x(1)/(h^3)/factor2;
c_2=(J*f_1^2+m);
```

```
xdot=zeros(3,1);
if (t<=inj_time)
   i_t=inj_current;
else
   i_t=0;
end

xdot(1)=x(2);
if (x(1)<=(-lift/2))
   xdot(2)=1/c_2*(-(b*f_1^2+bsp+bs)*x(2)-ksp*x(1)-
ks*(x(1)+lift/2)+Kt*i_t*f_1+f_t-J*f_2*f_1*x(2)^2);
elseif (x(1)<=(lift/2))
   xdot(2)=1/c_2*(-(b*f_1^2+bsp)*x(2)-ksp*x(1)+Kt*i_t*f_1+f_t-
J*f_2*f_1*x(2)^2);
else
   xdot(2)=1/c_2*(-(b*f_1^2+bsp+bs)*x(2)-ksp*x(1)-ks*(x(1)-
lift/2)+Kt*i_t*f_1+f_t-J*f_2*f_1*x(2)^2);
end


%%%%%%%%%%%%%%%%%%%%%%%%%%%%%%%%%%%%%%%%%%%%%%%%%%%%%%%%%%%%%%%%%%%%%%%%%%%%
% file name: flatd2.m
% by
% Woo Sok Chang
% 3/8/2001
% FFVD project in LEES, EECS, MIT

function xdot=flatd2(t,x)
global kp kd ki lift R L Kt J b r kv ks t1 t2 t3 t4 t5 t6 t7 tt h
       factor1 factor2 f_1 f_2  t_cross
global bs bg m bsp ksp fe1 fe2 trans_time a_0 w_0 interval_time c_2 c_1
       c_0 pp pv inj_time inj_current

x_r=0; v_r=0;f_t=0;

h=lift/2/sin(factor1*pi/2);

f_1=(1-(x(1)/h)^2)^(-1/2)/h/factor2;
f_2=(1-(x(1)/h)^2)^(-3/2)*x(1)/(h^3)/factor2;
c_2=(J*f_1^2+m);

xdot=zeros(3,1);

if (t<=inj_time)
   i_t=inj_current;
elseif ((t>=(2*t_cross-inj_time)) & (t<=(t_cross*2)))
   i_t=-inj_current;
   else
i_t=0;
   end

xdot(1)=x(2);
if (x(1)<=(-lift/2))
   xdot(2)=1/c_2*(-(b*f_1^2+bsp+bs)*x(2)-ksp*x(1)-
ks*(x(1)+lift/2)+Kt*i_t*f_1+f_t-J*f_2*f_1*x(2)^2);
elseif (x(1)<=(lift/2))
```

```
   xdot(2)=1/c_2*(-(b*f_1^2+bsp)*x(2)-ksp*x(1)+Kt*i_t*f_1+f_t-
J*f_2*f_1*x(2)^2);
else
   xdot(2)=1/c_2*(-(b*f_1^2+bsp+bs)*x(2)-ksp*x(1)-ks*(x(1)-
lift/2)+Kt*i_t*f_1+f_t-J*f_2*f_1*x(2)^2);
end


%%%%%%%%%%%%%%%%%%%%%%%%%%%%%%%%%%%%%%%%%%%%%%%%%%%%%%%%%%%%%%%%%%%%%%%%%%%%
% file name: cfr3.m
% by
% Woo Sok Chang
% 3/8/2001
% FFVD project in LEES, EECS, MIT

format long e
t_modified=[]; y_position=[]; y_velocity=[]; y_acceleration=[];

for i=1:length(t)
   if ((x(i,1)>0))
      t_cross=(t(i)+t(i-1))/2;
      break;
   end
end

for i=1:length(t)
   if (abs(x(i,1)-4*10^(-3))/(4*10^(-3))<0.00001)
      i_1=i;
      t_1=t(i_1);
      break;
   end
end

t_0=t_1/2;

for i=1:(i_1)
   t_modified=[t_modified;t(i)];
   y_position=[y_position;x(i,1)];
   y_velocity=[y_velocity;x(i,2)];
   y_acceleration=[y_acceleration;a(i)];
end

% t_0 is transferred to tt in flat2.m.

p_position=polyfit(t_modified,y_position,20);
p_velocity=polyfit(t_modified,y_velocity,19);
p_acceleration=polyfit(t_modified,y_acceleration,18);
f_position=polyval(p_position,t_modified);
f_velocity=polyval(p_velocity,t_modified);
f_acceleration=polyval(p_acceleration,t_modified);

pp=p_position; pv=p_velocity; pa=p_acceleration;

figure
plot(t_modified*10^3,y_position*10^3,t_modified*10^3,f_position*10^3)
grid
figure
```

```
plot(t_modified*10^3,y_velocity,t_modified*10^3,f_velocity)
grid
figure
plot(t_modified*10^3,y_acceleration,t_modified*10^3,f_acceleration)
grid
```

Table A.1. Parameters used for the simulations for Fig. 4.12.

Parameters	Value
Inertia in motor side (J)	$5.9 \cdot 10^{-6}$ (kg-m^2)
Friction in motor side (b)	0 (kg-m^2/s)
Torque constant (K_T)	0.07 (N-m/A)
Mass in the valve side (m_v)	0.083 (kg)
Friction in the valve side (b_v)	0 (kg/s)
Stiffness of springs (k)	$1.12 \cdot 10^5$ (N/m)
Resistance (R)	0.89 Ω
Flatness of NTF (a_1) in (7.1)	0.999999
Nominal transformer characteristic of NTF (a_2) in (7.1)	3.46
Valve lift (L)	8 (mm)

A.2 Matlab simulation programs and parameters for Fig. 5.4.

```
% This is the Matlab code to investigate the dynamic behaviors of
% the proposed EMVD, resulting in Fig. 5.4.
% Run flat1.m with flatd1.m in A-1 ( cfr3.m in A-1 ( flat2.m with
% flatd2.m in A-1 ( cfr4.m ( ncs.m with ncsd.m.

% cfr4.m is the program to find the curve-fitted position and velocity
% profiles during transition from the results of the flat2.m.
% This information is used for a reference input for ncs.m.

% ncs.m is the simulation program to get the time response of an
% EMVD of (4.11) with realistic parameters (see Table A-2)
% and a feedback controller.


%%%%%%%%%%%%%%%%%%%%%%%%%%%%%%%%%%%%%%%%%%%%%%%%%%%%%%%%%%%%%%%%%%%%%%%%%%%%%%%
% file name: cfr4.m
% by
% Woo Sok Chang
% 1/31/2001
% EMVD project in LEES, EECS, MIT

format long e
t_modified=[]; y_position=[]; y_velocity=[]; y_acceleration=[];

for i=1:length(t)
   if (x(i,1)>0)
      t_cross=(t(i)+t(i-1))/2;
      break;
   end
end

for i=1:length(t)
if (t(i)>t_cross*2)
      i_1=i;
      t_1=t(i_1);
      break;
   end
end

t_0=t_1/2;

for i=1:(i_1)
   t_modified=[t_modified;t(i)];
   y_position=[y_position;x(i,1)];
   y_velocity=[y_velocity;x(i,2)];
   y_acceleration=[y_acceleration;a(i)];
end

p_position=polyfit(t_modified,y_position,20);
p_velocity=polyfit(t_modified,y_velocity,19);
p_acceleration=polyfit(t_modified,y_acceleration,18);
f_position=polyval(p_position,t_modified);
f_velocity=polyval(p_velocity,t_modified);
f_acceleration=polyval(p_acceleration,t_modified);
```

```
pp=p_position; pv=p_velocity; pa=p_acceleration;

figure
plot(t_modified*10^3,y_position*10^3,t_modified*10^3,f_position*10^3)
grid
figure
plot(t_modified*10^3,y_velocity,t_modified*10^3,f_velocity)
grid
figure
plot(t_modified*10^3,y_acceleration,t_modified*10^3,f_acceleration)
grid


%%%%%%%%%%%%%%%%%%%%%%%%%%%%%%%%%%%%%%%%%%%%%%%%%%%%%%%%%%%%%%%%%%%%%%%%%%%%
% file name: ncs.m
% by
% Woo Sok Chang
% 5/7/2001
% EMVD project in LEES, EECS, MIT

global kp kd ki lift R L Kt J b r kv ks t1 t2 t3 t4 t5 t6 t7 tt h
       factor1 factor2 f_1 f_2 bs bg m bsp ksp fe1 fe2 trans_time
       a_0 w_0 x_0 interval_time c_2 c_1 c_0 pp pv pa inj_time t_cross
       inj_current r0 r1 r2 f0 nyu T myu2 f2 res

%res: resistance of motor winding [ohm]
res=0.89;

% These are the parameters to consider the friction in the NTF.
% But, in this simulation, for simplicity, these are neglected.
%r0=radius of a cam
%r1=outer radius of a roller [cm]
%r2=inner radius of a roller [cm]
%T=diameter of a roller [mm]
%nyu=constant in a roller bearing
%f0=constant in a roller bearing
%f2=constant in a roller bearing for Coulomb friction, ~ 1
%myu2=friction coeff in Coulomb friction

r0=1.5; r1=0.15; r2=T/2/10; T=3;

nyu=0;f0=0;myu2=0;f2=0;

%kp, kd, and ki are gains.

kd=7*10^3; kp=kd*1000; ki=kd*10^5;

% fe1, fe2; external gas force values at fully closed and open
% positions, respectively.
fe1=250; fe2=50;

% tt is an arbitrary number to determine the simulation ending time.
trans_time=3*10^-3;w_0=2*pi/trans_time;a_0=2*pi*lift/(trans_time)^2;
interval_time=trans_time;

tt=t_cross;
```

```
t1=tt*2;
t2=t1+interval_time;
t3=t1*2+interval_time;
t4=t1*2+2*interval_time;

% -/+lift/2 represents valve fully closed/open, respectively.
lift=8*10^-3;

% factor1 and factor2 represent a1 and a2 in (7.1).
% 8mm on the valve side corresponds to
% pi*factor1/factor2 on the rotor side.
factor1=0.999999; factor2=3.46;

%t0 & tf: simulation time
t0=0; tf=t4;

% Kt: torque constant; J: inertia on the actuator side;
% m: mass on the valve side; ksp: stiffness of valve springs
% b: viscous friction coeff on the actuator side
% ks: stiffness of valve seat; bs: viscous friction coeff of valve seat
% bg: viscous friction coeff on the valve side;
% bsp: viscous friction coeff of valve spring

Kt=7*10^-2; J=5.9*10^-6; m=0.083; ksp=1.12*10^5; b=8.4*10^-4;
ks=0; bs=0; bg=6; bsp=0; r=(J/m)^0.5;

% x_0=-lift/2 means the valve is initially fully closed.
x_0=-lift/2;

h=lift/2/sin(factor1*pi/2);
f_11_end=(1-(x_0/h)^2)^(-1/2)/h/factor2;
x_0_3=-ksp*x_0/(f_11_end*Kt*ki);

x0=[x_0 0 x_0_3]';

inj_time=0.3*10^-3; inj_current=20;

options = odeset('MaxStep',1e-5);
[t,x]=ode45('ncsd', [t0 tf], x0, options);

% Plot control input (current) u=i(t).
u=[]; a=[]; ex=[]; evx=[];
f_11=[]; f_22=[]; c_22=[]; i_t_jj=[];

omega11=[]; M011=[]; Fs11=[]; a211=[]; Fn11=[]; M111=[]; M11=[];
Tm11=[]; Tm011=[]; Tm111=[]; power11=[]; volt11=[]; voltr11=[];

for i=1:length(t)
   if (t(i)<=t1)
x_r
=pp(1)*t(i).^20+pp(2)*t(i).^19+pp(3)*t(i).^18+pp(4)*t(i).^17+pp(5)*t(i).
^16+pp(6)*t(i).^15 ...

+pp(7)*t(i).^14+pp(8)*t(i).^13+pp(9)*t(i).^12+pp(10)*t(i).^11+pp(11)*t(i
).^10+pp(12)*t(i).^9 ...
```

```
+pp(13)*t(i).^8+pp(14)*t(i).^7+pp(15)*t(i).^6+pp(16)*t(i).^5+pp(17)*t(i)
.^4+pp(18)*t(i).^3 ...
    +pp(19)*t(i).^2+pp(20)*t(i).^1+pp(21);
v_r =
pv(1)*t(i).^19+pv(2)*t(i).^18+pv(3)*t(i).^17+pv(4)*t(i).^16+pv(5)*t(i).^
15+pv(6)*t(i).^14 ...

+pv(7)*t(i).^13+pv(8)*t(i).^12+pv(9)*t(i).^11+pv(10)*t(i).^10+pv(11)*t(i
).^9 +pv(12)*t(i).^8 ...
     +pv(13)*t(i).^7+pv(14)*t(i).^6+pv(15)*t(i).^5+pv(16)*t(i).^4
+pv(17)*t(i).^3+pv(18)*t(i).^2 ...
     +pv(19)*t(i).^1+pv(20);
a_r =
pa(1)*t(i).^18+pa(2)*t(i).^17+pa(3)*t(i).^16+pa(4)*t(i).^15+pa(5)*t(i).^
14+pa(6)*t(i).^13 ...

+pa(7)*t(i).^12+pa(8)*t(i).^11+pa(9)*t(i).^10+pa(10)*t(i).^9+pa(11)*t(i)
.^8 +pa(12)*t(i).^7 ...
     +pa(13)*t(i).^6+pa(14)*t(i).^5+pa(15)*t(i).^4+pa(16)*t(i).^3
+pa(17)*t(i).^2+pa(18)*t(i).^1 ...
     +pa(19);
f_t=-((fe2-fe1)/t1*t(i) + fe1);

elseif (t(i)<=t2)
x_r=lift/2; v_r=0; a_r=0; f_t=-(fe2);

elseif (t(i)<=t3)
x_r =-(pp(1)*(t(i)-t2).^20+pp(2)*(t(i)-t2).^19+pp(3)*(t(i)-
t2).^18+pp(4)*(t(i)-t2).^17+pp(5)*(t(i)-t2).^16+pp(6)*(t(i)-t2).^15 ...
     +pp(7)*(t(i)-t2).^14+pp(8)*(t(i)-t2).^13+pp(9)*(t(i)-
t2).^12+pp(10)*(t(i)-t2).^11+pp(11)*(t(i)-t2).^10 +pp(12)*(t(i)-
t2).^9 ...
      +pp(13)*(t(i)-t2).^8 +pp(14)*(t(i)-t2).^7 +pp(15)*(t(i)-
t2).^6+pp(16)*(t(i)-t2).^5+pp(17)*(t(i)-t2).^4 +pp(18)*(t(i)-t2).^3 ...
      +pp(19)*(t(i)-t2).^2 +pp(20)*(t(i)-t2).^1 +pp(21));
v_r = -(pv(1)*(t(i)-t2).^19+pv(2)*(t(i)-t2).^18+pv(3)*(t(i)-
t2).^17+pv(4)*(t(i)-t2).^16+pv(5)*(t(i)-t2).^15+pv(6)*(t(i)-t2).^14 ...
       +pv(7)*(t(i)-t2).^13+pv(8)*(t(i)-t2).^12+pv(9)*(t(i)-
t2).^11+pv(10)*(t(i)-t2).^10+pv(11)*(t(i)-t2).^9 +pv(12)*(t(i)-t2).^8 ...
       +pv(13)*(t(i)-t2).^7+pv(14)*(t(i)-t2).^6+pv(15)*(t(i)-
t2).^5+pv(16)*(t(i)-t2).^4 +pv(17)*(t(i)-t2).^3+pv(18)*(t(i)-t2).^2 ...
       +pv(19)*(t(i)-t2).^1 +pv(20));
a_r = -(pa(1)*(t(i)-t2).^18+pa(2)*(t(i)-t2).^17+pa(3)*(t(i)-
t2).^16+pa(4)*(t(i)-t2).^15+pa(5)*(t(i)-t2).^14+pa(6)*(t(i)-t2).^13 ...
     +pa(7)*(t(i)-t2).^12+pa(8)*(t(i)-t2).^11+pa(9)*(t(i)-
t2).^10+pa(10)*(t(i)-t2).^9+pa(11)*(t(i)-t2).^8 +pa(12)*(t(i)-t2).^7 ...
     +pa(13)*(t(i)-t2).^6+pa(14)*(t(i)-t2).^5+pa(15)*(t(i)-
t2).^4+pa(16)*(t(i)-t2).^3 +pa(17)*(t(i)-t2).^2+pa(18)*(t(i)-t2).^1 ...
     +pa(19));

f_t=-((0-fe2)/(t3-t2)*(t(i)-t2) + fe2);

elseif (t(i)<=t4)
x_r=-lift/2; v_r=0; a_r=0; f_t=0;
end
```

```
if (t(i)<=inj_time)
   i_t_jj=[i_t_jj;inj_current];
elseif ((t(i)>=(t1-inj_time)) & (t(i)<=t1))
   i_t_jj=[i_t_jj;-inj_current];
   elseif ((t(i)>=t2) & (t(i)<=(t2+inj_time)))
      i_t_jj=[i_t_jj;-inj_current];
elseif ((t(i)>=(t3-inj_time)) & (t(i)<=t3))
   i_t_jj=[i_t_jj;inj_current];
  else
i_t_jj=[i_t_jj;0];
   end

if (t(i)<=t1)
kd=1.22*10^4; kp=kd*6000; ki=0;
elseif (t(i)<=t2)
kd=1.22*10^4; kp=kd*6000; ki=0;
elseif (t(i)<=t3)
kd=1.22*10^4; kp=kd*6000; ki=0;
elseif (t(i)<=t4)
kd=1.22*10^4; kp=kd*6000; ki=0;
end

   ex=[ex;x_r-x(i,1)];
   evx=[evx;v_r-x(i,2)];

h=lift/2/sin(factor1*pi/2);

if (abs(x(i,1))<=(lift/2))
f_11=[f_11;(1-(x(i,1)/h)^2)^(-1/2)/h/factor2];
f_22=[f_22;(1-(x(i,1)/h)^2)^(-3/2)*x(i,1)/(h^3)/factor2];
c_22=[c_22;(J*f_11(i)^2+m)];
else
f_11=[f_11;(1-(lift/2/h)^2)^(-1/2)/h/factor2];
f_22=[f_22;0];
c_22=[c_22;(J*f_11(i)^2+m)];
end

omega11=[omega11;abs(((r0/r1*f_11(i))^2+(1/r1*10^2)^2)^(1/2)*x(i,2)*60)]
;
M011=[M011;f0*10^(-7)*(omega11(i)*nyu)^(2/3)*T^3+f0*10^(-
7)*(abs(f_11(i)*x(i,2)*60)*nyu)^(2/3)*6.0^3];
Fs11=[Fs11;ksp*x(i,1)];
a211=[a211;1/r0/f_11(i)*10^2];
Fn11=[Fn11;abs(Fs11(i))*(1+a211(i)^2)^(0.5)];
M111=[M111;myu2*f2*T/2*Fn11(i)+myu2*f2*6.0/2*abs(ksp*x(i,1))];
M11=[M11;M011(i)+M111(i)];
Tm11=[Tm11;r0/r1*M11(i)*sign(x(i,2))*10^(-3)];
Tm011=[Tm011;r0/r1*M011(i)*sign(x(i,2))*10^(-3)];
Tm111=[Tm111;r0/r1*M111(i)*sign(x(i,2))*10^(-3)];

if (((t(i)<=inj_time)|((t(i)>=(t1-inj_time)) & (t(i)<=t1))|((t(i)>=t2) &
(t(i)<=(t2+inj_time)))|((t(i)>=(t3-inj_time)) & (t(i)<=t3))))
   u=[u;i_t_jj(i)-577/3*6000*(x(i,1)-x_r)-577/3*(x(i,2)-v_r)-ki*x(i,3)];
   elseif (((t(i)>t1)&(t(i)<t2))|(t(i)>t3))
   u=[u;i_t_jj(i)+(-60*10^3*6000*(x(i,1)-x_r)-60*10^3*(x(i,2)-v_r)-
ki*x(i,3))];
elseif (x(i,1)<=(-lift/2))
```

```
   u=[u;+c_22(i)/(f_11(i)*Kt)*(a_r-1/c_22(i)*(-
(b*f_11(i)^2+bsp+bs+bg)*x(i,2)...
         -ksp*x(i,1)-ks*(x(i,1)+lift/2)+(-Tm11(i))*f_11(i)+f_t-
J*f_22(i)*f_11(i)*x(i,2)^2)...
         -kp*(x(i,1)-x_r)-kd*(x(i,2)-v_r)-ki*x(i,3))];
elseif (x(i,1)<=(lift/2))
   u=[u;+c_22(i)/(f_11(i)*Kt)*(a_r-1/c_22(i)*(-
(b*f_11(i)^2+bsp+bg)*x(i,2)...
         -ksp*x(i,1)+(-Tm11(i))*f_11(i)+f_t-
J*f_22(i)*f_11(i)*x(i,2)^2)...
         -kp*(x(i,1)-x_r)-kd*(x(i,2)-v_r)-ki*x(i,3))];
elseif (x(i,1)>(lift/2))
   u=[u;+c_22(i)/(f_11(i)*Kt)*(a_r-1/c_22(i)*(-
(b*f_11(i)^2+bsp+bg)*x(i,2)...
         -ksp*x(i,1)-ks*(x(i,1)-lift/2)+(-Tm11(i))*f_11(i)+f_t-
J*f_22(i)*f_11(i)*x(i,2)^2)...
         -kp*(x(i,1)-x_r)-kd*(x(i,2)-v_r)-ki*x(i,3))];
end

power11=[power11;u(i)^2*res+u(i)*Kt*f_11(i)*x(i,2)];
volt11=[volt11;u(i)*res+Kt*f_11(i)*x(i,2)];
voltr11=[voltr11;u(i)*res];

if (x(i,1)<=(-lift/2))
   a=[a;1/c_22(i)*(-(b*f_11(i)^2+bsp+bs+bg)*x(i,2)-ksp*x(i,1)-
ks*(x(i,1)+lift/2)+(Kt*u(i)-Tm11(i))*f_11(i)...
         +f_t-J*f_22(i)*f_11(i)*x(i,2)^2)];
elseif (x(i,1)<=(lift/2))
   a=[a;1/c_22(i)*(-(b*f_11(i)^2+bsp+bg)*x(i,2)-ksp*x(i,1)+(Kt*u(i)-
Tm11(i))*f_11(i)+f_t-J*f_22(i)*f_11(i)*x(i,2)^2)];
   elseif (x(i,1)>(lift/2))
      a=[a;1/c_22(i)*(-(b*f_11(i)^2+bsp+bg)*x(i,2)-ksp*x(i,1)-
ks*(x(i,1)-lift/2)+(Kt*u(i)-Tm11(i))*f_11(i)...
         +f_t-J*f_22(i)*f_11(i)*x(i,2)^2)];
else
   a=[a;1/c_22(i)*(-(b*f_11(i)^2+bsp+bs+bg)*x(i,2)-ksp*x(i,1)-
ks*(x(i,1)-lift/2)+(Kt*u(i)-Tm11(i))*f_11(i)+...
         f_t-J*f_22(i)*f_11(i)*x(i,2)^2)];
end
end

figure
plot(t*10^3,x(:,1)*10^3,t*10^3,x(:,2),t*10^3,a/1000,t*10^3,Kt*u)
axis([0 t4*10^3 -10 10])
grid
figure
plot(t*10^3,u/10,t*10^3,volt11/10,t*10^3,power11/1000)
axis([0 t4*10^3 -10 10])
grid
figure
plot(t*10^3,ex*100000,t*10^3,evx*100)
axis([0 t4*10^3 -2 2])
grid

%%%%%%%%%%%%%%%%%%%%%%%%%%%%%%%%%%%%%%%%%%%%%%%%%%%%%%%%%%%%%%%%%%%%%%%%%%%%%%%
% file name: ncsd.m
% by
```

```
% Woo Sok Chang
% 5/7/2001
% EMVD project in LEES, EECS, MIT

function xdot=ncsd(t,x)
global kp kd ki lift R L Kt J b r kv ks t1 t2 t3 t4 t5 t6 t7 tt h
       factor1 factor2 f_1 f_2 bs bg m bsp ksp fe1 fe2 trans_time a_0
       w_0 interval_time c_2 c_1 c_0 pp pv pa inj_time t_cross
       inj_current r0 r1 r2 f0 nyu T myu2 f2 res

if (t<=t1)
x_r
=pp(1)*t.^20+pp(2)*t.^19+pp(3)*t.^18+pp(4)*t.^17+pp(5)*t.^16+pp(6)*t.^15
 ...

+pp(7)*t.^14+pp(8)*t.^13+pp(9)*t.^12+pp(10)*t.^11+pp(11)*t.^10+pp(12)*t.
^9 ...

+pp(13)*t.^8+pp(14)*t.^7+pp(15)*t.^6+pp(16)*t.^5+pp(17)*t.^4+pp(18)*t.^3
 ...
    +pp(19)*t.^2+pp(20)*t.^1+pp(21);
v_r =
pv(1)*t.^19+pv(2)*t.^18+pv(3)*t.^17+pv(4)*t.^16+pv(5)*t.^15+pv(6)*t.^14
...
     +pv(7)*t.^13+pv(8)*t.^12+pv(9)*t.^11+pv(10)*t.^10+pv(11)*t.^9
+pv(12)*t.^8 ...
     +pv(13)*t.^7+pv(14)*t.^6+pv(15)*t.^5+pv(16)*t.^4
+pv(17)*t.^3+pv(18)*t.^2 ...
     +pv(19)*t.^1+pv(20);
a_r =
pa(1)*t.^18+pa(2)*t.^17+pa(3)*t.^16+pa(4)*t.^15+pa(5)*t.^14+pa(6)*t.^13
...
     +pa(7)*t.^12+pa(8)*t.^11+pa(9)*t.^10+pa(10)*t.^9+pa(11)*t.^8
+pa(12)*t.^7 ...
     +pa(13)*t.^6+pa(14)*t.^5+pa(15)*t.^4+pa(16)*t.^3
+pa(17)*t.^2+pa(18)*t.^1 ...
     +pa(19);

f_t=-((fe2-fe1)/t1*t + fe1);

elseif (t<=t2)
   x_r=lift/2; v_r=0; a_r=0; f_t=-(fe2);

elseif (t<=t3)
x_r =-(pp(1)*(t-t2).^20+pp(2)*(t-t2).^19+pp(3)*(t-t2).^18+pp(4)*(t-
t2).^17+pp(5)*(t-t2).^16+pp(6)*(t-t2).^15 ...
      +pp(7)*(t-t2).^14+pp(8)*(t-t2).^13+pp(9)*(t-t2).^12+pp(10)*(t-
t2).^11+pp(11)*(t-t2).^10 +pp(12)*(t-t2).^9 ...
      +pp(13)*(t-t2).^8 +pp(14)*(t-t2).^7 +pp(15)*(t-t2).^6+pp(16)*(t-
t2).^5+pp(17)*(t-t2).^4 +pp(18)*(t-t2).^3 ...
      +pp(19)*(t-t2).^2 +pp(20)*(t-t2).^1 +pp(21));
v_r = -(pv(1)*(t-t2).^19+pv(2)*(t-t2).^18+pv(3)*(t-t2).^17+pv(4)*(t-
t2).^16+pv(5)*(t-t2).^15+pv(6)*(t-t2).^14 ...
       +pv(7)*(t-t2).^13+pv(8)*(t-t2).^12+pv(9)*(t-t2).^11+pv(10)*(t-
t2).^10+pv(11)*(t-t2).^9 +pv(12)*(t-t2).^8 ...
       +pv(13)*(t-t2).^7+pv(14)*(t-t2).^6+pv(15)*(t-t2).^5+pv(16)*(t-
t2).^4 +pv(17)*(t-t2).^3+pv(18)*(t-t2).^2 ...
```

```
       +pv(19)*(t-t2).^1 +pv(20));
a_r = -(pa(1)*(t-t2).^18+pa(2)*(t-t2).^17+pa(3)*(t-t2).^16+pa(4)*(t-
t2).^15+pa(5)*(t-t2).^14+pa(6)*(t-t2).^13 ...
     +pa(7)*(t-t2).^12+pa(8)*(t-t2).^11+pa(9)*(t-t2).^10+pa(10)*(t-
t2).^9+pa(11)*(t-t2).^8 +pa(12)*(t-t2).^7 ...
     +pa(13)*(t-t2).^6+pa(14)*(t-t2).^5+pa(15)*(t-t2).^4+pa(16)*(t-
t2).^3 +pa(17)*(t-t2).^2+pa(18)*(t-t2).^1 ...
     +pa(19));

f_t=-((0-fe2)/(t3-t2)*(t-t2) + fe2);

elseif (t<=t4)
   x_r=-lift/2; v_r=0; a_r=0; f_t=0;
end

if (abs(x(1))<=(lift/2))
f_1=(1-(x(1)/h)^2)^(-1/2)/h/factor2;
f_2=(1-(x(1)/h)^2)^(-3/2)*x(1)/(h^3)/factor2;
c_2=(J*f_1^2+m);
else
f_1=(1-(lift/2/h)^2)^(-1/2)/h/factor2;
f_2=0;
c_2=(J*f_1^2+m);
end

xdot=zeros(3,1);

if (t<=inj_time)
   i_t_j=inj_current;
elseif ((t>=(t1-inj_time)) & (t<=t1))
   i_t_j=-inj_current;
   elseif ((t>=t2) & (t<=(t2+inj_time)))
   i_t_j=-inj_current;
   elseif ((t>=(t3-inj_time)) & (t<=t3))
   i_t_j=inj_current;
   else
i_t_j=0;
end

if (t<=t1)
kd=1.22*10^4; kp=kd*6000; ki=kd*10^6; ki=0;
elseif (t<=t2)
kd=1.22*10^4; kp=kd*6000; ki=kd*10^6; ki=0;
elseif (t<=t3)
kd=1.22*10^4; kp=kd*6000; ki=kd*10^6; ki=0;
elseif (t<=t4)
kd=1.22*10^4; kp=kd*6000; ki=kd*10^6; ki=0;
end

omega=abs(((r0/r1*f_1)^2+(1/r1*10^2)^2)^(1/2)*x(2)*60);
M0=f0*10^(-7)*(omega*nyu)^(2/3)*T^3+f0*10^(-
7)*(abs(f_1*x(2)*60)*nyu)^(2/3)*6.0^3;

Fs=ksp*x(1);
a2=1/r0/f_1*10^2;
Fn=abs(Fs)*(1+a2^2)^(0.5);
M1=myu2*f2*T/2*Fn+myu2*f2*6.0/2*abs(ksp*x(1));
```

```
M=M0+M1;
Tm=r0/r1*M*sign(x(2))*10^(-3);

if (((t<=inj_time)|((t>=(t1-inj_time)) & (t<=t1))|((t>=t2) &
(t<=(t2+inj_time)))|((t>=(t3-inj_time)) & (t<=t3))))
   i_t=i_t_j+(-577/3*6000*(x(1)-x_r)-577/3*(x(2)-v_r)-ki*x(3));
elseif (((t>t1)&(t<t2))|(t>t3))
      i_t=i_t_j+(-60*10^3*6000*(x(1)-x_r)-60*10^3*(x(2)-v_r)-ki*x(3));
elseif (x(1)<=(-lift/2))
   i_t=+c_2/(f_1*Kt)*(a_r-1/c_2*(-(b*f_1^2+bsp+bs+bg)*x(2)-ksp*x(1)-
ks*(x(1)+lift/2)+(-Tm)*f_1+f_t-J*f_2*f_1*x(2)^2)...
      -kp*(x(1)-x_r)-kd*(x(2)-v_r)-ki*x(3));
elseif (x(1)<=(lift/2))
   i_t=+c_2/(f_1*Kt)*(a_r-1/c_2*(-(b*f_1^2+bsp+bg)*x(2)-ksp*x(1)+(-
Tm)*f_1+f_t-J*f_2*f_1*x(2)^2)...
      -kp*(x(1)-x_r)-kd*(x(2)-v_r)-ki*x(3));
elseif (x(1)>(lift/2))
   i_t=+c_2/(f_1*Kt)*(a_r-1/c_2*(-(b*f_1^2+bsp+bg)*x(2)-ksp*x(1)-
ks*(x(1)-lift/2)+(-Tm)*f_1+f_t-J*f_2*f_1*x(2)^2)...
      -kp*(x(1)-x_r)-kd*(x(2)-v_r)-ki*x(3));
end

power=i_t^2*res+i_t*Kt*f_1*x(2);

xdot(1)=x(2);

if (x(1)<=(-lift/2))
   xdot(2)=1/c_2*(-(b*f_1^2+bsp+bs+bg)*x(2)-ksp*x(1)-
ks*(x(1)+lift/2)+(Kt*i_t-Tm)*f_1+f_t-J*f_2*f_1*x(2)^2);
elseif (x(1)<=(lift/2))
   xdot(2)=1/c_2*(-(b*f_1^2+bsp+bg)*x(2)-ksp*x(1)+(Kt*i_t-Tm)*f_1+f_t-
J*f_2*f_1*x(2)^2);
elseif (x(1)>(lift/2))
   xdot(2)=1/c_2*(-(b*f_1^2+bsp+bg)*x(2)-ksp*x(1)-ks*(x(1)-
lift/2)+(Kt*i_t-Tm)*f_1+f_t-J*f_2*f_1*x(2)^2);
else
   xdot(2)=1/c_2*(-(b*f_1^2+bsp+bs+bg)*x(2)-ksp*x(1)-ks*(x(1)-
lift/2)+(Kt*i_t-Tm)*f_1+f_t-J*f_2*f_1*x(2)^2);
end
xdot(3)=-(x_r-x(1));
```

Table A.2. Parameters used for the simulations for Fig. 5.4.

Parameters	Value
Inertia in motor side (J)	$5.9 \cdot 10^{-6}$ (kg-m^2)
Friction in motor side (b)	$8.4 \cdot 10^{-4}$ (kg-m^2/s)
Torque constant (K_T)	0.07 (N-m/A)
Mass in the valve side (m_v)	0.083 (kg)
Friction in the valve side (b_v)	6 (kg/s)
Stiffness of springs (k)	$1.12 \cdot 10^5$ (N/m)
Resistance (R)	0.89 Ω
Flatness of NTF (a_1) in (7.1)	0.999999
Nominal transformer characteristic of NTF (a_2) in (7.1)	3.46
Valve lift (L)	8 (mm)

A.3 Matlab simulation programs and parameters for Fig. 5.5.

```
% This is the Matlab code to investigate the dynamic behaviors of
% an EMVD incorporating a linear transformer and a rotary motor,
% with realistic parameters (see Table A.3) resulting in Fig. 5.5.
% Run new2.m with newd2.m (a differential equation solver).


%%%%%%%%%%%%%%%%%%%%%%%%%%%%%%%%%%%%%%%%%%%%%%%%%%%%%%%%%%%%%%%%%%%%%%%%%%%%
% file name: new2.m
% by
% Woo Sok Chang
% 1/19/2000
% EMVD project in LEES, EECS, MIT

global kp kd ki lift R L Kt J b r kv ks t1 t2 t3 t4 t5 t6 t7 bs bg m
       bsp ksp fe1 fe2 trans_time a_0 w_0 x_0 interval_time c_2 c_1 c_0

%kp, kd, ki are P, D, and I gains of PID controller
kp=2.5*10^6; kd=1000; ki=4*10^9;

% fe1, fe2; external gas force values at fully closed and open
% positions, respectively.
fe1=250; fe2=50;

trans_time=3*10^-3; w_0=2*pi/trans_time; a_0=2*pi*lift/(trans_time)^2;
interval_time=trans_time;

t1=trans_time;t2=trans_time+interval_time;
t3=2*trans_time+interval_time; t4=2*trans_time+2*interval_time;
t5=3*trans_time+2*interval_time; t6=3*trans_time+3*interval_time;
t7=4*trans_time+3*interval_time;

% -/+lift/2 represents valve fully closed/open, respectively.
lift=8*10^-3;

%t0 & tf: simulation time
t0=0; tf=t4;

% Kt: torque constant; J: inertia on the actuator side;
% b: viscous friction coeff on the actuator side
% ks: stiffness of valve seat; bs: viscous friction coeff of valve seat
% m: valve mass; bg: viscous friction coeff on the valve side;
% bsp: viscous friction coeff of valve spring
%ksp=spring constant of valve spring

Kt=6.73*10^-2; J=1.1*10^-5; b=1.16*10^-5;ks=10^8; bs=407;
m=0.1; bg=0; bsp=0;

% r: modulus of mechanical transformer
% (angular vel.=linear vel./r; torque=force*r

r=(J/m)^0.5; ksp=(J/r^2+m)*(pi/trans_time)^2;

% x_0=-lift/2 means the valve is initially fully closed.
x_0=-lift/2;
```

```
x3_0=-ksp*x_0*r/(Kt*ki); x0=[x_0 0 x3_0]';

[t,x]=ode45('newd2', [t0 tf], x0);

% Plot control input (current) u=i(t) as well.
u=[]; a=[];

for i=1:length(t)
if (t(i)<=t1)
   x_r=-lift/2+a_0/w_0*t(i)-a_0/(w_0^2)*sin(w_0*t(i));
   v_r=a_0/w_0-a_0/w_0*cos(w_0*t(i));
      f_t=-((fe2-fe1)/t1*t(i) + fe1);
elseif (t(i)<=t2)
    x_r=lift/2;
    v_r=0;
       f_t=-(fe2);
elseif (t(i)<=t3)
   x_r=lift/2-a_0/w_0*(t(i)-t2)+a_0/(w_0^2)*sin(w_0*(t(i)-t2));
   v_r=-a_0/w_0+a_0/w_0*cos(w_0*(t(i)-t2));
      f_t=-((0-fe2)/(t3-t2)*(t(i)-t2) + fe2);
elseif (t(i)<=t4)
   x_r=-lift/2;
   v_r=0;
      f_t=0;
end

u=[u;-kp*(x(i,1)-x_r)-kd*(x(i,2)-v_r)-ki*x(i,3)];

if (x(i,1)<=(-lift/2))
   a=[a;1/c_2*(-(b/r^2+bsp+bs)*x(i,2)-ksp*x(i,1)-
ks*(x(i,1)+lift/2)+Kt*u(i)/r+f_t)];
else
   a=[a;1/c_2*(-(b/r^2+bsp)*x(i,2)-ksp*x(i,1)+Kt*u(i)/r+f_t)];
end
end

% x(1): valve position; x(2): valve velocity; u: motor current
figure
plot(t*10^3,x(:,1)*10^3,t*10^3,x(:,2),t*10^3,u/100,t*10^3,a/1000)
%legend('valve displacement: X[mm]','valve velocity: V[m/s]','motor
current: i[100A]','acceleration: a[1000m/sec^2')
axis([0 t4*10^3 -10 10])
grid
%title('Time response of an electromechanical engine valve')
%xlabel('time[msec]')
%ylabel('X[mm], V[m/s], i[100A], a[1000m/sec^2]')


%%%%%%%%%%%%%%%%%%%%%%%%%%%%%%%%%%%%%%%%%%%%%%%%%%%%%%%%%%%%%%%%%%%%%%%%%%%%%%%
% file name: newd2.m
% by
% Woo Sok Chang
% 1/19/2000
% EMVD project in LEES, EECS, MIT

function xdot=newd2(t,x)
global kp kd ki lift R L Kt J b r kv ks t1 t2 t3 t4 t5 t6 t7 bs bg m
```

```
      bsp ksp fe1 fe2 trans_time a_0 w_0 interval_time c_2 c_1 c_0

if (t<=t1)
   x_r=-lift/2+a_0/w_0*t-a_0/(w_0^2)*sin(w_0*t);
   v_r=a_0/w_0-a_0/w_0*cos(w_0*t);
   f_t=-((fe2-fe1)/t1*t + fe1);
elseif (t<=t2)
   x_r=lift/2; v_r=0; f_t=-(fe2);
elseif (t<=t3)
   x_r=lift/2-a_0/w_0*(t-t2)+a_0/(w_0^2)*sin(w_0*(t-t2));
   v_r=-a_0/w_0+a_0/w_0*cos(w_0*(t-t2));
   f_t=-((0-fe2)/(t3-t2)*(t-t2) + fe2);
elseif (t<=t4)
   x_r=-lift/2; v_r=0; f_t=0;
end

c_2=(J/r^2+m);

xdot=zeros(3,1);

% x(1)=valve position; x(2)=valve velocity;
% x(3)=integration of valve position error
% i_t=control input (current source) to plant; PID controller

i_t=(-kp*(x(1)-x_r)-kd*(x(2)-v_r)-ki*x(3));
xdot(1)=x(2);

if (x(1)<=(-lift/2))
   xdot(2)=1/c_2*(-(b/r^2+bsp+bs)*x(2)-ksp*x(1)-
ks*(x(1)+lift/2)+Kt*i_t/r+f_t);
else
   xdot(2)=1/c_2*(-(b/r^2+bsp)*x(2)-ksp*x(1)+Kt*i_t/r+f_t);
end
xdot(3)=x(1)-x_r;
```

Table A.3. Parameters used for the simulations for Fig. 5.5.

Parameters	Value
Inertia in motor side (J)	$1.1 \cdot 10^{-5}$ (kg-m^2)
Friction in motor side (b)	$1.16 \cdot 10^{-5}$ (kg-m^2/s)
Torque constant (K_T)	0.0673 (N-m/A)
Mass in the valve side (m_v)	0.1 (kg)
Friction in the valve side (b_v)	0 (kg/s)
Transformer modulus (r)	$(J/m_v)^{0.5} = 1.05 \cdot 10^{-2}$ (m/rad)
Transition time (t_o)	$3 \cdot 10^{-3}$ (s)
Stiffness of springs (k)	$(J/r^2+m_v) \cdot (\pi/t_o)^2$ $= 2.2 \cdot 10^5$ (N/m)
Valve lift (L)	8 (mm)

A.4 Matlab program for Fig. 7.4.

```
% This is the program to generate surface profiles of a disk cam
% (Fig. 7.4).


%%%%%%%%%%%%%%%%%%%%%%%%%%%%%%%%%%%%%%%%%%%%%%%%%%%%%%%%%%%%%%%%%%%%%%%%%%%%%%%
% file name: ntf.m
% by
% Woo Sok Chang
% 4/1/2002
% EMVD project in LEES, EECS, MIT

% for a disk cam
h_0=16*10^-3; r_0=4*10^-3; lift=8*10^-3;

theta_min=-26*pi/180; theta_max=26*pi/180;

theta=theta_min:0.01:theta_max;

g_theta=lift/2*sin(3.46*theta); dg_theta=lift/2*3.46*cos(3.46*theta);

x_0=-(sin(theta)).*(g_theta-h_0); y_0=(cos(theta)).*(g_theta-h_0);

d_x=-(cos(theta)).*g_theta-(sin(theta)).*dg_theta+h_0*cos(theta);
d_y=-(sin(theta)).*g_theta+(cos(theta)).*dg_theta+h_0*sin(theta);

if (atan(d_y./d_x)<0)
x_1=x_0+r_0*cos(pi/2-atan(d_y./d_x));
y_1=y_0+r_0*sin(pi/2-atan(d_y./d_x));
x_2=x_0+r_0*cos(-pi/2-atan(d_y./d_x));
y_2=y_0+r_0*sin(-pi/2-atan(d_y./d_x));
else
x_1=x_0+r_0*cos(pi/2+atan(d_y./d_x));
y_1=y_0+r_0*sin(pi/2+atan(d_y./d_x));
x_2=x_0+r_0*cos(-pi/2+atan(d_y./d_x));
y_2=y_0+r_0*sin(-pi/2+atan(d_y./d_x));
end

figure
plot(x_1,y_1,'r',x_0,y_0,'g',x_2,y_2,'b')
axis([-0.0182,0.0182,-0.03,0.0])
grid

% for TK's elevated disk cam
h_0=-16*10^-3; r_0=4*10^-3; lift=8*10^-3;

theta_min=-26*pi/180;
theta_max=26*pi/180;
theta=theta_min:0.01:theta_max;

g_theta=lift/2*sin(3.46*theta); dg_theta=lift/2*3.46*cos(3.46*theta);

x_0=-(sin(theta)).*(g_theta-h_0); y_0=(cos(theta)).*(g_theta-h_0);

d_x=-(cos(theta)).*g_theta-(sin(theta)).*dg_theta+h_0*cos(theta);
```

```
d_y=-(sin(theta)).*g_theta+(cos(theta)).*dg_theta+h_0*sin(theta);

if (atan(d_y./d_x)<0)
x_1=x_0+r_0*cos(pi/2-atan(d_y./d_x));
y_1=y_0+r_0*sin(pi/2-atan(d_y./d_x));
x_2=x_0+r_0*cos(-pi/2-atan(d_y./d_x));
y_2=y_0+r_0*sin(-pi/2-atan(d_y./d_x));
else
x_1=x_0+r_0*cos(pi/2+atan(d_y./d_x));
y_1=y_0+r_0*sin(pi/2+atan(d_y./d_x));
x_2=x_0+r_0*cos(-pi/2+atan(d_y./d_x));
y_2=y_0+r_0*sin(-pi/2+atan(d_y./d_x));
end

figure
plot(x_1,y_1,'r',x_0,y_0,'g',x_2,y_2,'b')
axis([-0.0182,0.0182,0.0,0.03])
grid
```

B Motor drive circuit [41]

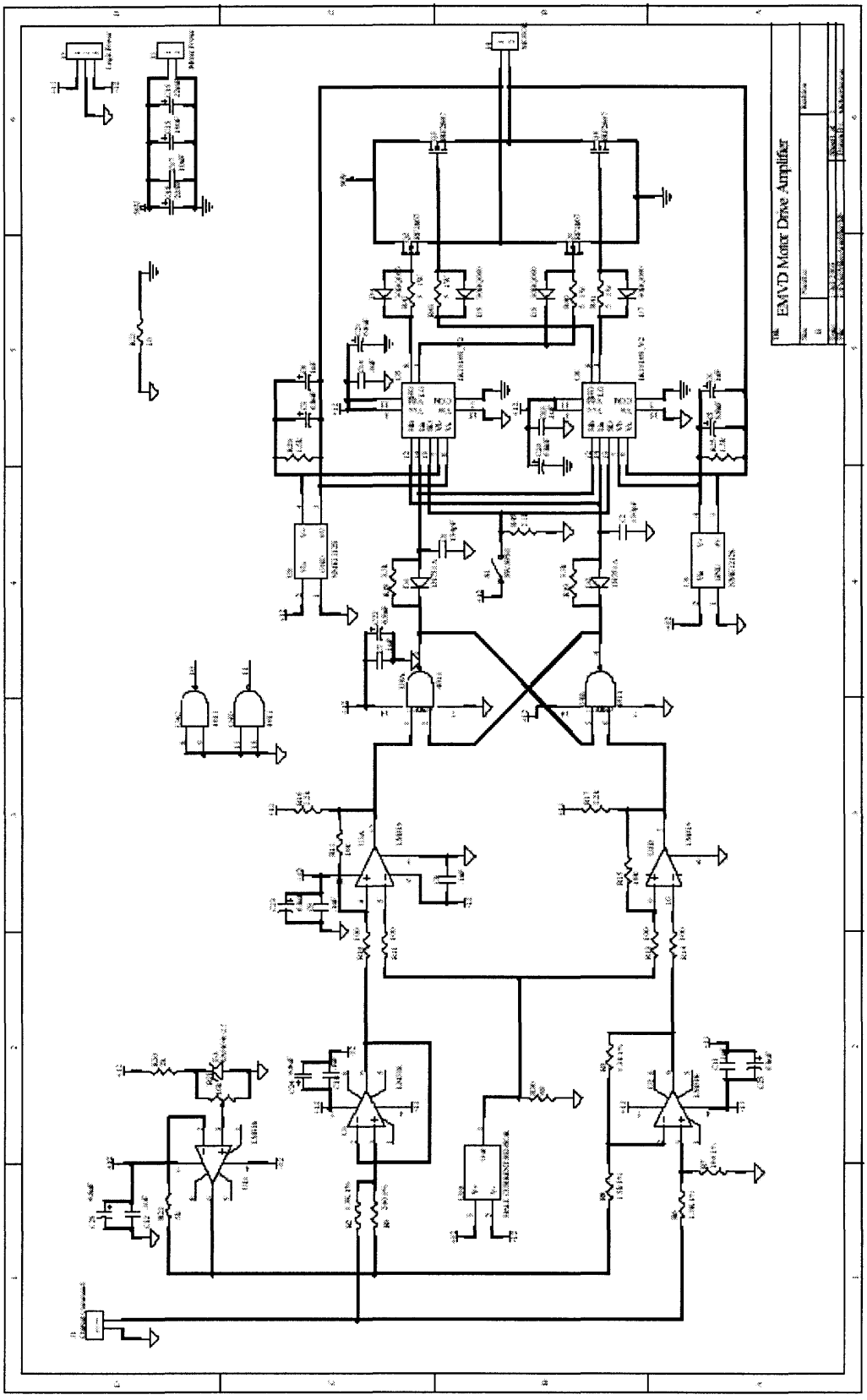

C Mechanical drawings

I designed the mechanical components and subsystems of the EMVD apparatus in 2-D and 3-D, and determined the geometric specifications including tolerances. Based on the 2-D and 3-D designs, Tushar Parlikar prepared the following drawings using the SolidWorks™, which were useful to confirm the designs.

C.1 Motor mount (front)

C.2 Motor mount (back)

C.3 Column I

C.4 Column II

C.5 Disk cam

C.6 Bearing housing

C.7 Bearing housing holder

C.8 Top plate

C.9 Bottom plate

C.10 Valve holder

C.11 Spring divider

C.12 Valve seat

C.13 Table

C.14 3-D view of the experimental apparatus

C.1

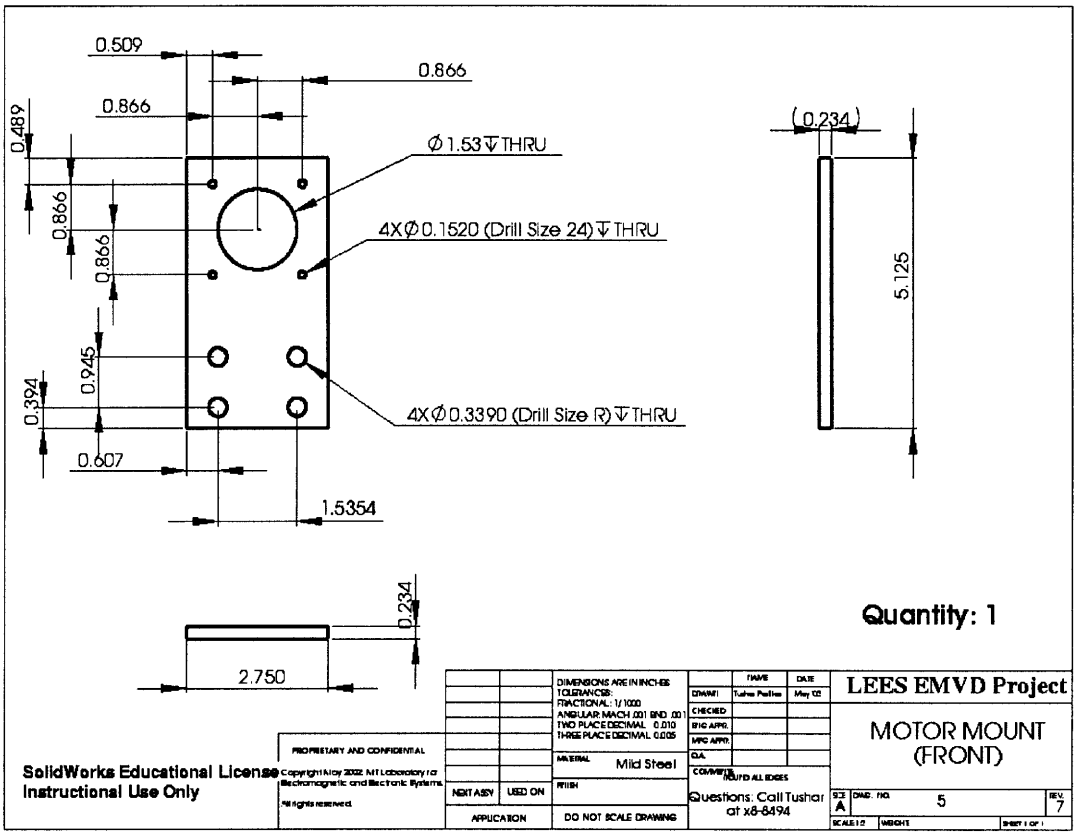
0.509
0.866
0.866
0.489
Ø1.53↧THRU
4XØ0.1520 (Drill Size 24)↧THRU
0.866
0.866
0.945
0.394
4XØ0.3390 (Drill Size R)↧THRU
0.607
1.5354
(0.234)
5.125
0.234
2.750
Quantity: 1
SolidWorks Educational License
Instructional Use Only
PROPRIETARY AND CONFIDENTIAL
Copyright May 2002, MIT Laboratory for Electromagnetic and Electronic Systems
All rights reserved
DIMENSIONS ARE IN INCHES
TOLERANCES:
FRACTIONAL: 1/1000
ANGULAR: MACH .001 BND .001
TWO PLACE DECIMAL .010
THREE PLACE DECIMAL .005
MATERIAL Mild Steel
FINISH
NEXT ASSY
USED ON
APPLICATION
DO NOT SCALE DRAWING
NAME
DATE
DRAWN Tushar Patkar May 02
CHECKED
ENG APPR.
MFG APPR.
Q.A.
COMMENTS
BREAK ALL EDGES
Questions: Call Tushar at x8-8494
LEES EMVD Project
MOTOR MOUNT (FRONT)
SIZE A
DWG. NO. 5
REV. 7
SCALE 1:2
WEIGHT
SHEET 1 OF 1

C.2

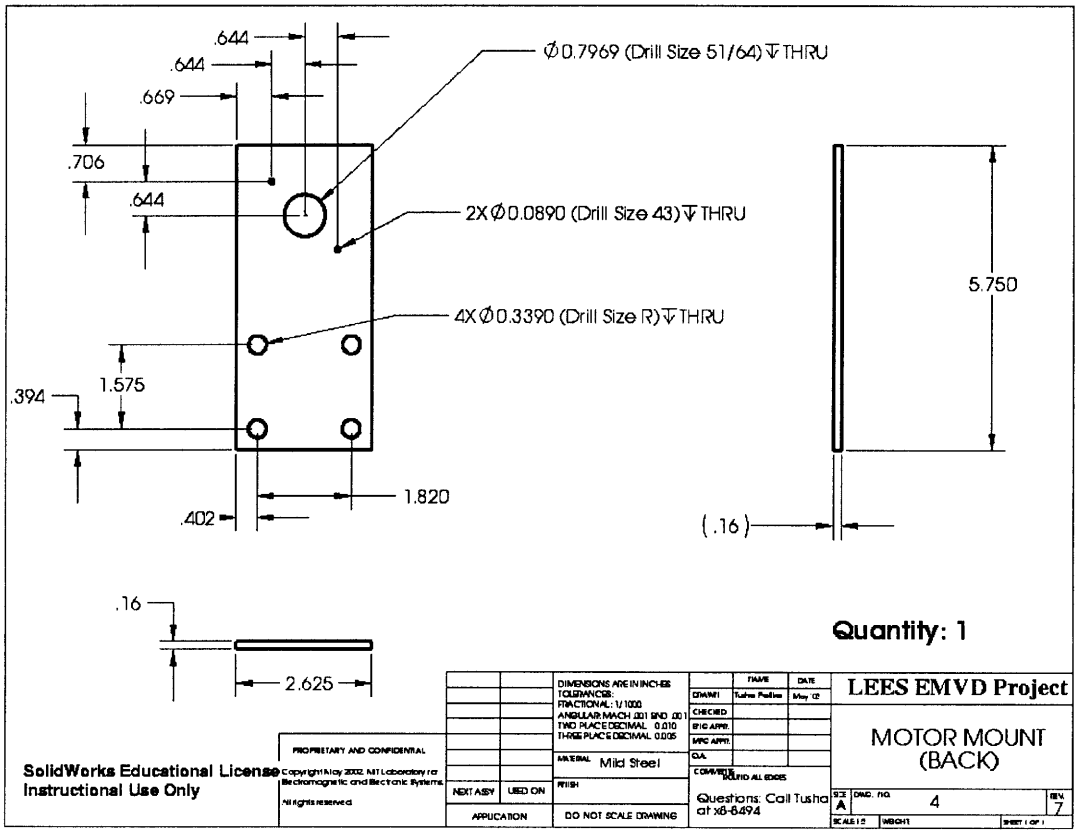
.644
.644
.669
Ø0.7969 (Drill Size 51/64)↧THRU
.706
.644
2XØ0.0890 (Drill Size 43)↧THRU
4XØ0.3390 (Drill Size R)↧THRU
5.750
1.575
.394
1.820
.402
(.16)
.16
2.625
Quantity: 1
SolidWorks Educational License
Instructional Use Only
PROPRIETARY AND CONFIDENTIAL
Copyright May 2002, MIT Laboratory for Electromagnetic and Electronic Systems
All rights reserved
DIMENSIONS ARE IN INCHES
TOLERANCES:
FRACTIONAL: 1/1000
ANGULAR: MACH .001 BND .001
TWO PLACE DECIMAL .010
THREE PLACE DECIMAL .005
MATERIAL Mild Steel
FINISH
NEXT ASSY
USED ON
APPLICATION
DO NOT SCALE DRAWING
NAME
DATE
DRAWN Tushar Patkar May 02
CHECKED
ENG APPR.
MFG APPR.
Q.A.
COMMENTS
BREAK ALL EDGES
Questions: Call Tushar at x8-8494
LEES EMVD Project
MOTOR MOUNT (BACK)
SIZE A
DWG. NO. 4
REV. 7
SCALE 1:2
WEIGHT
SHEET 1 OF 1

C.3

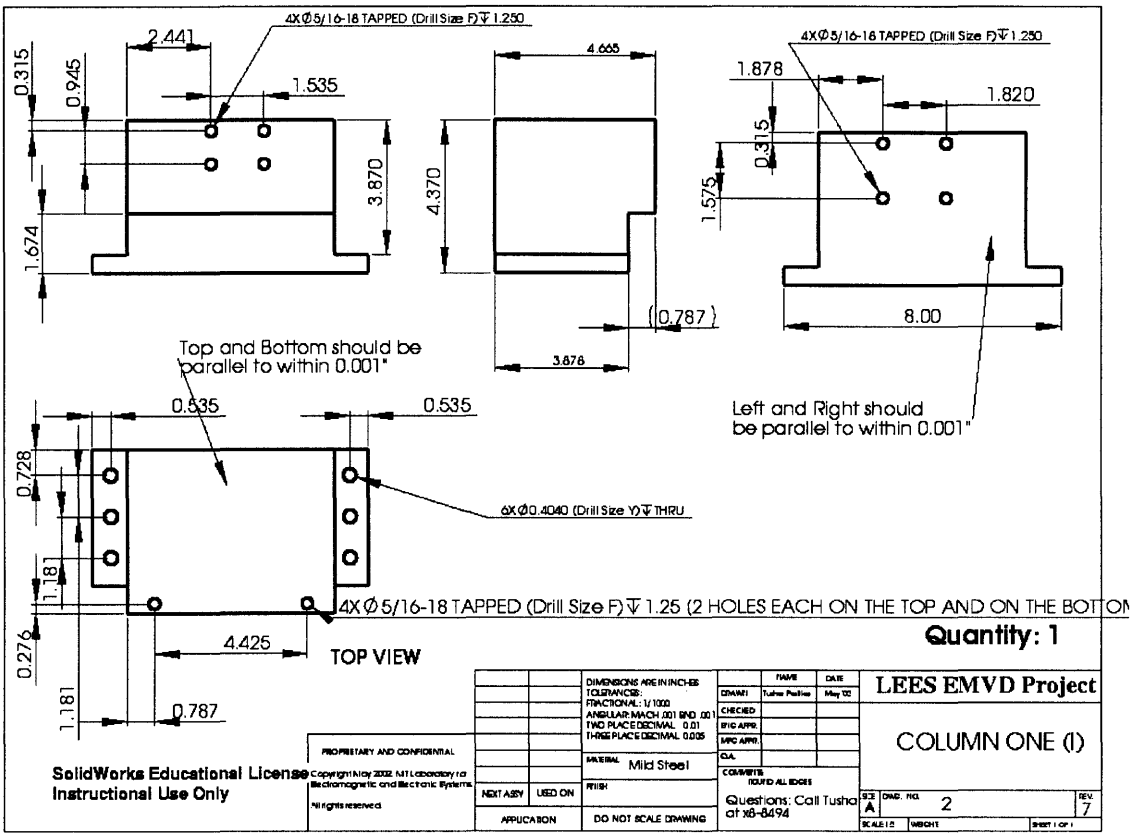
4XØ5/16-18 TAPPED (Drill Size F)↧1.250
2.441
1.535
0.315
0.945
3.870
1.674
4.665
4.370
(0.787)
3.876
4XØ5/16-18 TAPPED (Drill Size F)↧1.250
1.878
1.820
0.315
1.575
8.00
Top and Bottom should be parallel to within 0.001"
Left and Right should be parallel to within 0.001"
0.535
0.535
0.728
6XØ0.4040 (Drill Size Y)↧THRU
1.181
4XØ5/16-18 TAPPED (Drill Size F)↧1.25 (2 HOLES EACH ON THE TOP AND ON THE BOTTOM
Quantity: 1
0.276
4.425
TOP VIEW
1.181
0.787
SolidWorks Educational License
Instructional Use Only
PROPRIETARY AND CONFIDENTIAL
Mild Steel
DO NOT SCALE DRAWING
Questions: Call Tushar at x8-8494
LEES EMVD Project
COLUMN ONE (I)
2

C.4

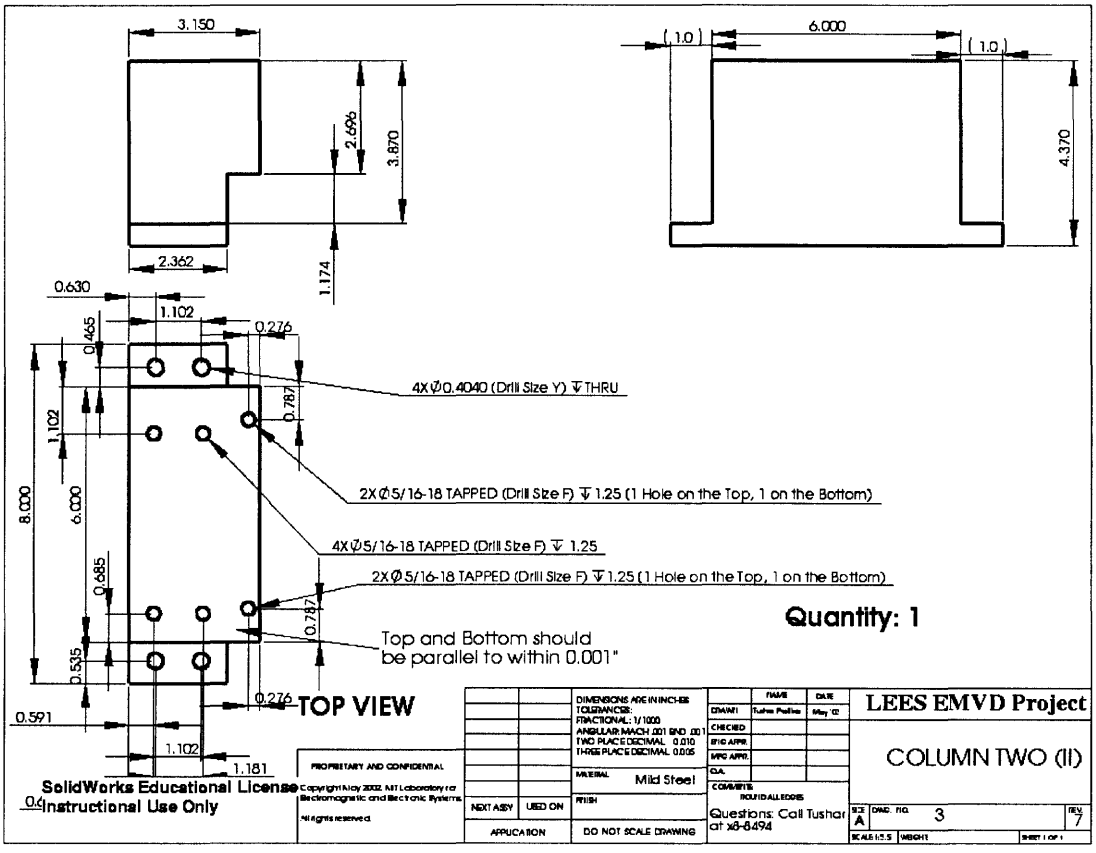
3.150
2.696
3.870
2.362
1.174
(1.0)
6.000
(1.0)
4.370
0.630
1.102
0.276
0.465
4XØ0.4040 (Drill Size Y)↧THRU
0.787
1.102
8.000
6.000
2XØ5/16-18 TAPPED (Drill Size F)↧1.25 (1 Hole on the Top, 1 on the Bottom)
4XØ5/16-18 TAPPED (Drill Size F)↧1.25
0.685
2XØ5/16-18 TAPPED (Drill Size F)↧1.25 (1 Hole on the Top, 1 on the Bottom)
0.787
Quantity: 1
Top and Bottom should be parallel to within 0.001"
0.535
0.276
TOP VIEW
0.591
1.102
1.181
SolidWorks Educational License
Instructional Use Only
PROPRIETARY AND CONFIDENTIAL
Mild Steel
DO NOT SCALE DRAWING
Questions: Call Tushar at x8-8494
LEES EMVD Project
COLUMN TWO (II)
3

C.5

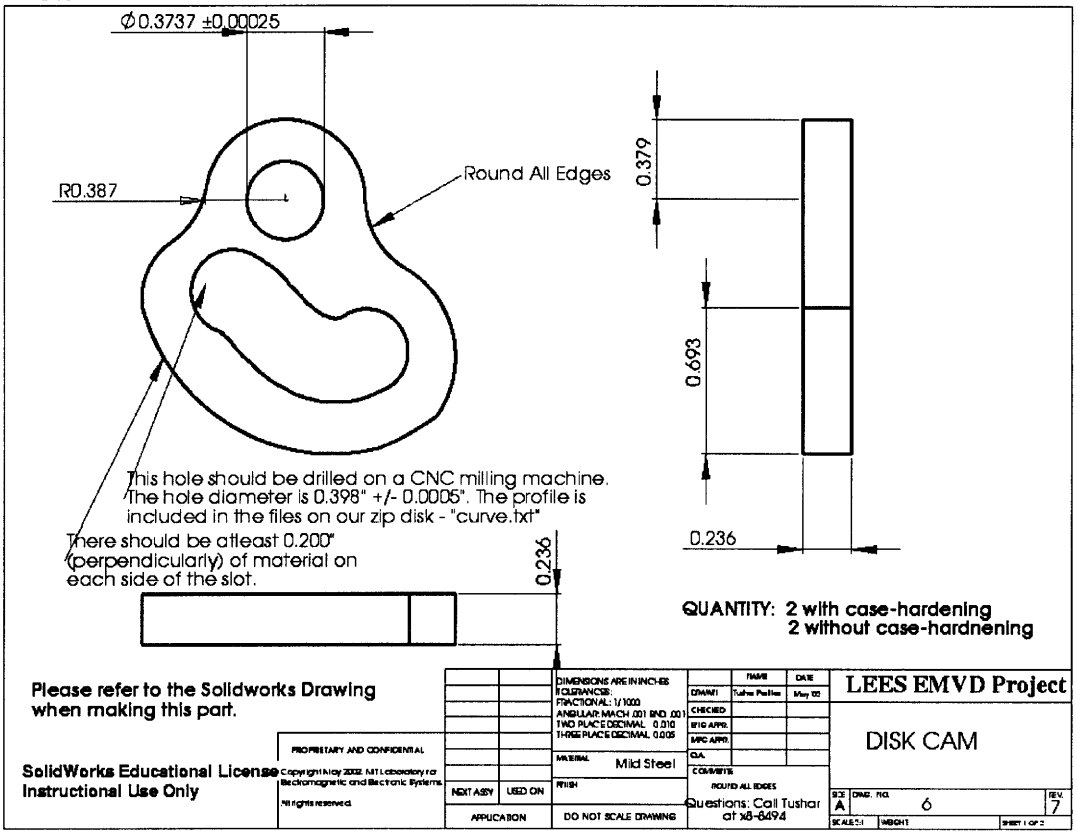
Ø0.3737 ±0.00025
R0.387
Round All Edges
0.379
0.693
0.236
This hole should be drilled on a CNC milling machine.
The hole diameter is 0.398" +/- 0.0005". The profile is
included in the files on our zip disk - "curve.txt"
There should be atleast 0.200"
(perpendicularly) of material on
each side of the slot.
0.236
QUANTITY: 2 with case-hardening
2 without case-hardnening
Please refer to the Solidworks Drawing
when making this part.
SolidWorks Educational License
Instructional Use Only
PROPRIETARY AND CONFIDENTIAL
Copyright May 2002 MIT Laboratory for Electromagnetic and Electronic Systems
All rights reserved.
DIMENSIONS ARE IN INCHES
TOLERANCES:
FRACTIONAL: 1/1000
ANGULAR: MACH .001 BND .001
TWO PLACE DECIMAL 0.010
THREE PLACE DECIMAL 0.005
MATERIAL Mild Steel
FINISH
NEXT ASSY
USED ON
APPLICATION
DO NOT SCALE DRAWING
NAME
DATE
DRAWN Tushar Parlikar May 02
CHECKED
ENG APPR.
MFG APPR.
Q.A.
COMMENTS
BREAK ALL EDGES
Questions: Call Tushar at x8-6494
LEES EMVD Project
DISK CAM
SIZE A
DWG. NO. 6
REV. 7
SCALE: 1:1
WEIGHT
SHEET 1 OF 2

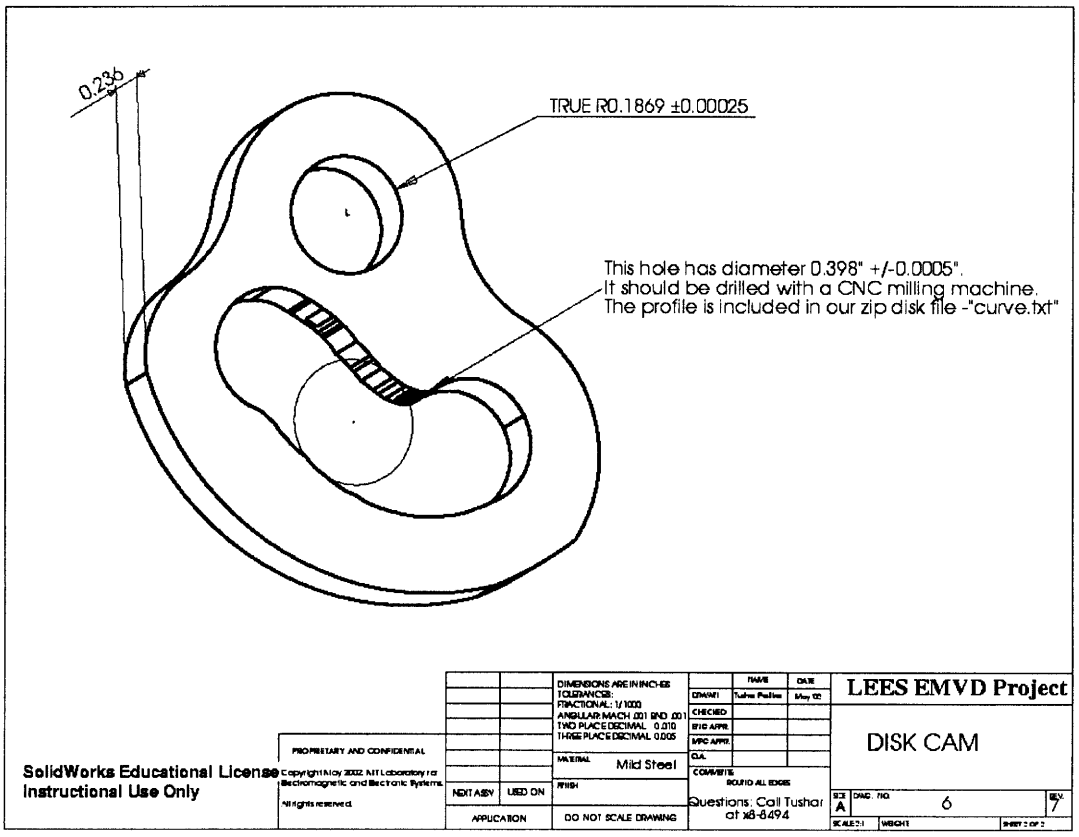
0.236
TRUE R0.1869 ±0.00025
This hole has diameter 0.398" +/-0.0005".
It should be drilled with a CNC milling machine.
The profile is included in our zip disk file -"curve.txt"
SolidWorks Educational License
Instructional Use Only
PROPRIETARY AND CONFIDENTIAL
Copyright May 2002 MIT Laboratory for Electromagnetic and Electronic Systems
All rights reserved.
DIMENSIONS ARE IN INCHES
TOLERANCES:
FRACTIONAL: 1/1000
ANGULAR: MACH .001 BND .001
TWO PLACE DECIMAL 0.010
THREE PLACE DECIMAL 0.005
MATERIAL Mild Steel
FINISH
NEXT ASSY
USED ON
APPLICATION
DO NOT SCALE DRAWING
NAME
DATE
DRAWN Tushar Parlikar May 02
CHECKED
ENG APPR.
MFG APPR.
Q.A.
COMMENTS
BREAK ALL EDGES
Questions: Call Tushar at x8-6494
LEES EMVD Project
DISK CAM
SIZE A
DWG. NO. 6
REV. 7
SCALE: 1:1
WEIGHT
SHEET 2 OF 2

C.6

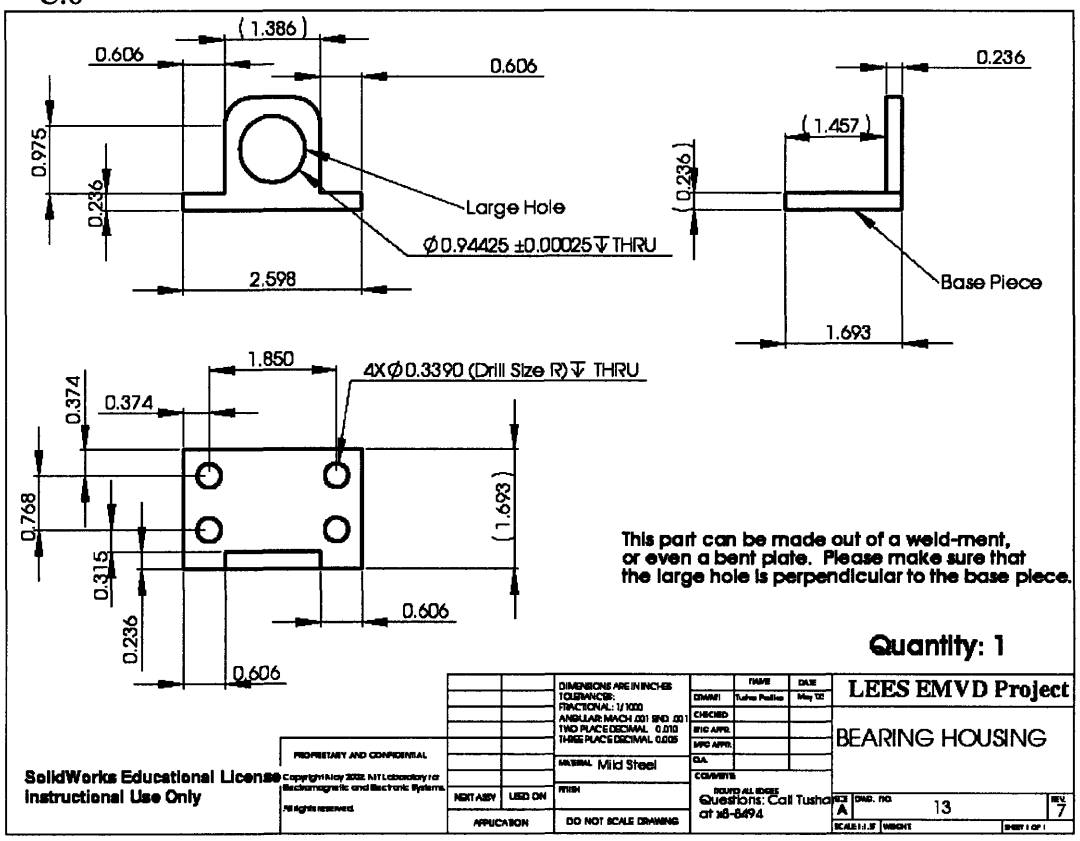

SolidWorks Educational License
Instructional Use Only

C.7

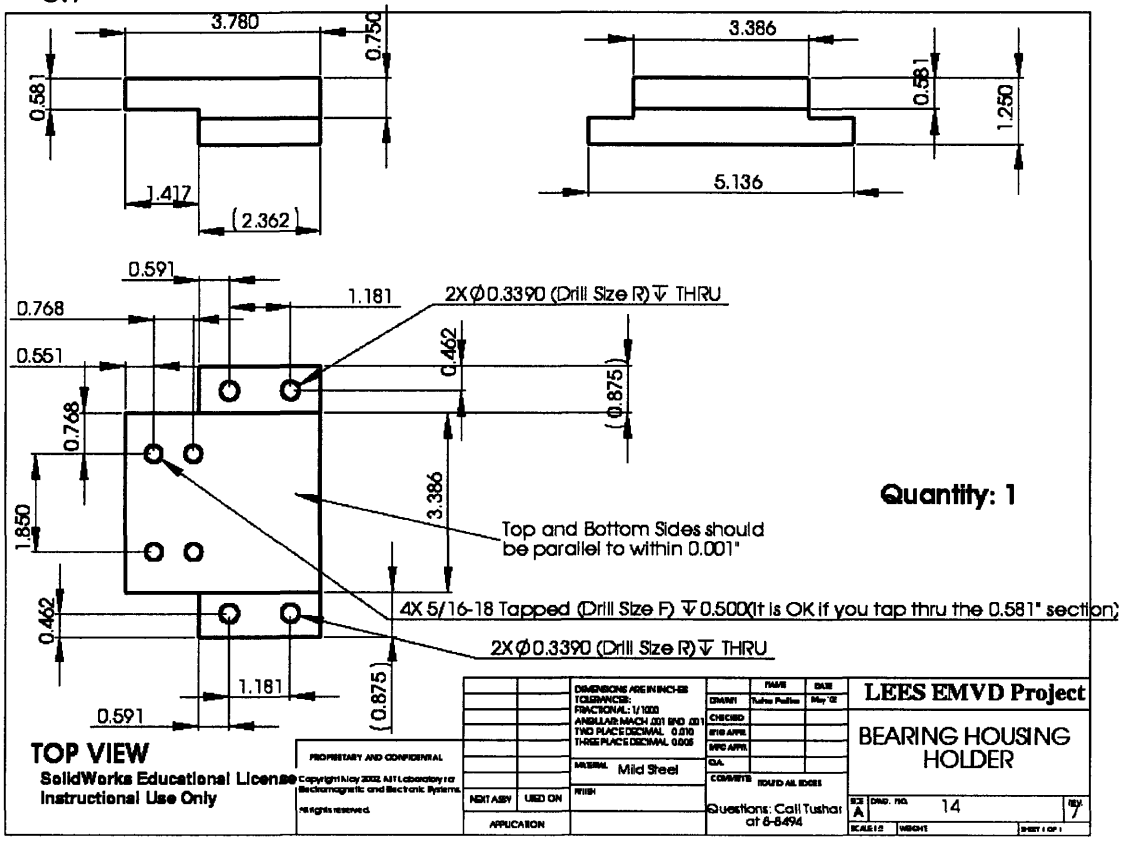

SolidWorks Educational License
Instructional Use Only

C.8

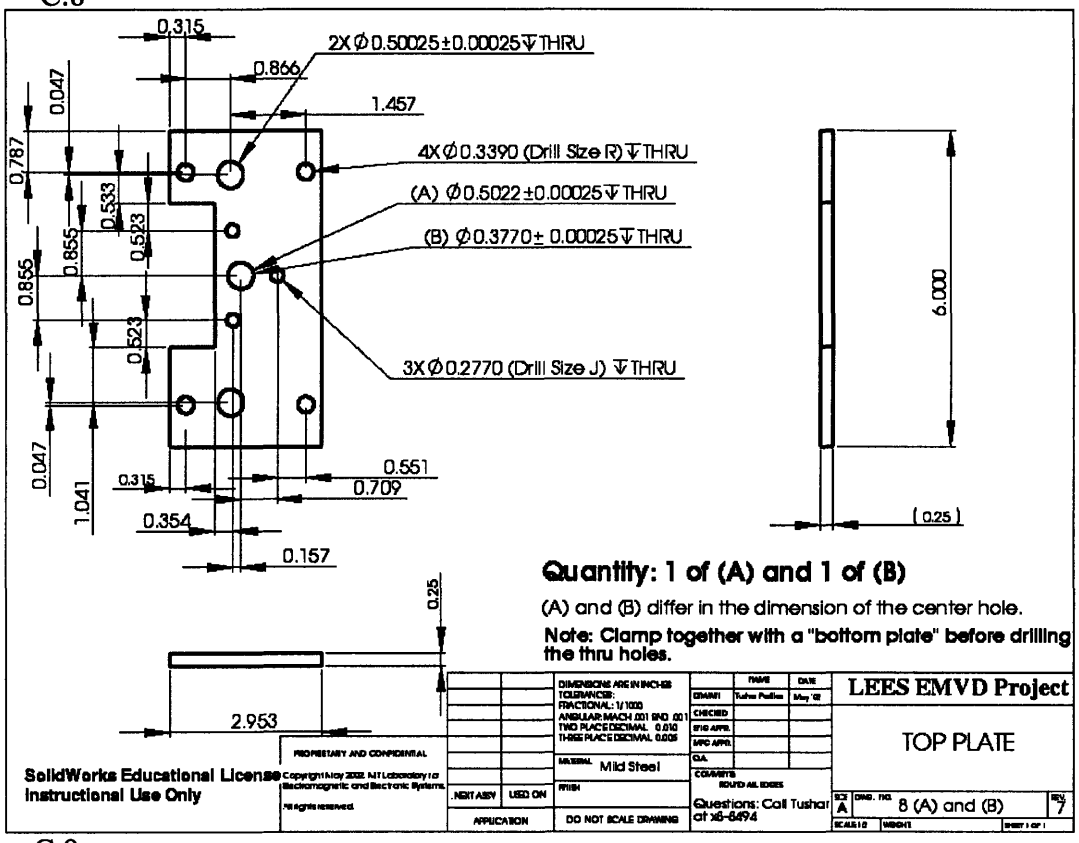
0.315
2X Ø0.50025±0.00025 ↧ THRU
0.866
1.457
0.047
0.787
4X Ø0.3390 (Drill Size R) ↧ THRU
(A) Ø0.5022±0.00025 ↧ THRU
0.533
0.523
0.855
(B) Ø0.3770± 0.00025 ↧ THRU
0.855
0.523
3X Ø0.2770 (Drill Size J) ↧ THRU
6.000
0.047
1.041
0.315
0.551
0.709
0.354
0.157
(0.25)
0.25
2.953
Quantity: 1 of (A) and 1 of (B)
(A) and (B) differ in the dimension of the center hole.
Note: Clamp together with a "bottom plate" before drilling the thru holes.
SolidWorks Educational License
Instructional Use Only
PROPRIETARY AND CONFIDENTIAL
Copyright May 2002 MIT Laboratory for Electromagnetic and Electronic Systems
All rights reserved.
DIMENSIONS ARE IN INCHES
TOLERANCES:
FRACTIONAL 1/1000
ANGULAR MACH .001 BND .001
TWO PLACE DECIMAL .010
THREE PLACE DECIMAL .005
MATERIAL Mild Steel
FINISH
NEXT ASSY
USED ON
APPLICATION
DO NOT SCALE DRAWING
DRAWN
Tushar Pedlow
May '02
CHECKED
ENG APPR.
MFG APPR.
Q.A.
COMMENTS
ROUND ALL EDGES
Questions: Call Tushar at x6-6494
LEES EMVD Project
TOP PLATE
SIZE A
DWG. NO. 8 (A) and (B)
REV. 7
SCALE 1/2
WEIGHT
SHEET 1 OF 1

C.9

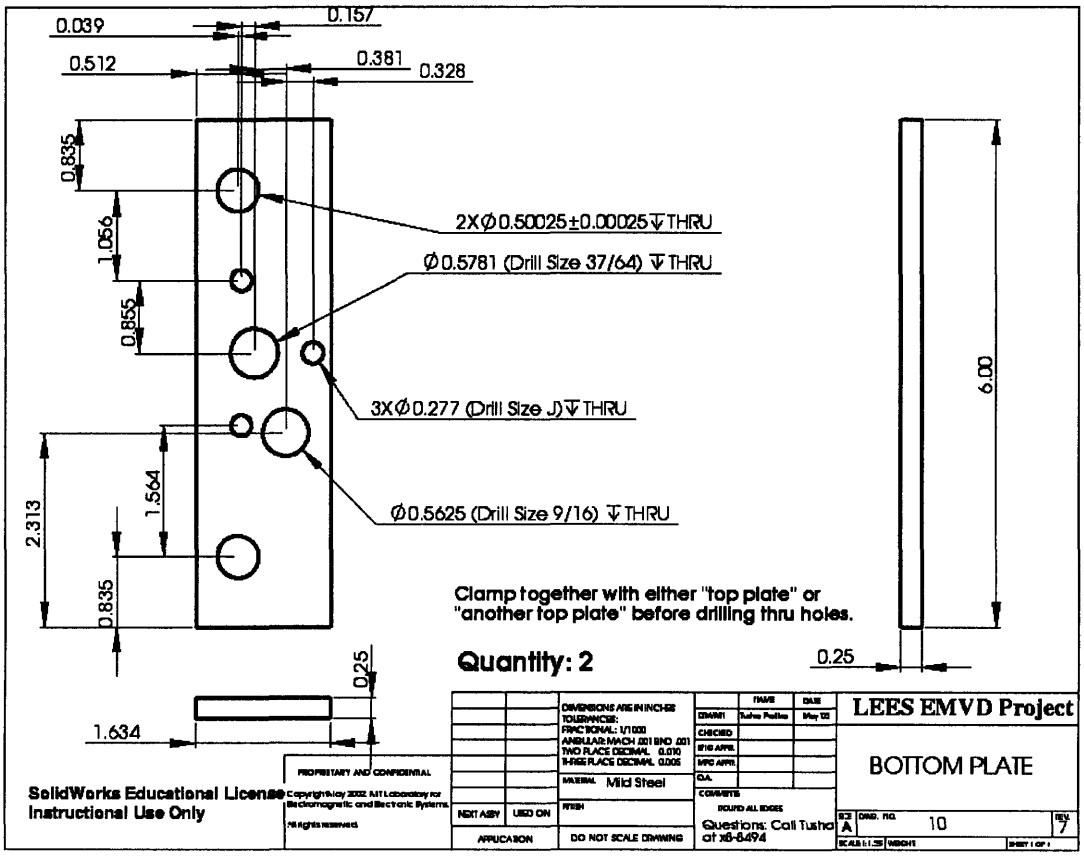
0.039
0.157
0.512
0.381
0.328
0.835
2X Ø0.50025±0.00025 ↧ THRU
1.056
Ø0.5781 (Drill Size 37/64) ↧ THRU
0.855
3X Ø0.277 (Drill Size J) ↧ THRU
6.00
2.313
1.564
Ø0.5625 (Drill Size 9/16) ↧ THRU
0.835
Clamp together with either "top plate" or "another top plate" before drilling thru holes.
Quantity: 2
0.25
0.25
1.634
SolidWorks Educational License
Instructional Use Only
PROPRIETARY AND CONFIDENTIAL
Copyright May 2002 MIT Laboratory for Electromagnetic and Electronic Systems
All rights reserved.
DIMENSIONS ARE IN INCHES
TOLERANCES:
FRACTIONAL 1/1000
ANGULAR MACH .001 BND .001
TWO PLACE DECIMAL .010
THREE PLACE DECIMAL .005
MATERIAL Mild Steel
FINISH
NEXT ASSY
USED ON
APPLICATION
DO NOT SCALE DRAWING
DRAWN
Tushar Pedlow
May '02
CHECKED
ENG APPR.
MFG APPR.
Q.A.
COMMENTS
ROUND ALL EDGES
Questions: Call Tushar at x6-6494
LEES EMVD Project
BOTTOM PLATE
SIZE A
DWG. NO. 10
REV. 7
SCALE 1/2
WEIGHT
SHEET 1 OF 1

C.10

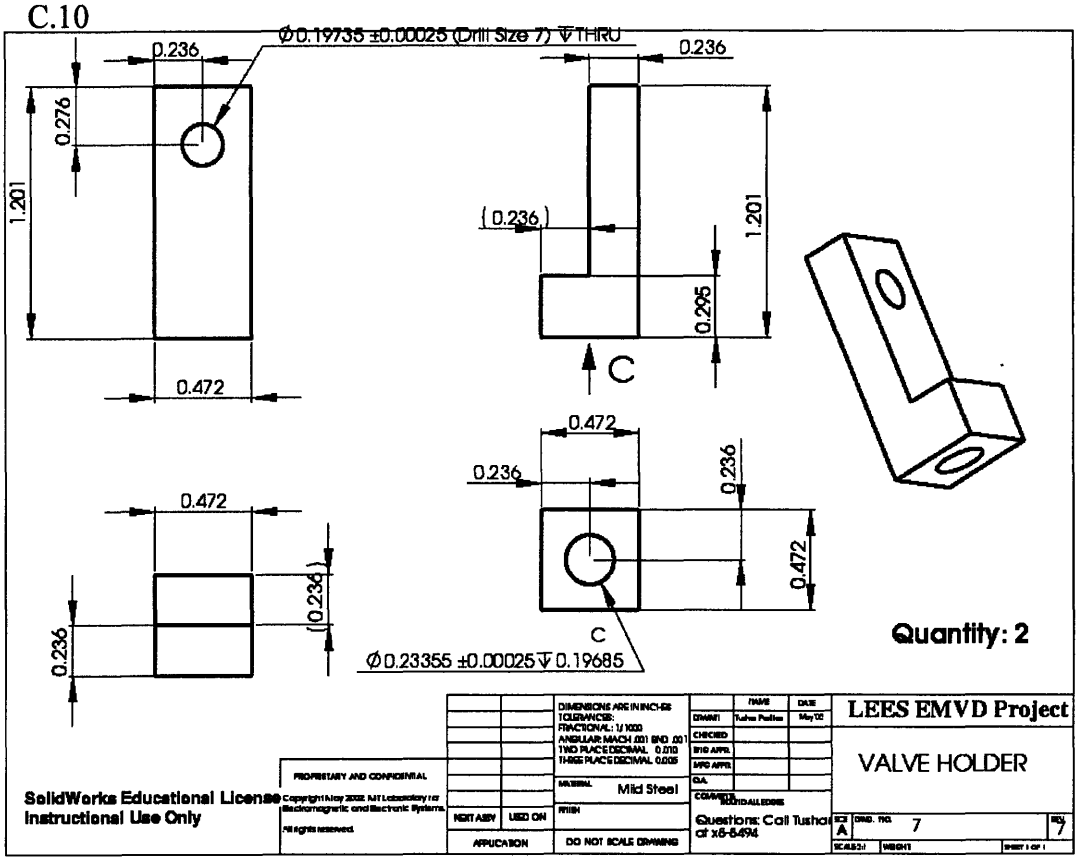
Ø0.19735 ±0.00025 (Drill Size 7) ↧THRU
0.236
0.276
1.201
0.472
0.236
1.201
0.295
C
0.472
0.236
0.236
0.472
0.472
0.236
0.236
C
Ø0.23355 ±0.00025↧0.19685
Quantity: 2
LEES EMVD Project
VALVE HOLDER
Mild Steel
DO NOT SCALE DRAWING
Questions: Call Tushar at x8-6494
SolidWorks Educational License
Instructional Use Only

C.11

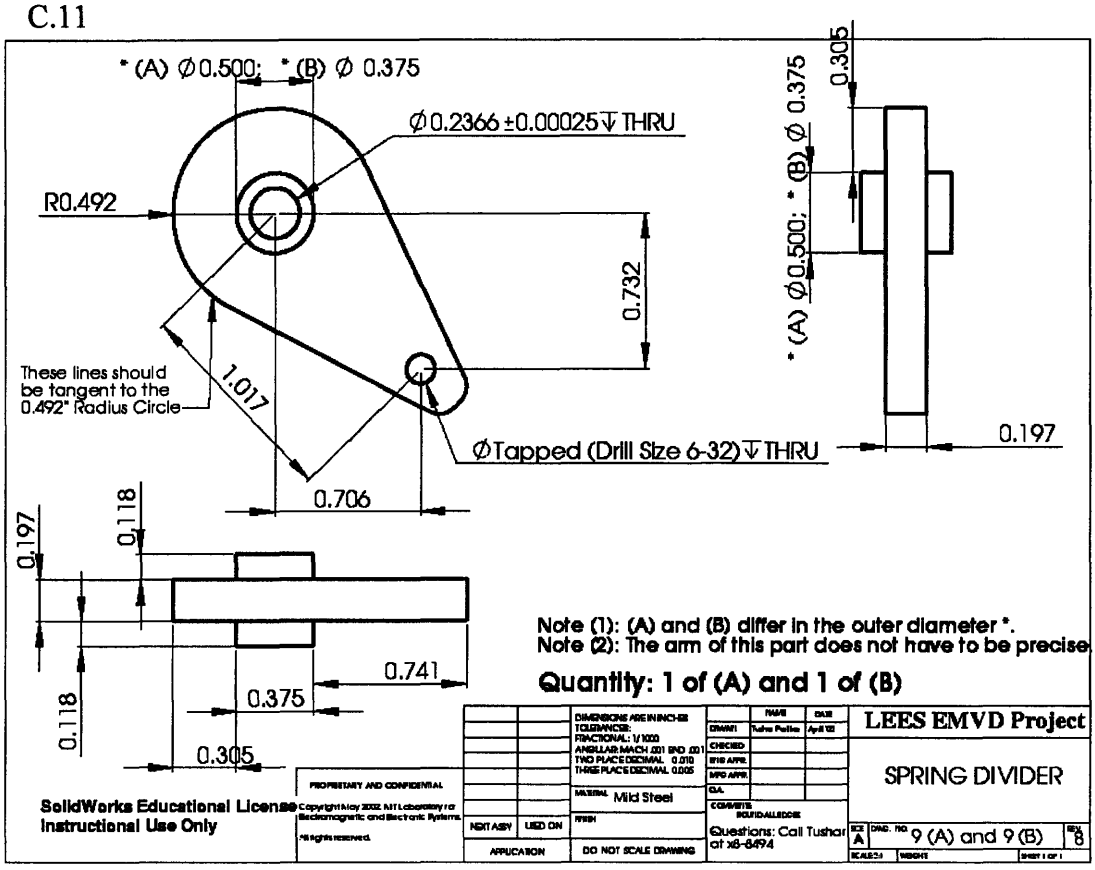
* (A) Ø0.500; * (B) Ø 0.375
Ø0.2366 ±0.00025↧THRU
R0.492
0.732
These lines should be tangent to the 0.492" Radius Circle
1.017
0.706
ØTapped (Drill Size 6-32)↧THRU
0.305
* (B) Ø 0.375
* (A) Ø0.500;
0.197
0.197
0.118
0.741
0.375
0.118
0.305
Note (1): (A) and (B) differ in the outer diameter *.
Note (2): The arm of this part does not have to be precise.
Quantity: 1 of (A) and 1 of (B)
LEES EMVD Project
SPRING DIVIDER
Mild Steel
DO NOT SCALE DRAWING
Questions: Call Tushar at x8-6494
SolidWorks Educational License
Instructional Use Only

C.12

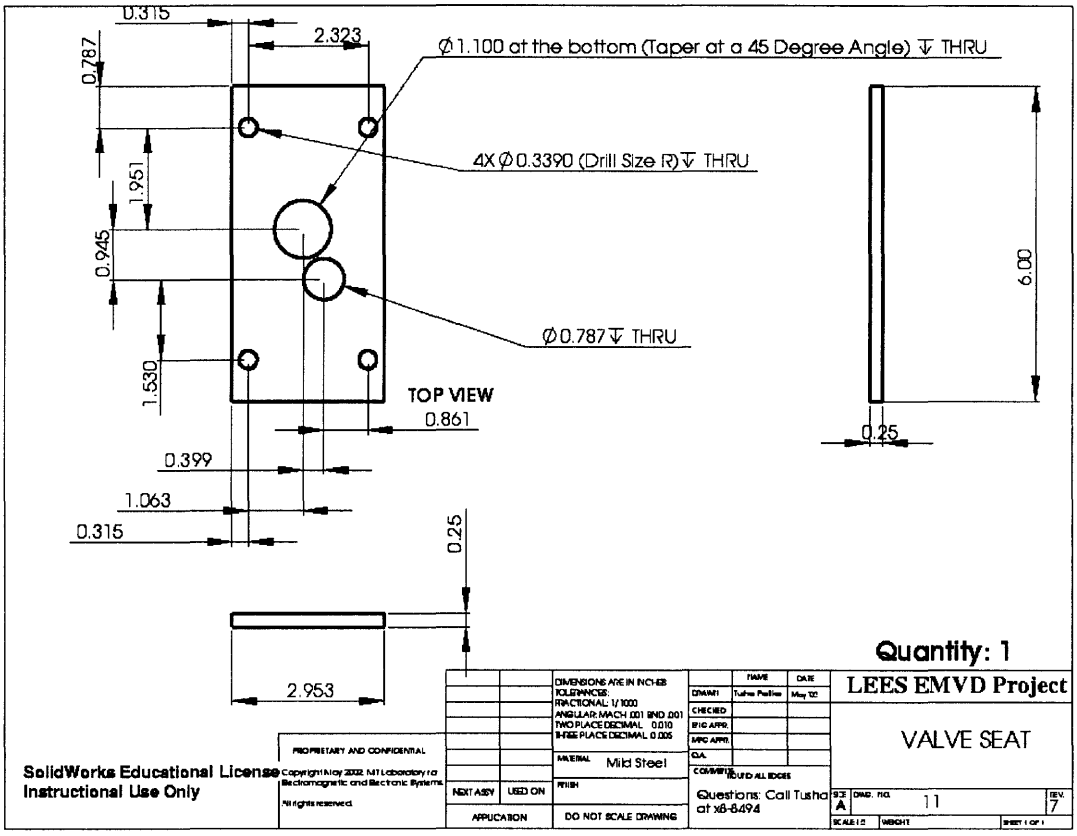
0.315
2.323
0.787
Ø1.100 at the bottom (Taper at a 45 Degree Angle) ↧ THRU
4X Ø0.3390 (Drill Size R) ↧ THRU
1.951
0.945
Ø0.787 ↧ THRU
1.530
TOP VIEW
0.861
0.399
1.063
0.315
0.25
2.953
6.00
0.25
Quantity: 1
DIMENSIONS ARE IN INCHES
TOLERANCES:
FRACTIONAL 1/1000
ANGULAR: MACH .001 BND .001
TWO PLACE DECIMAL .010
THREE PLACE DECIMAL .005
MATERIAL Mild Steel
FINISH
DO NOT SCALE DRAWING
DRAWN Tushar Patkar May '02
CHECKED
ENG APPR.
MFG APPR.
Q.A.
COMMENTS: BREAK ALL EDGES
Questions: Call Tushar at x8-8494
LEES EMVD Project
VALVE SEAT
SIZE A
DWG. NO. 11
REV. 7
SCALE: 1:5
WEIGHT
SHEET 1 OF 1
NEXT ASSY
USED ON
APPLICATION
PROPRIETARY AND CONFIDENTIAL
Copyright May 2002 MIT Laboratory for Electromagnetic and Electronic Systems
All rights reserved
SolidWorks Educational License
Instructional Use Only

C.13

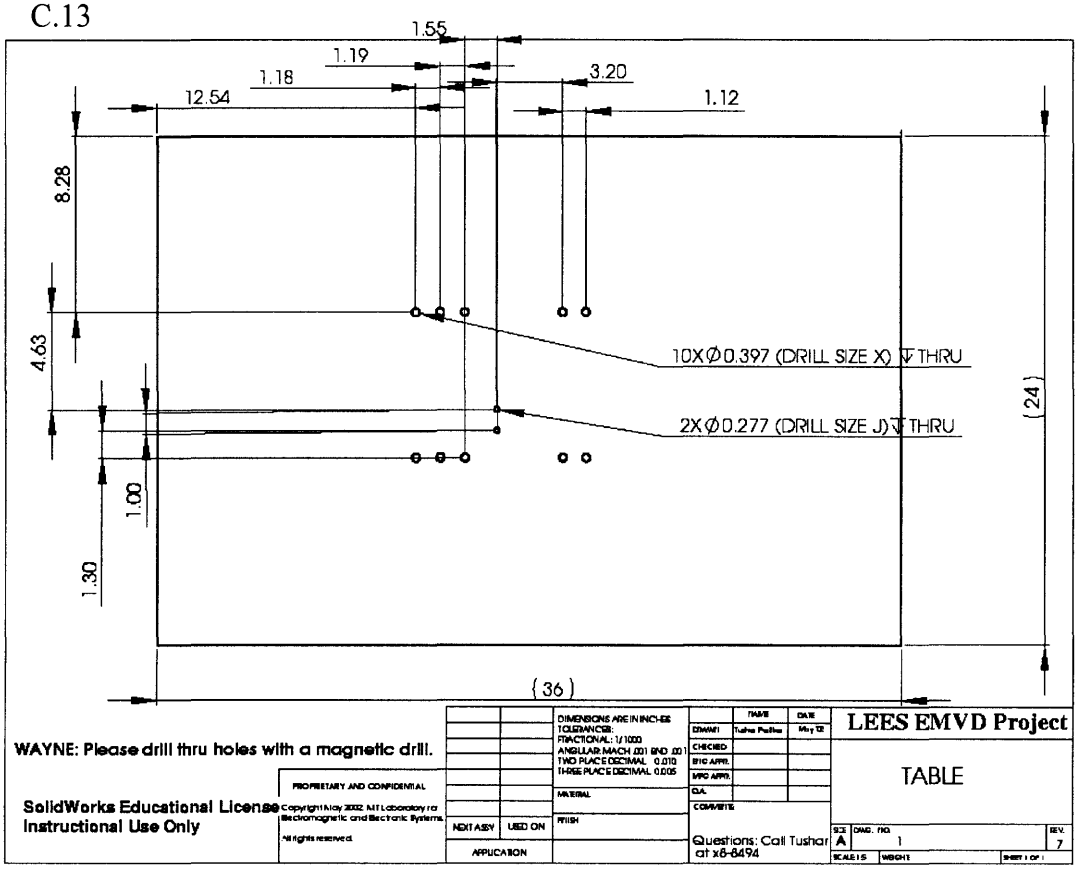
1.55
1.19
1.18
12.54
3.20
1.12
8.28
4.63
10XØ0.397 (DRILL SIZE X) ↧ THRU
2XØ0.277 (DRILL SIZE J) ↧ THRU
(24)
1.00
1.30
(36)
WAYNE: Please drill thru holes with a magnetic drill.
DIMENSIONS ARE IN INCHES
TOLERANCES:
FRACTIONAL: 1/1000
ANGULAR: MACH .001 BND .001
TWO PLACE DECIMAL .010
THREE PLACE DECIMAL .005
MATERIAL
FINISH
DO NOT SCALE DRAWING
DRAWN Tushar Patkar May '02
CHECKED
ENG APPR.
MFG APPR.
Q.A.
COMMENTS
Questions: Call Tushar at x8-8494
LEES EMVD Project
TABLE
SIZE A
DWG. NO. 1
REV. 7
SCALE: 1:5
WEIGHT
SHEET 1 OF 1
NEXT ASSY
USED ON
APPLICATION
PROPRIETARY AND CONFIDENTIAL
Copyright May 2002 MIT Laboratory for Electromagnetic and Electronic Systems
All rights reserved
SolidWorks Educational License
Instructional Use Only

C.14. 3-D view of the experimental apparatus.

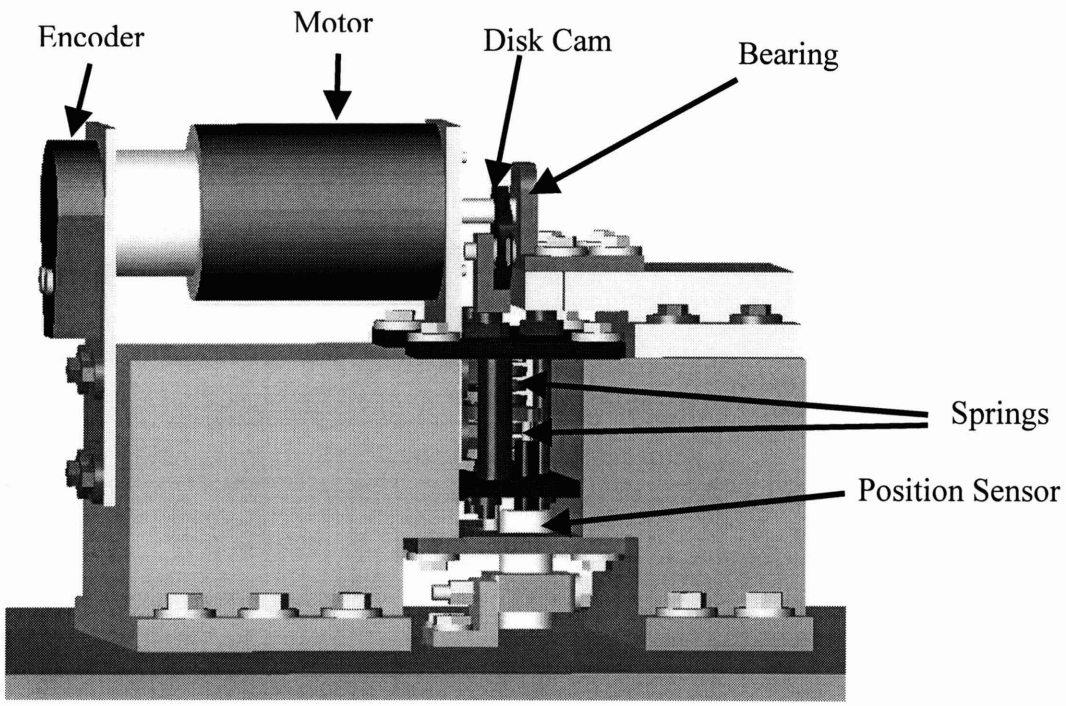

References

[1] T. W. Asmus, "Perspectives on applications of variable valve timing," *SAE Paper* 910445, 1991.

[2] M. M. Schlechter and M. B. Levin, "Camless engine," *SAE Paper* 960581, 1996.

[3] T. Dresner and P. Barkan, "A review of variable valve timing benefits and modes of operation," *SAE Paper* 891676, 1989.

[4] J. B. Heywood, *Internal Combustion Engine Fundamentals*, McGraw-Hill, 1988.

[5] *SAE Handbook*, 4th ed., Stuttgart, Germany, Bosch, Oct. 1996.

[6] W. Giles, "Fundamentals of valve design and material selection," *SAE Paper* 660471, 1966.

[7] R. Ernst et al., "Advanced optimization techniques in valvetrain design," *SAE Paper* 932004, 1993.

[8] R. R. Henry and B. P. Lequesne, "A novel, fully flexible, electro-mechanical engine valve actuation system," *SAE Paper* 970249, 1997.

[9] C. Dopson and T. Drake, " Emissions optimization by camshaft profile switching," *SAE Paper* 910838, 1991.

[10] W. Demmelbauer-Ebner, A. Dachs, and H. P. Lenz, " Variable valve actuation systems for the optimization of engine torque," *SAE Paper* 910447, 1991.

[11] J. G. Kassakian, H.-C. Wolf, J. M. Miller, and C. J. Hurton, "Automotive electrical systems circa 2005," *IEEE Spectrum*, pp. 22-27, Aug. 1996.

[12] T. Dresner and P. Barkan, "A review and classification of variable valve timing mechanisms," *SAE Paper* 890674, 1989.

[13] T. Ahmad and M. A. Theobald, "A survey of variable-valve-actuation technology," *SAE Paper* 891674, 1989.

[14] R. Steinberg, et al., "A fully continuous variable cam timing concept for intake and exhaust phasing," *SAE Paper* 980767, 1998.

[15] L. Mikulic, et al., "Variable gas exchange systems for S.I. engines--layout and experimental data," *SAE Paper* 920296, 1992.

[16] H. Nakamura, et al., "Development of gear parts for VVT unit," *SAE Paper* 970337, 1997.

[17] M. Matsuki, et al., "Development of a lean-burn engine with a variable valve timing mechanism," *SAE Paper* 960583, 1996.

[18] A. Titolo, "The variable valve timing system--application on a V8 engine," *SAE Paper* 910009, 1991.

[19] R. Flierl and M. Kluting, "The third generation of valvetrains – new fully variable valvetrains for throttle-free load control," *SAE Paper* 2000-01-1227, 2000.
[20] L. A. Gould, W. E. Richeson, and F. L. Erickson, "Performance evaluation of a camless engine using valve actuators with programmable timing," *SAE Paper* 910450, 1991.
[21] F. Pischinger and P. Kreuter, "Electromagnetically operating actuators," *U.S. Patent* 4,455,543, June 19, 1984.
[22] P. Kreuter, P. Heuser, and M. Schebitz, "Strategies to improve SI-engine performance by means of variable intake lift, timing, and duration," *SAE Paper* 920449, 1992.
[23] M. A. Theobald, B. Lequesne, and R. Henry, "Control of engine load via electromagnetic valve actuator," *SAE Paper* 940816, 1994.
[24] M. Pischinger, et al., "Benefits of the electromechanical valve train in vehicle operation," *SAE paper* 2000-01-1223, 2000.
[25] "Camless BMW engine still faces hurdles," *Automotive Industries*, p. 34, Oct. 1999.
[26] "Renault research," *Automotive Engineering International*, p. 114, Mar. 2000.
[27] "Emission control," *Automotive World*, pp. 10-15, Apr. 2000.
[28] S. Butzmann, et al., "Sensorless control of electromagnetic actuators for variable valve train," *SAE paper* 2000-01-1225, 2000.
[29] "Camless engine," *Automotive Engineering International*, p. 36, Feb. 2000.
[30] M. Gottschalk, "Electromagnetic valve actuator drives variable valvetrain," *Design News*, Nov. 1, 1993.
[31] F. Y. Chen, *Mechanics and design of cam mechanicsms*, New York, Pergamon Press, 1982, p. 466, p. 71.
[32] W. S. Chang, *An electromechanical vale drive incorporating a nonlinear mechanical transformer*, Ph.D. Thesis Proposal, Massachusetts Institute of Technology, Dec. 2001.
[33] W. S. Chang, J. G. Kassakian, and T. A. Keim, "An electromechanical vale drive incorporating a nonlinear mechanical transformer," *U.S. Patent Application* 60/322813, June 2000.
[34] W. S. Chang, T. Parlikar, J. G. Kassakian, and T. A. Keim, "An electromechanical vale drive incorporating a nonlinear mechanical transformer," *SAE Paper* 2003-01-0036, 2003.
[35] W. S. Chang, T. Parlikar, M. Seeman, D. J. Perreault, J. G. Kassakian, and T. A. Keim, "A new electromagnetic valve actuator," *IEEE Workshop on Power Electronics in Transportation*, pp. 109-118, Auburn Hills, MI, Oct. 2002.
[36] SAE Spring Committee, *Spring Design Manual*, 2nd ed., Warrendale, PA, Society of Automotive Engineers, Inc., 1996, pp. 321-356.

[37] D. C. Karnopp, D. L. Margolis, R. C. Rosenberg, *System dynamics: a unified approach*, 2nd ed., John Wiley & Sons, Inc., 1990.

[38] J.-J. Slotine and W. Li, *Applied Nonlinear Control*, Englwood Cliffs, NJ, Prentice-Hall Inc., 1991.

[39] A. B. Plunkett, "A current-controlled PWM transistor inverter drive," *IEEE/IAS Annual Meeting Conference*, pp. 789-792, 1979.

[40] D. M. Brod and D. W. Novotny, "Current control of VSI-PWM inverters," *IEEE Transactions on Industrial Applications*, vol. 21, no. 4, pp. 562-570, 1985.

[41] M. Seeman, T. Parlikar, W. S. Chang, and D. P. Perreault, *Design and implementation of a motor drive amplifier*, Technical Report, Laboratory for Electromagnetic and Electronic Systems, Massachusetts Institute of Technology, May 2002.

[42] T. Parlikar, *Experimental implementation of an electromagnetic engine valve*, M.S. Thesis, Department of Electrical Engineering and Computer Science, Massachusetts Institute of Technology, Feb. 2003.

[43] H. K. Khalil, *Nonlinear Systems*, 2nd ed., Upper Saddle River, New Jersey, Prentice Hall, 1996.

[44] K. Ogata, *Modern Control Engineering*, 2nd ed., Prentice-Hall International, Inc., 1990, pp. 699-713.